

**GAZİANTEP UNIVERSITY GRADUATE
SCHOOL OF NATURAL & APPLIED SCIENCES**

**AN EXPERIMENTAL INVESTIGATION ON
THE ANALYSIS OF FLOW DYNAMICS IN
COLLAPSIBLE ELASTIC TUBES**

**Ph.D. THESIS
IN
MECHANICAL ENGINEERING**

**BY
VEDAT ORUÇ
FEBRUARY 2007**

**An Experimental Investigation on the Analysis of Flow
Dynamics in Collapsible Elastic Tubes**

**Ph.D. Thesis
in
Mechanical Engineering
University of Gaziantep**

**Supervisor
Prof. Dr. Melda ÇARPINLIOĞLU**

**by
Vedat ORUÇ
February 2007**

T.C.
GAZİANTEP UNIVERSITY
GRADUATE SCHOOL OF
NATURAL & APPLIED SCIENCES
MECHANICAL ENGINEERING DEPARTMENT

Name of the thesis : An Experimental Investigation on the Analysis of Flow Dynamics in Collapsible Elastic Tubes
Name of the student : Vedat ORUÇ
Exam date : 01 February 2007

Approval of the Graduate School of Natural and Applied Sciences

Prof. Dr. Sadettin ÖZYAZICI
Director

I certify that this thesis satisfies all the requirements as a thesis for the degree of Doctor of Philosophy.

Prof. Dr. Melda ÇARPINLIOĞLU
Head of Department

This is to certify that we have read this thesis and that in our opinion it is fully adequate, in scope and quality, as a thesis for the degree of Doctor of Philosophy.

Prof. Dr. Melda ÇARPINLIOĞLU
Supervisor

Examining Committee Members

Prof. Dr. Kahraman ALBAYRAK

Prof. Dr. Beşir ŞAHİN

Prof. Dr. Melda ÇARPINLIOĞLU

Assoc. Prof. Dr. Hüseyin AKILLI

Assoc. Prof. Dr. M. Yaşar GÜNDOĞDU

ABSTRACT

AN EXPERIMENTAL INVESTIGATION ON THE ANALYSIS OF FLOW DYNAMICS IN COLLAPSIBLE ELASTIC TUBES

ORUÇ, Vedat

Ph.D. in Mechanical Engineering

Supervisor: Prof. Dr. Melda ÇARPINLIOĞLU

February 2007, 169 pages

In this study airflow through collapsible elastic tubes was experimentally investigated. The experimental set-up was designed and constructed as a result of literature survey. In the experiments, Penrose tubes having a wall thickness of 0.55 mm and silicone rubber tubes having a wall thickness of 1 mm, 2 mm and 3mm were used. The inside diameter of the tubes are 25.4 mm and three different tube lengths were tested such as the ratios of tube length to the tube inside diameter would be 10, 7.5 and 5. The elastic tube was placed without any tension in an airtight box known as Starling resistor and it was attached to pieces of metal pipes at both of its ends. Airflow was steadily supplied to the system by means of a screw-type compressor. The steady air flow rate was regulated between 0.0049 m³/s and 0.0214 m³/s. When the internal and external pressure difference of the tube in which air flowed through it was negative on applying pressure into the Starling resistor, the self excited oscillations were observed in most of the cases and flow was therefore unsteady. However the oscillations were not observed in some cases depending on the tube type (the 3 mm thick silicone rubber tube) and flow rate. The time dependent pressure and velocity measurements were stored on the computer by means of a data acquisition system. The measurements of pressure at the inlet and exit of the tube and the velocity at the exit of the tube had been performed at the onset of oscillations. The frequency of the oscillations had been determined by applying Fast Fourier Transform (FFT) to these measurements. The experimentally determined frequency of the oscillations values were between 18 Hz and 35 Hz. It was seen that the properties of the tube (wall-thickness, length, inside diameter, tube material) and

magnitude of the flow rate seriously affected pressure and velocity measurements. Therefore it was emphasized that these parameters should be considered in the collapsible tube flow investigations. The experimental results were also compared with the theoretical calculations based on linear stability theory obtained from literature. The frequency value obtained from the calculations was seen to be in the range of measurement results. The flows through collapsible tubes are up-to-date topic and the studies are continuing on them due to the fact that they are basically related to physiological flows and biomechanical applications. Therefore this experimental study which had been presented in detail may be considered to be beneficial for the investigators dealing with this topic. In addition, since water had been used as fluid in most of the previous experimental studies related to the subject, it was considered that it might be useful to test also airflow in collapsible tubes. Consequently, the performed investigation in which this gap was taken into consideration can be said to have significance in this respect.

Key Words: tube law, transmural pressure, fluid-solid interaction, self-excited oscillations, Starling resistor, collapsible tube flow, data acquisition, wave speed, Womersley number

ÖZET

ÇÖKELEBİLEN ELASTİK TÜPLERDEKİ AKIŞ DİNAMİĞİNİN ANALİZİNE YÖNELİK DENEYSEL BİR ARAŞTIRMA

ORUÇ, Vedat

Doktora Tezi, Makina Mühendisliği Bölümü
Tez Yöneticisi: Prof. Dr. Melda ÇARPINLIOĞLU
Şubat 2007, 169 sayfa

Bu çalışmada çökelebilen elastik tüplerdeki hava akışı deneysel olarak araştırılmıştır. Deneysel düzeneği literatür araştırması sonucu tasarlanıp imal edilmiştir. Deneysel tüplerde cidar kalınlığı 0.55 mm olan Penrose tüp ve cidar kalınlığı 1 mm, 2 mm ve 3 mm olan silikon tüpler kullanılmıştır. Tüplerin iç çapı 25.4 mm olup tüp uzunluğunun tüp iç çapına oranı 10, 7.5 ve 5 olacak şekilde üç farklı tüp uzunluğu test edilmiştir. Elastik tüp, Starling resistor olarak bilinen hava sızdırmaz bir kutu içerisine herhangi bir gerilme verilmeden her iki ucunda metal boru parçalarına takılmıştır. Hava akışı vida tipi bir kompresörle zamana bağımsız olarak sisteme sağlanmıştır. Zamana bağımsız akış miktarı $0.0049 \text{ m}^3/\text{s}$ ile $0.0214 \text{ m}^3/\text{s}$ arasında ayarlanmıştır. Starling resistor'e basınç uygulayarak içinden hava akan tüpün iç ve dış basınç farkı negatif olduğu zaman çoğu durumda kendiliğinden salınımlar gözlenmiş ve akış bu yüzden zamana bağımlı hale gelmiştir. Ancak tüp çeşidine (3 mm kalınlığındaki silikon tüp) ve akış miktarına bağlı olarak bazı durumlarda salınımlar gözlenmemiştir. Zamana bağımlı basınç ve hız ölçümleri bir veri toplama sistemiyle bilgisayara kaydedilmiştir. Salınımların başladığı anda tüp giriş ve çıkışındaki basınç ölçümleri ve tüp çıkışındaki hız ölçümleri yapılmıştır. Bu ölçümlere hızlı Fourier dönüşümü (FFT) uygulayarak salınımların frekansı belirlenmiştir. Deneysel olarak belirlenen salınımların frekans değerleri 18 Hz ile 35 Hz arasında kalmıştır. Tüp özelliklerinin (cidar kalınlığı, uzunluk, iç çap, tüp malzemesi) ve akış miktarının, basınç ve hız ölçümlerini önemli ölçüde etkilediği görülmüştür. Bu yüzden bu parametrelerin çökelebilen tüp akışları araştırmalarında dikkate alınması gerektiği vurgulanmıştır. Ayrıca deneysel sonuçlar, literatürden

alınan lineer stabilite teorisine bađlı olan teorik hesaplamalarla karřılařtırılmıřtır. Hesaplamalar sonucu bulunan frekans deđerinin ölçümlerden elde edilen aralık içerisinde kaldıđı görülmüřtür. Çökelebilen tüplerdeki akıřlar esas olarak fizyolojik akıřlara ve biyomekanik uygulamalara bađlantılı olduđundan, güncel bir konu olup üzerinde çalıřmalar devam etmektedir. Bu yüzden detaylı olarak sunulan bu deneysel çalıřmanın konu alanındaki arařtırcılara yararlı olacađı düşünülebilir. Ayrıca konuyla ilgili geçmiřteki deneysel çalıřmaların çođunda akıřkan olarak su kullanıldıđından, çökelebilen tüplerde hava akıřının da test edilmesinin yararlı olabileceđi düşünölmüřtür. Dolayısıyla bu açıklıđı dikkate alarak yapılan arařtırmanın bu anlamda önem tařıdıđı söylenebilir.

Anahtar Kelimeler: tüp yasası, transmural basınç, akıřkan-katı etkileřimi, kendiliđinden oluřan salınımlar, Starling resistor, çökelebilen tüp akıřı, veri toplama, dalga hızı, Womersley sayısı

ACKNOWLEDGMENTS

I want to express my gratitude to Prof. Dr. Melda ÇARPINLIOĞLU, my Ph.D. supervisor. She helped me to complete the study with her inspiration and great efforts to explain things clearly and simply. Throughout my thesis-writing period, she provided lots of good ideas and sound advice.

I am indebted to my friend Mr. Salih KILINÇ due to his help with the programming and data acquisition. I wish to express my sincere appreciation to Dr. Orhan ÇAKIR from Dicle University, Mechanical Engineering Department for his encouragement. In addition the support by Dr. Sedat KOLUKISA and Dr. Haluk KEJANLI is acknowledged. Furthermore, I remember here Dr. M. Aydın KETANİ who sincerely expected my success during the study. By the way, I would like to cite my cousin Mr. Orhan GÜNGÖRDÜ who has a special place in my heart.

I want to thank Ms. Melahat ŞEN and Ms. Elif AŞKIN, the secretaries in the Mechanical Engineering Department of Gaziantep University, for assisting me in many different ways. I also thank the personnel in the workshop of the department; Mr. İbrahim KORKMAZ deserves special mention. I haven't forgotten the assistance by Mr. Eyüp DOĞAN from Electrical and Electronics Engineering Department.

Special thanks are due to the financial support of TÜBİTAK under the research project no. 105M301. The staff of Öz Diyarbakır Travel Agency is also worthy of my thanks for making safely the distance between Diyarbakır and Gaziantep shorter.

I save the last and greatest thanks for my family due to their continuous patience, support, and encouragement during the study. In my opinion they've been more tired than me. I'm especially grateful to my big-brother, Nurullah ORUÇ who allowed so much time during construction of the experimental set-up. I also wish to mention about my brother Osman ORUÇ due to his continuous heartening through the study. I cannot further explain their contribution to this study by means of words. Thus, briefly, to my family I dedicate this thesis.

CONTENTS

	page
ABSTRACTii
ÖZET	iv
ACKNOWLEDGMENTS	vi
CONTENTS	vii
LIST OF TABLES	x
LIST OF FIGURESxi
LIST OF SYMBOLS	xv
CHAPTER 1: INTRODUCTION	1
CHAPTER 2: LITERATURE SURVEY4
2.1. Introduction	4
2.2. The Basic Definitions Related to the Subject	4
2.2.1. Derivation of 1D model	8
2.2.2. Analysis of 1D model	12
2.3. Theoretical Studies	14
2.3.1. Lumped parameter models	14
2.3.2. One-dimensional (1D) models	15
2.3.3. Two-dimensional (2D) and three dimensional (3D) models	16
2.4. Experimental Studies	18
2.4.1. Studies on pressure / flow characteristics and flow limitation	18
2.4.2. Studies on flow field measurement	24
2.5. Conclusion	25
CHAPTER 3: EXPERIMENTAL SET-UP, MEASURING DEVICES and DATA ACQUISITION SYSTEM	27
3.1. Introduction	27
3.2. Experimental Set-up	27
3.2.1. Airtight chamber: Starling resistor	29
3.2.2. Test tubes	29

3.3. Measurements and Measuring Devices	30
3.3.1. Flow rate measurement	31
3.3.2. Pressure measurement	31
3.3.3. Velocity measurement with hot-wire anemometer	32
3.3.4.1. Determination of the hot-wire probe position in the pipe cross-section	33
3.4. Data Acquisition System.	35
3.4.1. Hardware of data acquisition system	36
3.4.2. Software of data acquisition system	36
3.5. Control of Time Dependent Data Acquisition	37
3.6. Checking of Reliability of the Measurements	37
3.7. Conclusion	38

CHAPTER 4: PRELIMINARY EXPERIMENTS FOR DETERMINING

EXTERNAL PRESSURE INITIATING TUBE COLLAPSE	40
4.1. Introduction	40
4.2. Experimental Protocols	40
4.2.1. Non-oscillating flow case	41
4.2.2. Oscillating flow case	43
4.2.3. Analysis of non-oscillating and oscillating flow cases simultaneously	50
4.3. Conclusion	55

CHAPTER 5: ANALYSIS OF THE TEST CASES

AT THE ONSET OF SELF-EXCITED OSCILLATIONS	57
5.1. Introduction	57
5.2. Unsteady Pressure and Velocity Measurement Results	58
5.3. The Effects of Q , h , L Parameters on $p_{e,c}$ and f	61
5.3.1. Variation of f and $p_{e,c}$ with Q	62
5.3.2. Determination of the effect of L	63
5.3.3. Determination of the effect of h	64
5.4. Evaluation of Experimental Results In Terms of Dimensionless Parameters	65
5.5. Conclusion	70

CHAPTER 6: THEORETICAL CALCULATIONS OF FREQUENCY and COMPARISON WITH MEASUREMENTS AT THE ONSET OF OSCILLATIONS	72
6.1. Introduction	72
6.2. Linear Stability Theory	72
6.3. Tube Law Calculations	76
6.4. Calculations of f & u_c By Using Linear Stability Theory and Comparison With Experimental Data	78
6.5. Conclusion	82
 CHAPTER 7: CONCLUSION and SUGGESTIONS FOR FURTHER INVESTIGATIONS	 83
REFERENCES	86
TABLES	93
FIGURES	102
APPENDICES	148
Appendix 1: Specifications of the Compressor	149
Appendix 2: Specifications of Pressure Transmitter for p_e Measurement	150
Appendix 3: Technical Data of Ascon (M1-3000) Digital Process Controller	151
Appendix 4: Technical Specifications of Pressure Transducers for p_1 and p_2 Measurement	153
Appendix 5: Technical Specifications of The Hot-Wire Anemometer and Its Probe	154
Appendix 6: Features of The Das-1602 Hardware	156
Appendix 7: Testing and Calibration of The Das-1602 Hardware	157
Appendix 8: Time Dependent Data Accumulation Control Program	160
 CURRICULUM VITAE	 168

LIST OF TABLES	page
Table 3.1. Properties of the test tubes	94
Table 4.1. Specification of the experimental test cases	95
Table 4.2. Oscillating test cases	95
Table 4.3. Non-oscillating test cases	96
Table 5.1. The experimental data for flow through P_L tube at the onset of oscillations	97
Table 5.2. The experimental data for flow through P_M tube at the onset of oscillations	97
Table 5.3. The experimental data for flow through P_S tube at the onset of oscillations	97
Table 5.4. The experimental data for flow through $S_{1,L}$ tube at the onset of oscillations	98
Table 5.5. The experimental data for flow through $S_{1,M}$ tube at the onset of oscillations	98
Table 5.6. The experimental data for flow through $S_{1,S}$ tube at the onset of oscillations	98
Table 5.7. The experimental data for flow through $S_{2,L}$ tube at the onset of oscillations	99
Table 5.8. The experimental data for flow through $S_{2,M}$ tube at the onset of oscillations	99
Table 5.9. The experimental data for flow through $S_{2,S}$ tube at the onset of oscillations	99
Table 6.1. Calculations of some parameters based on [13] in reference to the experimental measurements at the onset of oscillations for the flow through Penrose tube	99
Table 6.2. Calculations of some parameters based on [13] in reference to the experimental measurements at the onset of oscillations for the flow through silicone rubber tube ($h=1$ mm)	100
Table 6.3. Calculations of some parameters based on [13] in reference to the experimental measurements at the onset of oscillations for the flow through silicone rubber tube ($h=2$ mm)	101

LIST OF FIGURES	page
Figure 2.1. A schematic representation of Starling resistor	103
Figure 2.2. A sketch for Δp versus Q with (a) $p_{m,1}$ fixed (flow limitation), (b) $p_{m,2}$ fixed (pressure-drop limitation), (c) Conrad's [1] protocol	104
Figure 2.3. A schematic relation between p_m and A (tube law) showing typical tube cross-sections	104
Figure 2.4. Computations from [40] demonstrating 3D buckling and collapse of a tube held open at each end, supporting an internal flow; external compression increases from panel (a) to panel (d)	104
Figure 3.1. A schematic representation of the experimental set-up without data acquisition system	105
Figure 3.2. A schematic representation of the experimental set-up together with its data acquisition system and measuring devices	106
Figure 3.3. Steady turbulent flow measurements with Pitot tube at three different Re in order to show that flow is fully developed before entering to the test section	107
Figure 3.4. Dimensions of the rigid attachment	107
Figure 3.5. Axial force-deflection test applied to the sample of test tubes (P, S ₁ , S ₂ , S ₃) for the determination of E	108
Figure 3.6. Calibration curve of pressure transmitter (E913) and digital process controller (M1-3000) combination	109
Figure 3.7. Calibration curve of Omega pressure transducer	109
Figure 3.8. Calibration of hot-wire anemometer probe	109
Figure 3.9. Cross-sectional velocity distribution at $5.12D_0$ downstream of S _{1,L} in steady flow for $Re = 5,300$ with $p_e = 0$	110
Figure 3.10. Cross-sectional velocity distribution at $5.12D_0$ downstream of S _{1,L} in steady flow for $Re = 51,000$ with $p_e = 0$	110

Figure 3.11. Velocity distribution at $6.3D_0$ downstream of $S_{1,M}$ in oscillating flow for $Re = 61,000$ with $p_e = 2.12$ kPa	110
Figure 3.12. Sample measurement cases with hot wire anemometer to check the accuracy of the measurements	111
Figure 3.13. FFT analysis of Figure 3.12	111
Figure 4.1. Variation of $p_1, p_2, \Delta p, Q$ and $p_{tm,2}$ with p_e for a non-oscillating case through $S_{1,L}$	112
Figure 4.2. Variation of $p_1, p_2, \Delta p, Q$ and $p_{tm,2}$ with p_e for a non-oscillating case through $S_{3,L}$	113
Figure 4.3. Variation of $p_1, p_2, \Delta p, Q$ and $p_{tm,2}$ with p_e for a non-oscillating case through $S_{1,M}$	114
Figure 4.4. Variation of $p_1, p_2, \Delta p, Q$ and $p_{tm,2}$ with p_e for a non-oscillating case through $S_{2,M}$	115
Figure 4.5. Variation of $p_1, p_2, \Delta p, Q$ and $p_{tm,2}$ with p_e for a non-oscillating case through $S_{1,S}$	116
Figure 4.6. Variation of $p_1, p_2, \Delta p, Q$ and $p_{tm,2}$ with p_e for a non-oscillating case through $S_{3,S}$	117
Figure 4.7. Variation of $p_1, p_2, \Delta p, Q$ and $p_{tm,2}$ with p_e for an oscillating case through $S_{1,L}$	118
Figure 4.8. Variation of $p_1, p_2, \Delta p, Q$ and $p_{tm,2}$ with p_e for an oscillating case through $S_{2,L}$	119
Figure 4.9. Variation of $p_1, p_2, \Delta p, Q$ and $p_{tm,2}$ with p_e for an oscillating case through P_M	120
Figure 4.10. Variation of $p_1, p_2, \Delta p, Q$ and $p_{tm,2}$ with p_e for an oscillating case through $S_{1,M}$	121
Figure 4.11. Variation of $p_1, p_2, \Delta p, Q$ and $p_{tm,2}$ with p_e for an oscillating case through P_S	122
Figure 4.12. Variation of $p_1, p_2, \Delta p, Q$ and $p_{tm,2}$ with p_e for an oscillating case through $S_{1,S}$	123
Figure 4.13. Variation of Δp with p_e through $S_{1,L}$ tube for a range of Q	124
Figure 4.14. Variation of Δp with p_e through $S_{2,L}$ tube for a range of Q	124
Figure 4.15. Variation of Δp with p_e through $S_{3,L}$ tube for a range of Q	125

Figure 4.16. Variation of Δp with p_e through P_L tube for a range of Q	125
Figure 4.17. Variation of Δp with p_e for the tubes of $L/D_0 = 10$	125
Figure 4.18. Variation of Q with $p_{e,c}$ for indicating the effect of h	126
Figure 4.19. Variation of Q with $p_{e,c}$ for indicating the effect of L	127
Figure 4.20. Variation of $Re(h/L)$ with $p_{e,c}/K_p$	128
Figure 5.1. Variation of pressure and velocity with time at the onset of oscillations for the flow through $S_{1,M}$ tube ($\bar{p}_1 = 3.2$ kPa, $\bar{p}_2 = 2$ kPa, $\bar{u}_{os} = 43.93$ m/s)	129
Figure 5.2. FFT analysis of Figure 5.1 (at the peak, $f = 19.60$ Hz for the three cases)	130
Figure 5.3. Variation of pressure and velocity with time at the onset of oscillations for the flow through $S_{2,S}$ tube ($\bar{p}_1 = 3.01$ kPa, $\bar{p}_2 = 1.38$ kPa, $\bar{u}_{os} = 27.84$ m/s)	131
Figure 5.4. FFT analysis of Figure 5.3 (at the peak, $f = 28.89$ Hz for the three cases)	132
Figure 5.5. Variation of pressure and velocity with time at the onset of oscillations for the flow through P_L tube ($\bar{p}_1 = 1.37$ kPa, $\bar{p}_2 = 1.1$ kPa, $\bar{u}_{os} = 15.27$ m/s)	133
Figure 5.6. FFT analysis of Figure 5.5 (at the peak, $f = 19.06$ Hz for the three cases)	134
Figure 5.7. Variation of f and $p_{e,c}$ with Q at the onset of oscillations for the flow through P_L , P_M and P_S tubes	135
Figure 5.8. Variation of f and $p_{e,c}$ with Q at the onset of oscillations for the flow through $S_{1,L}$, $S_{1,M}$, and $S_{1,S}$ tubes	136
Figure 5.9. Variation of f and $p_{e,c}$ with Q at the onset of oscillations for the flow through $S_{2,L}$, $S_{2,M}$, and $S_{2,S}$ tubes	137
Figure 5.10. Variation of $p_{e,c}$ with Q to show the effect of length of the test tubes at the onset of oscillations	138
Figure 5.11. Variation of f with Q to show the effect of length of the test tubes at the onset of oscillations	139

Figure 5.12. Variation of $p_{e,c}$ with Q to show the effect of thickness of the test tubes at the onset of oscillations	140
Figure 5.13. Variation of f with Q to show the effect of thickness of the test tubes at the onset of oscillations	141
Figure 5.14. Mean flow resistance versus downstream transmural pressure in dimensionless form at the onset of oscillations	142
Figure 5.15. Variation of Womersley number with dimensionless downstream transmural pressure at the onset of oscillations	143
Figure 5.16. Mean oscillating flow velocity versus downstream transmural pressure in dimensionless form at the onset of oscillations	144
Figure 6.1. Relationship between dimensionless fluid speed (S) and wave number (k) given in reference [13] for $b/D_0 = 0.108$	145
Figure 6.2. Tube law for the test tubes obtained by using equations (6.14 and 6.15)	145
Figure 6.3. The relationship between A/A_0 and b/D_0 obtained by utilizing the experimental data presented in reference [8]	146
Figure 6.4. The relationship between S and k determined by using linear stability theory presented in reference [13] for $b/D_0 = 0.108$	146
Figure 6.5. Variation of f with b determined by using linear stability theory for the flow through test tubes at the onset of oscillations	147

LIST OF SYMBOLS

A	: cross-sectional area of the collapsible tube
A_0	: cross-sectional area of the unstretched (circular) tube
a	: constant number given by eqn. (6.3)
B	: bending stiffness to elastance ratio (eqn. 6.7)
b	: half distance between the opposing walls of the buckled tube
c	: wave speed (eqn. 2.9 or eqn. 6.5)
D_0	: inside diameter of the unstretched tube
E	: modulus of elasticity of the tube material
E_w	: elastance (tube law defined with eqn. 6.6)
E_s	: specific elastance (eqn. 6.8)
f	: frequency of oscillations
G	: ratio fluid friction to wall damping (eqn. 6.10)
h	: tube wall thickness
K_p	: circumferential bending stiffness of the tube (eqn. 3.1)
k	: dimensionless wave number
L	: tube length
ℓ	: rigid attachment length
M	: wall to fluid mass ratio (eqn. 6.9)
N	: number of acquired data
$P(A)$: tube law
$P(\alpha)$: dimensionless tube law (eqn. 6.14)
p	: local internal pressure of the fluid
p_1	: pressure at the upstream end of the elastic tube
\bar{p}_1	: mean upstream pressure of the oscillating flow
p_2	: pressure at the downstream end of the elastic tube
\bar{p}_2	: mean downstream pressure of the oscillating flow
Δp	: axial pressure drop along the length of the tube = $p_1 - p_2$
p_d	: downstream outlet pressure (see Figure 2.1)
p_e	: external pressure of the tube
$p_{e,c}$: external pressure at collapse
p_{tm}	: local transmural pressure = $p - p_e$
$p_{tm,1}$: upstream transmural pressure = $p_1 - p_e$
$p_{tm,2}$: downstream transmural pressure = $p_2 - p_e$
p_u	: upstream inlet pressure (see Figure 2.1)

Q	: volume flow rate of steady flow
Q_c	: volume flow rate at $p_{e,c}$
Q_{os}	: average oscillating flow rate
R	: frictional resistance factor
R_0	: radius of the circular tube
R_1	: upstream flow resistance (see Figure 2.1)
R_2	: downstream flow resistance (see Figure 2.1)
R_f	: friction factor of fluid (eqn. 6.11)
R_w	: wall damping coefficient
r	: radial position from the pipe center
r'	: the limiting position of the hot-wire probe close to the wall
Re	: steady flow Reynolds number ($Re = \bar{u}D_0 / \nu_f$)
S	: speed index ($S = \bar{u} / c$ and see eqns. 6.1, 6.4)
T	: longitudinal tension in the tube wall
t	: time
U_e	: effective cooling velocity of the hot wire anemometer
u	: axial fluid velocity
\bar{u}	: cross-sectionally averaged axial fluid velocity
u_c	: critical flow velocity at which oscillations generate (eqn. 6.4)
u_{os}	: oscillating flow velocity
\bar{u}_{os}	: mean oscillating flow velocity
V_A	: output voltage of the hot wire anemometer
V_p	: output voltage of the pressure transducer
W	: Womersley number (eqn. 5.3)
x	: axial distance (flow direction)

Greek Letters:

α	: dimensionless area ratio = A / A_0
ρ_f	: fluid density
ρ_w	: density of the tube material
ν	: Poisson's ratio of the elastic tube
ν_f	: fluid kinematic viscosity
ω	: angular frequency (eqn. 6.12)
ω^*	: dimensionless angular frequency (eqn. 6.2)

CHAPTER 1

INTRODUCTION

If a fluid flows through a collapsible tube or channel, interactions between fluid-mechanical and elastic forces can lead to a variety of biologically significant phenomena, including nonlinear pressure-drop/flow-rate relations, wave propagation, and the generation of instabilities. Understanding the physical origin and nature of these phenomena remains an important experimental, computational and analytical challenge, involving unsteady flows, large-amplitude fluid-structure interactions, free-surface flows, and intrinsically two-dimensional or three-dimensional motion.

Virtually all fluid carrying vessels in the body are elastic and can collapse when the transmural (internal minus external) pressure, p_{tm} falls below a critical value. At large positive values of p_{tm} such a tube is distended and stiff, and at large negative values the cross-sectional area is either very small, it being reduced to two narrow channels separated by a flat region of contact between the opposite walls, which is again a very stiff configuration, or it may fall to zero. There is an intermediate range of values of p_{tm} in which the cross-section is very compliant and even the small pressure drop through the tube may be enough to cause a large reduction in area, i.e., collapse.

Examples of physiological deformable vessels are systemic veins above the heart, arteries compressed by a sphygmomanometer cuff, or within the chest, intramyocardial coronary blood vessels during systole, the urethra during micturition, large intrathoracic airways during forced expiration or coughing, etc. The steady and unsteady flow through the veins near the heart is qualitatively similar to the flow through collapsible tubes. In all of these systems flow is significantly modified by transmural pressure-induced motion of the wall.

The airways throughout the respiratory system are deformable to a degree, and flow-structure interactions underlie some important pulmonary conditions. Expiratory flow limitation is of particular significance: An increase in effort (driving pressure drop) during forced expiration can lead to no increase, and possibly a decrease, in the flux of expired air, essentially because the alveolar (driving upstream) pressure leads to compression of conducting airways. This maneuver is frequently accompanied by *wheezing* which results from a flow-induced instability of deformable airway walls. Inspiration may lead to flow-induced upper-airway obstruction (contributing to *sleep apnea*) and instabilities that generate *snoring noises*. More controlled noise generation arises in the human larynx, where flow-induced oscillations of the vocal chords generate speech. Flow through the larynx generates instabilities of the vocal chords, which excite acoustic modes in the upper airways.

Self-excited oscillations, in particular, relate to the wheezing and *Korotkoff sounds* which are used clinically to measure systolic and diastolic arterial blood pressure, heard during brachial artery collapse under an arm cuff. Understanding fully mechanisms driving these oscillations remains a major research goal. Therefore the analysis and interpretation of collapsible tube flow experiments can be expected to explain these spontaneous oscillations arising in the above-mentioned vessels and comparable structures.

Flow in collapsible tubes also presents an interesting and extremely challenging fluid-mechanical problem in its own right as well as it has physiological relevance. Thus the study of flows in elastic tubes is of considerable interest in many biomedical and biomechanical applications. The prevalence of vessel collapse and variety of associated phenomena have made it a topic of great interest to biomechanical engineers.

In this study, due to the above cited importance, airflow in collapsible tubes has been experimentally investigated. The aim of the first chapter is to present some applications of collapsible tube flows and to present the outline of the thesis. Chapter 2 is related to the literature survey on the subject. Firstly the basic definitions and terms are introduced, and then the derivation of one-dimensional model is given. The classification of previous work has been done by considering that whether the study

is theoretical or experimental. An experimental set-up utilized in the study has been constructed by referring to the literature which points out that the necessity of investigations with airflow in the collapsible tubes.

Chapter 3 represents the details of the experimental set-up constructed for the present investigation. The test tubes which were used in the study are given together with their technical specifications. The measuring instruments and the data acquisition system are clearly introduced. The measuring principles, data acquisition methods and data processing techniques have been presented in the chapter.

The preliminary experimental results obtained without data acquisition system are given in Chapter 4. Before time dependent measurements, the initial experiments with conventional measuring methods by means of manometers have been carried out to understand the basic behaviour of the flow. This section offers a significant idea about the flow due to its inclusion of wide range of explanatory data.

The time dependent pressure and velocity measurements are the subject of Chapter 5 which is related to the analysis of experimental results obtained at the onset of self-excited oscillations. Time dependent pressure and velocity fluctuations and frequency of the oscillations are presented. The effects of flow rate, tube's material type, tube length and tube wall thickness on the oscillations were determined. In addition, some dimensionless parameters connected with experimental measurements were defined. The relationships between these non-dimensional parameters were studied and the significance of them was suggested.

Chapter 6 includes some theoretical calculations based on the linear stability theory. The results obtained from these calculations correspond to the onset of oscillations similarly to the results obtained in Chapter 5. The necessary equations for the calculations had been derived from the literature and they were specified in accordance with the calculations. The chapter represents important results due to the fact that although a number of approximations have been followed during the computations, but the theoretical results seem to agree with the measurements.

Chapter 7 outlines general conclusions of the present investigation and includes some suggestions for the future studies concerned with the collapsible tube flows.

CHAPTER 2

LITERATURE SURVEY

2.1. INTRODUCTION

In this chapter previous studies on collapsible tube flows are reviewed in detail. The studies of collapsible tube flows are sometimes considered to begin since 1969 [1] so it is appropriate to acknowledge that the subject has a rather longer history. There are some relevant review papers [2–6] which summarize well the previous work on the subject.

The available literature was mainly classified in two groups as theoretical studies and experimental studies. Almost in all of the experiments water was typically used as flowing fluid. However there are a few studies in which air was used as fluid in the experimental investigations [7,8]. The experimentally generated flows are essentially three-dimensional. However analytically and numerically the problem is challenging so that simplification down to two-dimensional or one-dimensional is usual.

In the following sections initially some basic definitions concerned to the collapsible tube flows are expressed and equations to derive one-dimensional model are presented due to a number of the model's applications in the literature. Then an attempt will be made to present important theoretical and experimental studies.

2.2. THE BASIC DEFINITIONS RELATED TO THE SUBJECT

There have been a lot of experiments using collapsible tubes designed to investigate flow-induced collapse. A famous study is the use of a collapsible tube by Starling and his colleagues [9]. A length of collapsible tube, made of silicone rubber or latex, is mounted horizontally between two rigid tubes to which it is clamped and is surrounded by a rigid airtight chamber. The independently controlled pressure inside

the chamber is external pressure (p_e) to the tube. Thus an airtight chamber including the collapsible tube, as shown in Figure 2.1, acquired a still-popular name: *Starling resistor*. It is simple to operate, exhibits dramatic flow-structure interactions and presents a wealth of modelling opportunities.

Considering the Starling resistor system, incompressible fluid flows along the tube from a constant-head reservoir. The pressures at the upstream and downstream ends of the collapsible segment, p_1 and p_2 , respectively are measured and may be controlled by valves providing additional upstream flow resistance, R_1 and downstream flow resistance, R_2 in the rigid parts of the apparatus. In general, two principal results have been obtained from these experiments:

- i. Above a critical value, the flow rate (Q) depends on the difference between p_1 and p_e , and is independent of the axial pressure drop, $\Delta p = p_1 - p_2$ along the length of the tube (*flow limitation*). It has been generally claimed in the literature that flow limitation is commonly associated with large-amplitude flow-induced oscillations, although it has not been established in the experiments [10] and computations [11] that whether the two phenomena are causally linked. The investigations [8,12,13] indicate that flow limitation is a necessary but not sufficient condition for the onset of oscillations.
- ii. Even in experiments designed to investigate steady-pressure relationships, commonly unsteady flow has been observed: large-amplitude *self-excited oscillations* which are manifested as audible sounds develop in the tube cross-sectional area.

In most investigations reported in the literature Q was measured as a function of variations in either p_1 , p_2 or p_e while the other two were held constant. The information about flow through a collapsible tube can be presented in terms of the pressure gradient Δp across the tube as a function of Q through the tube. The curve of Δp versus Q is called a *Characteristic Curve* (Figure 2.2). It is a common and useful method of presenting flow information for all kinds of systems. Δp represents flow rate through the tube. The stresses in the wall and p_m determine its geometry.

Flow-structure interactions lead to a strongly non-linear relation between Δp and Q . The type of curve obtained depends on what is held constant while Q is varied.

If a flow is driven through a Starling resistor, then as p_e is increased a constriction typically forms first toward the collapsible tube's downstream end where internal pressure, p is lowest. Various experimental protocols can then be followed (as given in [6], for example) such as increasing Δp while keeping the upstream transmural pressure, $p_{m,1} = p_1 - p_e$ fixed. It is found that the relation between Δp and the steady flow Q is as shown schematically in Figure 2.2(a). It should be noted here that time-averaged quantities are shown in Figure 2.2 in cases when the flow becomes unstable. Increasing Δp initially causes Q to increase: here, typically, $p_1 > p_2 > p_e$ and the tube is everywhere inflated. However, increasing Δp (for example by reducing p_2) leads to a reduction in downstream transmural pressure, $p_{m,2} = p_2 - p_e$ which causes the tube to collapse at its downstream end (with $p_1 > p_e > p_2$). Collapse can then surprisingly lead to a reduction in Q as Δp rises. Since Q cannot increase pass some threshold, this is an example of *flow-limitation* and usually *self-excited oscillations* accompany this behaviour. In reference [3], this version of the experiment is cited to be directly relevant to forced expiration from the lung [14] to venous return [15] and to micturition through the urethra [16].

Other protocols with the Starling resistor also yield nonlinear $\Delta p/Q$ relations. Increasing Δp while holding $p_{m,2}$ constant leads to *pressure-drop limitation*, namely a limit on the maximum possible Δp , Figure 2.2(b). This experiment is not directly applicable to any particular physiological condition, however it comes out that $p_{m,2}$ is a natural control parameter for at least one of the theoretical models [17] that have been proposed.

In the experimental investigation of reference [1] p_e and the downstream outlet pressure, p_d were fixed, as well as R_2 . In this case (Figure 2.2.c),

- i. initially $p_e > p_1 > p_2$: the tube is collapsed along its entire length, offers a high resistance to flow, and Δp rises sharply to produce a small increase in Q ;
- ii. then $p_1 > p_e > p_2$: the tube inflates at its upstream end remaining collapsed downstream, the resistance to flow falls dramatically and Δp falls as Q increases;
- iii. finally $p_1 > p_2 > p_e$: the tube is uniformly inflated, offers low resistance to flow and large increases in Q are provided by small increases in Δp .

The breakdown of steady flow through a collapsible tube appears to occur if cross-sectionally averaged steady fluid velocity (\bar{u}) in the tube exceeds the local value of the speed of propagation of small amplitude pressure waves (c) so that signals cannot be propagated upstream and the flow is *supercritical* ($\bar{u} > c$). The mechanism for the onset of unsteady behaviour is then analogous to *choking* of sonic gas flow in a nozzle, and can be analysed by a *one-dimensional (1D) model* in which local internal pressure of the fluid (p), the cross-sectional area (A) and \bar{u} are taken to be functions of time (t) and longitudinal distance (x). The fluid mass and momentum equations are complemented by a *tube law* which represents the elastic properties of the tube, namely $p_m = p - p_e$ at any point is taken to be single-valued function of A at that point. The relationship between p_m and A (tube law) is schematically shown in Figure 2.3. When $p_m > 0$, the tube has circular cross-section, and is under an extensional hoop stress. A tube is typically very stiff in this state (A changes very little as p_m increases). If p_m is reduced below zero, the tube initially remains circular, but is now under compression. At a critical pressure, the tube buckles, initially to an elliptical cross-section. The compression is now balanced by bending stresses in the most highly curved parts of the tube wall. In this state the tube becomes highly compliant: small reductions in p_m lead to large reductions in A . As p_m is reduced further, the opposite walls of the tube come into contact first at a point, and then along a line (points A and B in Figure 2.3 respectively). Thereafter, the tube forms two distinct lobes in which bending stresses are large, and further area reductions are difficult.

A stable, supercritical flow can be produced which experiences an abrupt, spontaneous deceleration to *subcritical flow* ($\bar{u} < c$). The abrupt deceleration is termed an *elastic jump* analogous to a shock wave in gas dynamics or a hydraulic jump in free surface flows. The propagation of an elastic jump through the region beneath a sphygmomanometry cuff has been proposed as a mechanism capable of producing Korotkoff sounds [18].

It was convenient in [4] to distinguish between what are generally called *self-excited oscillations* (relatively low-frequency oscillations for which membrane inertia is not a critical factor) and *flutter* (high-frequency oscillations for which membrane inertia is generally significant), although this distinction is sometimes blurred.

After introducing basic terminology and definitions frequently cited in the literature, it is useful at this point to review the basic equations in order to obtain the 1D model which has been a fruitful tool for theoreticians to study the flow through collapsible tubes.

2.2.1. Derivation of 1D model

Ignoring the effect of gravitational forces, the axial component of the momentum equation is given in reference [6,19,20] with the following equation:

$$\frac{\partial \bar{u}}{\partial t} + \bar{u} \frac{\partial \bar{u}}{\partial x} = -\frac{1}{\rho_f} \frac{\partial p}{\partial x} - R\bar{u} \quad (2.1)$$

Here $\bar{u} = \bar{u}(x,t)$ is the cross-sectional average axial fluid velocity, $p = p(x,t)$ is the fluid pressure, ρ_f is the fluid density. The authors define that $R > 0$ is a frictional resistance factor whose value depends on $A(x,t)$, namely the term $R\bar{u}$ represents viscous resistance.

The continuity equation in general case (three dimensional, compressible, unsteady) is

$$\frac{\partial(\rho_f \bar{u} dydz) dx}{\partial x} + \frac{\partial(\rho_f \bar{v} dx dz) dy}{\partial y} + \frac{\partial(\rho_f \bar{w} dx dy) dz}{\partial z} = - \frac{\partial(\rho_f dx dy dz)}{\partial t} \quad (2.2)$$

where \bar{u} , \bar{v} and \bar{w} represent average flow velocities in x , y and z directions, respectively. Note that cross-sectional area is not considered to be constant in equation (2.2), but it is also changing with the flow direction. This is the required case in collapsible tube flows since area is varying with respect to the pressure difference across the tube wall. As a result, for 1D (x direction) and incompressible (ρ_f is being a constant parameter; its derivative is zero) flow case, equation (2.2) reduces to

$$\frac{\partial(\bar{u} dydz) dx}{\partial x} = - \frac{\partial(dydz) dx}{\partial t} \quad (2.3)$$

where $dydz = A$ is the cross-sectional area in x direction, so that the continuity equation for 1D, incompressible collapsible tube flow analysis is obtained as

$$\frac{\partial A}{\partial t} + \frac{\partial(\bar{u} A)}{\partial x} = 0 \quad (2.4)$$

which has also been evaluated in [6,19,20] as the same form.

Equations (2.1 and 2.4) need to be augmented by a constitutive model for the wall. In the earliest 1D models ([19]), this was provided by a functional relationship between the local transmural pressure $p_m(x,t) = p(x,t) - p_e$ and $A(x,t)$. This relationship is referred to as the *tube law* and expressed in the form

$$p_m = P(A) \quad (2.5)$$

$$p - p_e = P(A)$$

where the function $P(A)$ represents the tube law. Note that the functional form equation (2.5) of the tube law allows axial variations of the vessel's elastic properties

(reflecting for example, changes in the unstretched tube cross-sectional area or variations in the vessel's wall thickness and modulus of elasticity).

Valuable insight into the behaviour of collapsible tubes can be gained from the steady version of equations (2.1, 2.4, 2.5). It is assumed that the elastic properties of the vessel are independent of axial position. Eliminating p from equations (2.1) and (2.5) then, the three steady equations can be combined to give the rate of change of A with x , i.e., $\frac{dA}{dx}$. Starting with the steady case of equation (2.1);

$$\bar{u} \frac{d\bar{u}}{dx} = -\frac{1}{\rho_f} \frac{dp}{dx} - R\bar{u} \quad (2.6)$$

Equation (2.5) can be written as

$$p = P(A) + p_e$$

$$\frac{dp}{dx} = \frac{dP(A)}{dx} + \frac{dp_e}{dx}$$

since p_e is constant, $\frac{dp_e}{dx} = 0$

$$\frac{dp}{dx} = \frac{dP(A)}{dx}$$

this term is then inserted into (2.6) and the obtained result is

$$\bar{u} \frac{d\bar{u}}{dx} = -\frac{1}{\rho_f} \frac{dP(A)}{dx} - R\bar{u} \quad (2.7)$$

Steady case for equation (2.4) is

$$\frac{d(\bar{u}A)}{dx} = 0, \text{ which can be expressed as:}$$

$$A \frac{d\bar{u}}{dx} + \bar{u} \frac{dA}{dx} = 0$$

$$\frac{d\bar{u}}{dx} = -\frac{\bar{u}}{A} \frac{dA}{dx}$$

inserting into (2.7)

$$\bar{u} \left(-\frac{\bar{u}}{A} \frac{dA}{dx} \right) = -\frac{1}{\rho_f} \frac{dP(A)}{dx} - R\bar{u}$$

$$\frac{dA}{dx} = \left(\frac{1}{\rho_f} \frac{dP(A)}{dx} + R\bar{u} \right) \frac{A}{\bar{u}^2}$$

$$\frac{dA}{dx} = \frac{A}{\rho_f \bar{u}^2} \frac{dP(A)}{dx} + \frac{RA}{\bar{u}}$$

$$1 = \frac{A}{\rho_f \bar{u}^2} \frac{dP(A)}{dA} + \frac{RA}{\bar{u}} \frac{dx}{dA} \quad (2.8)$$

It is emphasized by considerations of wave travel that the more distensible tube, the slower waves would propagate along it. This idea had been realized by Young [21] and the wave speed was defined by

$$c^2 = \frac{A}{\rho_f} \frac{dp_m}{dA} \quad (2.9)$$

where c is the speed of propagation of long, small-amplitude pressure waves along the tube when its cross-sectional area is A . Equation (2.9) expresses in modern notation what the author analysed and therefore it is also known as *Young's equation*. Inserting this definition into equation (2.8) yields,

$$1 = \frac{c^2}{\bar{u}^2} + \frac{RA}{\bar{u}} \frac{dx}{dA}$$

$$\frac{dx}{dA} = \left(1 - \frac{c^2}{\bar{u}^2}\right) \frac{\bar{u}}{RA}$$

$$\frac{dA}{dx} = \frac{\bar{u}^2}{\bar{u}^2 - c^2} \frac{RA}{\bar{u}}$$

$$\frac{dA}{dx} = \frac{-R\bar{u}A}{c^2 - \bar{u}^2} \tag{2.10}$$

Equations related to 1D model have been analysed, for example, in [6,20,22] which give a thorough discussion of all the three types of phenomena (choking, flow limitation and elastic jump) that occur in steady flow. It should be pointed out here that obtaining equation (2.10) enables to comment on the cases related to the collapsible tube flows by means of 1D model approximation. Therefore it would be useful to analyse the outcome of this theory, that is, equation (2.10) is examined for some possible cases outlined in the next section.

2.2.2. Analysis of 1D Model

Assume that at an upstream station, the tube is circular and $\bar{u} < c$. Since $R > 0$ then equation (2.10) shows that dA/dx is negative which means that the tube's collapse increases in the flow direction. Continuity requires that the flow rate ($Q = \bar{u}A$) is constant so as A decreases, \bar{u} increases; $d\bar{u}/dx > 0$, namely the flow is accelerated in the streamwise direction. If the tube is long enough, a point will in general be reached at which \bar{u} is predicted to be equal to c (*speed index*, $S = \bar{u}/c \rightarrow 1$) and so $dA/dx = -\infty$. Clearly this situation is physically unrealisable, by this stage referred

to as *choking*, which is similar to that found in compressible gas flow, the steady flow model will have broken down: steady flow at the proposed Q , from the assumed upstream conditions, is not possible according to this simple model. If Q and the upstream area are held fixed and the model is a correct one for steady flow, then unsteady behaviour must follow. A number of researchers (for example [23]) have gone further and suggested that the presence of a point at which $S = 1$ is the prime mechanism for the initiation of unsteady behaviour (self-excited oscillations). However, it was found in [8] that while flow-induced oscillations in a tube with large wall inertia occurred only when the flow was limited, the onset of flow speed could be as low as $S \approx 0.3$.

Alternatively if the flow is supercritical ($S > 1$) at some point along the tube, the variations in downstream conditions cannot propagate upstream; this underlies the wave-speed mechanism of flow limitation as determined in [24].

One-dimensional collapsible tube equations can be expected to have shock-like solutions similar to those found in gas flows through Laval nozzles. Experimentally, in [25] shock like structures (elastic jumps) are easily generated in collapsible tube flow. Within the framework of the 1D model, elastic jumps are predicted to occur in situations where $S > 1$ is generated somewhere in a collapsible tube. This is experimentally done by pinching the tube at a far upstream location; the reduction in A increases \bar{u} while associated reduction in wall stiffness simultaneously reduces c . The resulting supercritical flow is still governed by equation (2.10), which now predicts that $dA/dx > 0$. Hence A increases and the reduction in \bar{u} leads to a situation in which $dA/dx \rightarrow +\infty$ at some point. As in the case of choking, this locally violates the model's assumptions. However, a shock-like transition region in which \bar{u} is reduced from super- to subcritical instead develop upstream of the point where $dA/dx \rightarrow +\infty$ would occur.

It is clear that the one-dimensional model contains much that is relevant to the self-excited oscillations of real collapsible tubes in the laboratory. The previous theoretical studies including 1D model are reviewed in the following sections.

2.3. THEORETICAL STUDIES

There have been several models to investigate theoretically the collapsible tube flows and these can be divided into the following groups:

- i. lumped parameter models
- ii. one-dimensional models
- iii. two-dimensional models
- iv. three-dimensional models

Much of this modelling effort was recorded in [6,20,22]. In the next sections, these models are described and the related previous studies are presented for each of the models.

2.3.1. Lumped Parameter Models

In this model (the earliest theoretical models of flow in collapsible tubes) the geometry of the collapsible segment is represented by one or two time-dependent variables such as A at the narrowest point and the elastic properties are represented by a single-valued relationship between A and p_m at the narrowest point. Such models do predict self-excited oscillations in certain circumstances and serve to emphasize the important constraints exerted on such oscillations by the mechanical properties of the upstream and downstream rigid segments. The studies given in references [1,26-31] are among those who have predicted self-excited oscillations with such a model.

Lumped parameter model has been used in reference [32] on the basis of ignoring the effect of flow separation at the collapsed part of the tube. The authors have suggested that the effect of viscosity was essential (contrary to a number of previous studies, in which the flow separation in the collapsed part have been considered to be the primary cause of the instability, the authors have studied the problem from the viewpoint that instability is primarily due to loss characteristics determined from fluid viscosity). The theoretical amplitudes and frequencies of self-excited oscillations qualitatively agreed well with experimental results.

While lumped parameter models successfully offer many important flow features (such as important role played by the fluid in the rigid parts of the system) they fail to describe wave propagation, for example. Therefore a more sophisticated approach is warranted.

2.3.2. One-Dimensional (1D) Models

The basic equations to have a 1D model are presented in Section 2.2.1 which results with equation (2.10) so that the previous works used 1D model are given here. The aim of both sets of models is to predict the fluid speed at which oscillations begin and their frequencies. However, the weakness of the lumped-parameter models is that they cannot incorporate wave propagation and therefore cannot distinguish between subcritical and supercritical flow. The weakness of most one dimensional models is that although they predict the onset of unsteady behaviour at a particular point in the tube, they have not been used to model the developing oscillations.

A 1D model was presented in [19] to describe the flow through a collapsible tube. Results were presented for the special case of steady flow. Predicted Δp versus Q characteristics agree qualitatively with the available experimental data. Comparison of the theoretical results in [19] with the experimental results in [23] had given support that oscillations result from fluid velocity, \bar{u} approaching phase velocity of small amplitude pressure waves, c .

Some numerical integration results of the fully nonlinear one-dimensional equations have been shown in [33]. Some of the computed time series, for example of p_2 , look quite similar to the measurements of [34].

The 1D flow model in [35] assumes two additional features both of which should be important in the region downstream of the narrowest point. One is longitudinal tension in the tube wall. The other new feature is the recognition that flow through a constriction will separate, a process leading to enhanced energy loss and therefore substantially incomplete pressure recovery in the region downstream of the

narrowest point. The energy loss downstream of the narrowest point had already been identified in [36] as important in lumped parameter models.

The direct viscous term $R\bar{u}$ in equation (2.1) has been neglected in the 1D model [17]. The principal results can be summarized as follows:

- i. when there is no energy loss in the collapsible tube downstream of the narrowest point, then there exists a critical value of the Q , dependent on the longitudinal tension above which the steady problem has no solution. In other words, the presence of tension alone does not abolish choking.
- ii. whenever there is any downstream energy loss, then a steady solution exists for all positive values of Q and tension. Since some energy loss is inevitable, it follows that the breakdown of steady flow is not caused by choking, in other words, the non-existence of a steady flow at the chosen parameter values, but must arise through instability of the steady solution.

It is determined in [4] that neglecting frictional effects, choking can be predicted, but including dissipation, either through a distributed frictional term in [37] or through the term given in [35], leads to a rich variety of self-excited oscillations. These oscillations arise in distinct frequency bands. Then it has been concluded in [4] that while 1D models provide significant insights, they fail to provide reliable quantitative matches with experiment. The authors have stated that the 1D model can exhibit significant qualitative deficiencies (particularly in describing energy losses associated with unsteady flow separation). Furthermore, a 1D framework cannot be guaranteed to capture all possible modes of instability known to be present in systems involving flows over compliant surfaces. Thus, in the 1990s, attention turned to the development of rational two-dimensional models.

2.3.3. Two-Dimensional (2D) and Three Dimensional (3D) Models

A closely related physical model system was introduced in [38]. It consists of a 2D channel, one wall of which has a segment replaced by a membrane under longitudinal tension. Viscous flow is driven by an imposed Δp . The deformation of the membrane is determined by p_e and Q . Despite the practical difficulties of

producing 2D flows experimentally, this system has attracted considerable theoretical attention since it avoids the complications of fully three-dimensional flows found in the Starling resistor, while still exhibiting phenomena such as flow limitation and self-excited oscillations.

The steady and unsteady numerical simulations of two-dimensional flow in a collapsible channel have been carried out in [11] to investigate whether there is a causal link between the self-excited oscillations and the flow limitation which typically occurs when $p_{m,1}$ is held constant while Q and pressure gradient along the collapsible channel can vary independently. This was the first time that collapse and flutter have been examined together, self-consistently, in the same model problem. Multiple steady solutions were found for a range of $p_{m,1}$ and Q . The stability of these steady solutions was tested in order to check the correlation between flow limitation and self-excited oscillations (the latter being a consequence of unstable steady solutions). Both stable and unstable solutions were found when flow was limited. They concluded that there is not a definite link between flow limitation and the instability of the steady solutions (and hence self-excited oscillations). However, some degree of collapse of the membrane is essential to destabilise the steady solutions, and in order to provide the energy loss needed for the generation of self-excited oscillations.

The 2D physical model is a rational and realisable system which can be interpreted as an approximation to the flow in a strongly collapsed three-dimensional tube. However, it is clear that the model ignores many potentially important 3D effects such as:

- i. the strong three-dimensionality of the flow field during phases when the tube collapse moderate,
- ii. the significant differences between flow separation in 2D and 3D flows,
- iii. the drastic changes in wall stiffness as the tube changes from an axisymmetric to a non-axisymmetrically buckled state.

The first step towards the development of a rational computational model of flow in 3D collapsible tubes was undertaken in [39]. It has been shown in [40] that how

nonaxisymmetric buckling of the tube (Figure 2.4) contributes to nonlinear pressure-flow relations that can exhibit flow limitation through purely viscous mechanisms. For short tubes under compression, the buckling instability may be subcritical, leading to hysteresis in the pressure-flow relation, so that an initially open tube snaps through to a collapsed state that under certain conditions may have the tube's opposite walls in contact. Stokes-flow simulations in [40] show excellent agreement with experiment (Figure 2.4). It is known from the experiments of [41] that the non-axisymmetric collapse of thin walled elastic tubes only induces small extensional deformations of the tube wall. Therefore, a linear stress-strain relationship with two elastic constants (modulus of elasticity and Poisson's ratio) was used as the constitutive equation.

2.4. EXPERIMENTAL STUDIES

2.4.1. Studies on Pressure / Flow Characteristics and Flow Limitation

The earliest experiments on flows in collapsible tubes can be remarked with the studies given in [1,42]. A thin-walled Penrose tube attached to rigid tubes at both ends in [1]. The wall-thickness (h), the circular inside diameter (D_0) and the length of the tube (L) were 0.33 mm, 12.7 mm and 89 mm, respectively. The fluid was water in this study. Particular interest was the pressure-flow behaviour relating to *flow limitation*. When $p_{m,1}$ was set constant and $p_{m,2}$ reduced, Q initially increased as the tube remained inflated. However at negative $p_{m,2}$ the tube was collapsed and Q was independent of Δp . Conrad's [1] influential study of pressure-flow relationships was built on a foundation of considerable physiological interest in collapsing vessels. In this paper systematic data on Δp versus Q with variation of either p_e or R_2 was presented. Furthermore, the criterion for the existence of self-excited oscillations was identified. He indicated that the relation between Δp and Q was sigmoid with a middle section of negative slope representing negative incremental resistance. Oscillations were predicted to occur only when operating point lay on the negative slope in his experiments.

The relationship between flow characteristics and tube deformation was studied in [43] when water flowed in a collapsible tube subjected to p_e . Experiments were carried out for silicone rubber tubes of $h = 0.4$ mm, $h = 0.8$ mm and $h = 1.6$ mm. The values of D_0 were 8mm and 20mm while $L = 10D_0$ and $L = 20D_0$. It was observed that the collapsible tube was deformed according to conditions of flows and finally followed by self-excited oscillations. The frequency of self-excited oscillations (f) has taken nearly uniform value independently of $p_{m,2}$ and these indicated higher values under the condition of thicker tube or shorter tube length. The phenomena of self-excited oscillations were verified to be classified into some regions; the small amplitude region characterized by the low-frequency ($f = 10.25$ Hz) self-excited oscillation, the intermediate region characterized by the large change in the frequency ($f = 16$ Hz), and the large amplitude region characterized by the high-frequency ($f = 20$ Hz) self-excited oscillation.

The results of pressure-flow (water) behaviour have been obtained in [44] for a Penrose tube ($L = 120$ mm, $D_0 = 12$ mm, $h = 0.2$ mm) under steady and unsteady upstream conditions. In all cases the mean results indicated the presence of flow limitation. However the effect of increasing either the frequency or amplitude of p_1 fluctuations tended to reduce the magnitude of the maximum Q .

An experimental investigation was made in [45] for the pressure-flow (water) behaviour of a collapsible tube which had the same properties given in [44] subjected to p_2 fluctuations. The Reynolds number ($Re = \bar{u}D_0 / \nu_f$ where ν_f is the kinematic viscosity of the fluid) based on mean inlet conditions was 600. The forcing pressure frequency was 3.33 Hz. These p_2 waves were observed to be transmitted upstream beyond the point of collapse. Flow limitation was exhibited in the mean pressure-flow results and the mean flow rate was not significantly affected by the amplitude or frequency of pressure fluctuations. However, the flow amplitude and tube oscillations were reduced at the higher frequency.

$\Delta p - Q$ characteristics in *thick-walled* tubes was examined in [46] under the conditions of flow rate limitation when $p_{m,1}$ was held constant. The fluid was water and the tubing was silicone rubber of $D_0 = 13$ mm and $h = 2.4$ mm; the unsupported length was $17D_0$. In this uniform tube, it was found that at the onset of flow-rate limitation, Q decreased typically much greater, relative to the flow-limited Q values themselves, than has been reported by others using thinner tubes and lower Q values. Flow-rate limitation was seldom accompanied by large-amplitude self-excited oscillation; the latter was mostly exhibited only during the transition to or from maximum flow to the flow-limited state. The authors concluded that flow limitation itself was not associated with self-excited oscillation.

The idea of this association goes back at least to [23] in which it was found that the outbreak of spontaneous oscillations to coincide with the fluid speed, \bar{u} reaching the pressure wave speed, c . This is the choking condition of gas dynamic analogy which has been used in [47] to explain flow limitation in the collapsible urethra.

Flow limitation without oscillation was also observed in [8]. The authors concluded that flow limitation is associated with flutter, rather than lower-frequency oscillations, and that flow limitation is a necessary but not sufficient precondition for the generation of flutter in tubes.

Oscillations observed at veins during heart-lung bypass operations are regarded to be a kind of self-excited oscillations of collapsible tubes. The cause of oscillations has been explained independently as choking [23], negative resistance effects [26, 27] or separation hysteresis [48].

Korotkoff sound generation is closely related to self-excited oscillation of the tube wall. The mechanism for self-excited oscillations were attributed to flow separation [26], negative pressure-flow characteristics [22,49,50] and supercritical flow [16, 51]. An extensive review on the mechanism of Korotkoff sound generation was given in [36]. The propagation of a single pressure wave in a collapsible tube have been taken into account in [52] and the drawn conclusion was that Korotkoff sounds,

particularly at diastole, are associated with the steepening of the wavefront during propagation.

The characteristics of a self-excited oscillation of flow (water) through a collapsible tube have been experimentally investigated in [53]. In the experiments Penrose tube ($D_0 = 5.7\text{mm}$, $h = 0.15\text{ mm}$, $L = 160\text{ mm}$) and natural rubber tube ($D_0 = 6\text{ mm}$, $h = 1.2\text{ mm}$, $L = 160\text{ mm}$) were used. The tube was immersed in water inside the airtight box. The fluid was water and as a result, the following facts have been clarified:

- i. The oscillation takes place no matter when the static operating point may be in the negative or the positive slope region of the $\Delta p - Q$ curve.
- ii. The frequency of oscillation increases approximately in proportion to p_e and Δp . For example by considering Penrose tube, the frequency range was $5\text{ Hz} < f < 17\text{ Hz}$ for $0.98\text{kPa} < p_e < 5.88\text{kPa}$ and $1\text{ kPa} < \Delta p < 6\text{ kPa}$. Similarly, in the case of natural rubber, $10\text{ Hz} < f < 35\text{ Hz}$ for $29.24\text{ kPa} < p_e < 37.21\text{ kPa}$ or $0\text{ kPa} < \Delta p < 25\text{ kPa}$.

The characteristics of self-excited oscillation of airflow through collapsible tube in an airtight box were investigated in [54]. A Penrose tube with $D_0 = 5.7\text{mm}$, $h = 0.15\text{ mm}$ and $L = 160\text{ mm}$ was tested. A theoretical analysis was made on the initiation of the oscillation. As a result it was found that a self-excited oscillation of the flow through the tube took place in a wide range of the flow condition. Especially it was found that in a particular condition a strong resonant oscillation accompanied with a sharp sound occurred, and that the frequency of the resonant one (1250 Hz) was 4 or 5 times as high as that of the ordinary one (270 Hz). When the ordinary oscillation changed to the resonant one, Δp increased by 1.5 to 2 times (from 6 kPa to 10 kPa) and Q slightly decreased (from $0.0008\text{ m}^3/\text{s}$ to $0.0007\text{ m}^3/\text{s}$).

The equilibrium behaviour of flow in collapsible tubes was studied in [55]. Thick walled ($h = 2.4\text{ mm}$, $D_0 = 13.3\text{ mm}$) silicone rubber tube connected to rigid pipes upstream and downstream was externally pressurized to cause collapse while aqueous fluid flowed through propelled by a constant upstream reservoir head. Three

types of equilibrium were found: stable equilibrium (steady flow) at high R_2 , self-excited oscillations at low R_2 , and unattainable (by varying p_e) or exponentially unstable equilibrium at intermediate R_2 . The self-excited oscillations were highly non-linear and appeared in four, apparently discrete, frequency bands: 2.7 Hz, 3.8–5.0 Hz, 12–16 Hz and 60–63 Hz, suggesting that the possible oscillation modes may be harmonically related. Comparison of c calculated from local pressure-area relation for the tube with \bar{u} indicated that supercritical velocities were attained in the course of the self-excited oscillations.

The results of experiments with flow of water on a simple system incorporating a thin-walled silicon rubber ($D_0 = 12.7\text{mm}$, $h = 0.13\text{mm}$) subjected to a range of pressure differences between its ends and across its walls were reported in [56]. The centre of interest was to determine the conditions under which the tube will experience self-excited oscillation of its walls and nature of these oscillations. It was significant that no oscillations were detected for Re below about 1500 which was considerably higher than that found in the veins of a resting patient (approximately $Re = 450$). As expected Q varied in general, except, at the onset of oscillation ($10\text{ Hz} < f < 35\text{ Hz}$) when it suffered a fairly abrupt decrease from its steady full flow value.

The flutter in collapsible tubes was studied in [8] as a possible mechanism for the generation of respiratory wheezes. The pressure-flow relationships and the wall oscillations of thick-walled (h/R_0 values are 1:1.7 to 1:3, where R_0 is the inside radius of the tube at zero p_{ms} , in other words, it is the inside radius of the unstretched circular tube) self-supporting latex tubes mounted between rigid pipes were measured. A high-impedance vacuum pump was connected to the downstream end. Upstream and downstream valves were used to control corresponding R values. They found loud sounds and tube wall oscillations that occurred only when the tubes were buckled and flow limiting. The overall range of oscillatory frequencies was 260–750 Hz for airflow. The oscillatory frequencies were higher at higher fluid velocities and with narrower distance between opposing flattened walls, resulting from increasing downstream suction pressure and $p_{m,2}$ becoming more negative. They concluded that viscid flutter in soft tubes is the more probable mechanism for

the generation of oscillations in the soft tube model and is a possible mechanism for the generation of respiratory wheezes.

Indirect evidence links self-excited oscillation of flow through collapsed tubes with choking. This was tested in [10] by measuring both $c - \bar{u}$ and c as functions of A during self-excited oscillation. The wave speed c was derived from the local slope of the pressure/area relationship. The results confirmed what had been suggested by theory [17] that there is no threshold in terms of Q or \bar{u} at which choking begins, because of the dispersive properties of the system.

The causes of self-excited oscillations of flow in collapsible tubes were experimentally investigated in [57]. The fluid was water in the system. In the experiments, the deformations of a silicone rubber tube ($L = 98$ mm, $D_0 = 7$ mm and $h = 1$ mm) were measured with a laser displacement meter. Thereby \bar{u} and c at the throat, based on the static tube law, could be compared. The stability of an experimental system with a long (1.96 m) downstream pipe was compared with a short (0.48 m) downstream pipe. It was found that $S > 1$ was attained with a long downstream pipe. Negative resistance for the silicone tube in the set-up was also verified. The oscillations for the short downstream pipe seemed to occur without either supercritical flow or negative resistance.

Similarly, causes of self-excited oscillations of collapsible tube flow (water) have been investigated in [58] for the same test tube in [57]. The results have clarified that \bar{u} approaches c , which is estimated from the tube law and that a supercritical flow and subcritical flow occur alternately during oscillations. Although causes such as unsteady flow separation were not examined in that study, a self-excited oscillation with a frequency of 4–10 Hz (mean Q was 4.9×10^{-5} m³/s and $p_e = 19.6$ kPa) caused by supercritical flow close to choking has been verified experimentally and theoretically.

2.4.2. Studies on Flow Field Measurement

Compliant tubes attain a complex three-dimensional geometry when p_e exceeds p and the tube is partially collapsed. A self-excited oscillation often takes place in flow through a collapsible tube. However, the mechanism of oscillation has not yet been revealed. The knowledge of the local flow field in the collapsible tube during oscillation is indispensable for the determination of mechanism of the oscillation. The local flow field has not yet been measured extensively, however, due to the difficulty caused by a very large motion of the tube wall. Experimental investigations of flow through collapsible tubes have been limited, because invasive measurements alter the flow condition. In particular, it is impossible to measure the tube geometry invasively since any contact with a measuring device alters the dynamic equilibrium of the tube wall. Thus there is no experimental evidence on the exact three-dimensional geometry of the tube under steady or unsteady flow conditions.

Experimental measurements of the three-dimensional geometry of collapsible tubes that were subjected to steady flow (water) have been presented in [41]. Results were shown for two tubes of the same material (latex) and internal diameter ($D_0 = 27$ mm) but with different wall thicknesses ($h = 0.8$ mm and $h = 1.6$ mm). Measurements of static tube laws yielded favourable results which are in accord with previous experimental and theoretical works. Steady state flows were also examined and the geometry measurements were followed by pressure and flow measurements. An attempt to compare the measured data with the one-dimensional theoretical model yielded results that are significantly different. The authors had expressed that improvements in both the experimental procedure and theoretical modelling were necessary. They have concluded that theoretical models should be directed towards approximations that better simulate the flow pattern within the tube cross-section. In addition, tube law models should incorporate a more accurate representation of the mechanical characteristics of the wall at collapse conditions.

Velocity fields in collapsible tubes have not been extensively investigated. A non-invasive technique is demanded, and of these only LDA has been used. The first

reported data are those of [18], but the results were confined to measurements of centerline velocity at seven axial locations.

The flow field within a self-oscillating transparent flexible tube was experimentally studied in [59] by employing flow visualization, velocity and pressure measurements. The fluid was water and the tube's material was silicone elastomer ($L = 80$ mm, $D_0 = 8$ mm and $h = 0.2$ mm). The main observations made were as follows:

- i. The tube oscillations occurred under low and positive p_{im} (of the order of 50 mm water), independently of p_e , Q and settings of the constrictions. Under these pressures, the tube being compliant, was set to an oscillatory motion initiated by a flow asymmetry.
- ii. There was a phase difference between the upstream and downstream of the tube pressure signals, the latter being in advance. That is, during the shrinking of the tube, p_2 started first being reduced, whereas later on the p_1 started increasing, and specifically a little before the tube neck approached the end of the tube.
- iii. The frequency of oscillations increased with increasing difference between p_e and the time-mean p_2 (for example, $f = 1.5$ Hz at $p_e - p_2 = -1.18$ kPa, but f increased to 5 Hz when $p_e - p_2$ was -6.1 kPa) without however being able to define a certain relationship between these two parameters.

2.5. CONCLUSION

Theoretical and experimental investigations on flow in collapsible tubes have been continuing since some phenomena such as self-excited oscillations, flow limitation and the relationship between these has not been determined yet. It is deduced from the literature survey that the mechanisms which drive these oscillations have not been fully understood yet.

It is clear that disregarding physiological relevance the studies on this special flow field will be necessary to reveal the above-mentioned phenomena from the point of

view of fluid dynamics due to the incompleteness of the general theory. The existence of only a limited number of previous experimental works using air as fluid in collapsible pipes is another gap in the related literature. Therefore an experimental set-up was designed and constructed to investigate airflow through collapsible tubes without paying attention to the physiology owing to the fact that the main objective is not to obtain quantitative results for direct physiological applications. Subsequently the experimental research has been conducted to analyse the airflow through Penrose tube and silicone rubber tubes with different L and h . Moreover different type collapsible tube testing is seen to be necessary in order to have more general results.

CHAPTER 3

EXPERIMENTAL SET-UP, MEASURING DEVICES and DATA ACQUISITION SYSTEM

3.1. INTRODUCTION

In this chapter the experimental set-up with its components, utilized measuring devices with their calibration, measuring principles are presented. The data acquisition system used with the experimental set-up is also described.

3.2. EXPERIMENTAL SET-UP

An experimental set-up was designed and constructed for the investigation based on the literature survey. It was mainly composed of an airtight chamber (Starling resistor) including a collapsible tube with its rigid attachments and connected rigid piping system before and after the chamber. The measurements were obtained by means of data acquisition system, in principal. However to reveal the pressure values at which the tube wall collapses or oscillates an initial experimentation was achieved without data acquisition system, namely by considering utilization of manometers (Figure 3.1) for the measurements. Therefore a schematic representation of the experimental set up can be given as in combination with manometers (Figure 3.1) or electronic devices, i.e., data acquisition system (Figure 3.2) for the measurements. The experimental set-up which is shown in Figure 3.2 has been introduced in the studies given in [60,61]. Airflow was supplied by means of a screw type compressor LUPAMAT which has model of LKV 30/8-PLC (Appendix-1) in combination with a pressurized air tank. Compressor controls airflow rate, Q relative to the consumption in the system by means of a proportional valve which consequently provided a constant network pressure during discharge to the atmosphere. The pressure regulator

at the exit of the compressor provided high sensitivity in Q control in its covered range.

The upstream and downstream rigid pipes with inside diameter of 25.4 mm, outside diameter of 40 mm and length of 2 m were used in the experimental set-up. This means that the rigid pipe length is approximately 80 times of its inside diameter. It will be seen in the next chapter that all flow cases studied here are turbulent since in the laminar flow experiments oscillations have not developed. However one of the main motivations under the present investigation has been to analyse the oscillating flows in collapsible tubes. According to reference [62] typical entry lengths for the establishment of fully developed turbulent pipe flow may be theoretically taken as 60 times of inside pipe diameter. The steady flow entering to the test section is therefore achieved as fully developed by considering the abovementioned case about the experimental set-up. This has been also verified experimentally by Figure 3.3 in which three different Re as 16200, 26350 and 36150 are present. These values also well explain that the flow is turbulent. It is seen in Figure 3.3 that the velocity distribution across the pipe cross-section is symmetrical (although only the Pitot tube traverse between pipe center and its wall is shown, but it was the same for the traverse across the full pipe diameter) thus flow is said to be developed at the measurement station and it enters to the test section. Meanwhile the average velocities for each case were calculated by means of integration of velocity distribution across the pipe cross-section and the ratios of mean velocity to the maximum velocity at the pipe center ($r=0$), \bar{u}/u_{\max} are determined to be 0.83, 0.827 and 0.821 as shown in Figure 3.3. According to $1/7^{\text{th}}$ power law, $\bar{u}/u_{\max} = 0.817$ for fully developed turbulent pipe flows [62]. It is seen that the measured \bar{u}/u_{\max} values are so close to the theoretical requirement of $1/7^{\text{th}}$ power law; the flow entering to the test section can once again be said that fully developed due to the above confirmations.

The hot wire anemometer in combination with its 55P14 type miniature wire probe by Dantec Electronic was located at the exit of the Starling resistor on the rigid pipe at station according to L which caused a distance from the exit of the collapsible tube

to the probe location to be $5.12 D_0$, $6.30 D_0$ or $7.56 D_0$, respectively. The extended information for the test rig is presented in the following sections.

3.2.1. Airtight chamber: Starling resistor

The airtight chamber including the test tubes is prismatic in geometry and it has internal dimensions of 39 cm x 15 cm x 14 cm. It was checked that the size of it is large enough for p_e not to be affected by the developed self-excited oscillations. The chamber was composed of a steel plate welded to angle iron. The front sides and top side of the chamber were made of glass plates that were stuck on the angle iron to visualize the test tube during flow. The topside of the chamber was a removable cover, which was fastened to by nuts and bolts with a rubber gasket forming a tight seal (see Figure 3.1). The pressure in the chamber p_e was controlled by providing air through a valve located at the bottom side of the steel plate in combination with a manual air pump.

The test tubes were placed in the centre of the Starling resistor in combination with upstream and downstream rigid attachments (Figure 3.4) made of brass with inside diameter of 25.4 mm and 3 different ℓ values as 17.5 mm, 47 mm and 79 mm for enabling attachment of the test tubes of different L/D_0 . Two pairs of O-rings were used to form a tight sealing of the rigid attachments to the test tube and connection of the airtight chamber to upstream and downstream rigid pipes.

3.2.2. Test tubes

The latex and silicone rubber test tubes of $D_0 = 25.4$ mm supplied by the manufacturer firms MRK Healthcare (India) and Silicone Engineering (England) respectively were used in the study. In order to determine the influence of tube geometrical characteristics, silicone rubber test tubes of three different thickness $h = 1$ mm, $h = 2$ mm and $h = 3$ mm and Penrose test tube of a single thickness $h = 0.55$ mm at lengths specified by the subscripts “L, M, and S” meaning long, medium and short samples respectively were used. Test tube geometrical dimensions were measured by a micrometer having a sensitivity of ± 0.01 mm.

The specifications of the test tubes are given in Table 3.1 together with a tube coding system proposed. The modulus of elasticity (E) of the tubes was determined according to BS 903 [63] in the axial force-deflection test. The samples to be tested were cut from each Penrose and silicone rubber tubes and the results have been obtained as shown in Figure 3.5 for P, S₁, S₂ and S₃, respectively. Since the relationship between stress and strain is non-linear for elastic materials, E was taken corresponding to approximately 10% strain in conformity with the approach utilized in [45]. Poisson's ratio (ν) of the test tube material was assumed to be 0.48 which is an approximate value for rubber materials. The *circumferential bending stiffness* (K_p) of the test tubes was calculated [19,22,45,64] by the following relationship

$$K_p = \frac{1}{12} E \frac{(h/R_0)^3}{(1-\nu^2)} \quad (3.1)$$

The latex tube so called Penrose tube P and silicone rubber S₁ are in *thin-walled* which by definition has a radius-to-thickness ratio greater than ten ($R_0/h > 10$) while S₂ and S₃ are in *thick-walled* class (since $R_0/h < 10$). The test tube placement in the Starling resistor was such that no longitudinal tension was applied by fixing the distance between the rigid attachments to the length of the tube.

3.3. MEASUREMENTS and MEASURING DEVICES

The steady flow measurements were achieved by means of inclined type alcohol manometers. However for unsteady flow case pressure and velocity measurements were done using gage type pressure transducers and constant temperature hot wire anemometer, respectively. The electronic signals from these devices were acquired through the hardware board of the data acquisition system. Some accessories such as a digital multimeter, an oscilloscope, signal generator, DC power supply were used for the calibration of pressure transducers, hot wire anemometer, and the hardware board of the data acquisition system used with the experimental set-up.

3.3.1. Flow Rate Measurement

The steady flow rate was measured at $6D_0$ upstream of the Starling resistor in collaboration with a pitot tube and an inclined alcohol manometer (Figure 3.1) with a sensitivity of 10 Pa which leads to the sensitivity in Q measurement to be ± 0.0015 m³/s. All the manometer's alcohol level readings were converted into the standard atmospheric temperature and pressure values. Since Pitot tube measures the total of the static and dynamic pressure values, the alcohol level in the manometer's leg is a definite indication of the dynamic pressure of the flow. Because it corresponds to the difference of total pressure from the Pitot tube and static pressure that is measured from the static pressure tapping located on the rigid pipe wall. Therefore the mean velocity of the steady flow was calculated from dynamic pressure measurements. Then steady flow rate was determined by multiplying mean steady flow velocity with cross-sectional area of the rigid pipe.

3.3.2. Pressure Measurement

The external pressure p_e was measured with a 2-wire pressure transmitter of Bourdon Haenni (Model: E913) in combination with a digital process controller produced by Ascon (Model: M1-3000). The digital process controller can directly display the output of the pressure transmitter in various units such as mA, mV, V, bar or psi, so that the unit of psi was selected as the output of M1-3000. The calibration of E913 and M1-3000 combination was achieved by using an alcohol manometer simultaneously and the result is shown in Figure 3.6. Since the manometer's reading and digital process controller's output are in agreement the accuracy of M1-3000 has thus been verified by referring this figure. The measurement range of the transmitter was between 0 and 25 kPa and the operation of the manual air pump was such that increase in p_e as low as 20 Pa for each increment was possible. The detailed technical specifications of E913 and M1-3000 are given in Appendix 2 and Appendix 3, respectively.

The steady Δp measurement was done with another inclined manometer (Figure 3.1). However the time dependent values of p_1 and p_2 were measured as shown in Figure

3.2 with the pressure transducers by Omega (Model: PX951-010G5V). The location of pressure tapping on the upstream and downstream rigid attachments was at a distance of $0.7D_0$ (Figure 3.4) in reference to the literature [44]. This distance is actually close enough to the tube end to measure oscillating flow pressure more sensitively. Technical specifications of the pressure transducers are given in Appendix 4. The output of the pressure transducer was voltage which was converted into the unit of Pascal with respect to calibration of the instrument as shown in Figure 3.7. The calibration was carried out as follows: The upstream pressure p_1 was selected as reference pressure which was measured at various flow rate values by means of an alcohol manometer for steady flow case. Then corresponding p_1 values were measured with pressure transducer for the same flow rate values. The voltage outputs of the transducer were recorded and these were directly assigned to the previously measured p_1 values obtained from the manometer. This process had resulted in the following relation:

$$p = 13.79(V_p) \quad (3.2)$$

where V_p is the output voltage of the pressure transducer, p is the pressure in kPa.

3.3.3. Velocity Measurement with Hot-wire Anemometer

The velocity measurement for the present research was conducted by means of a Constant Temperature Anemometer (CTA). The hot-wire probe should be placed at the possible nearest location to the collapsed and oscillating tube wall to measure the velocity more sensitively. The measurement station of the hot wire probe was at the exit of the Starling resistor (Figure 3.2) with a distance of $2.45D_0$. Therefore it corresponds to the distances of $5.12D_0$, $6.30D_0$ and $7.56D_0$ from the exit end of the collapsible tubes for long, medium and short tubes (for example, $S_{2,L}$, $S_{1,M}$, and P_S), respectively. The velocity measurement system was based on a CTA main unit in the centre between the sensing probe and the hardware of software signal processing equipment. The measurement started with the probe which was connected via a bridge to the CTA main unit. Hardware signal processing of the output from the CTA

main unit was made by means of a plug-in module. This was followed with a computer for further data processing. The components in this measurement were a probe, a bridge, a CTA main unit, a hardware installed on the computer and software for signal processing.

The axial velocity measurements were conducted with the CTA Hot-wire Anemometer manufactured by DANTEC. The components of the measurement system used for the axial velocity determination were 55P14 type miniature wire probe, the main unit (56C01 CTA), the bridge (56C17 CTA), the linearizer (56N21), the plug-in data acquisition board (DAS-1602) installed on a computer and the standard software package (DAS-1600) supplied by the manufacturer firm of the board (Keithley). Technical specifications of the CTA and the used probe are given in Appendix 5.

The calibration of CTA was simply based on the comparison of the voltage outputs of the anemometer with the effective air velocity measurements obtained from a pitot-static tube and an alcohol manometer. Therefore a pitot-static tube which was mounted on the rigid pipe was placed to a definite radial position. Air velocities calculated from dynamic pressure measurements conducted by Pitot tube for different flow rates were recorded. Then the voltage outputs of the anemometer were recorded for the corresponding probe position and flow conditions, so that the calibration result can be given as in Figure 3.8. Thus the following equation was obtained from the CTA calibration:

$$U_e = 30.24V_A^3 - 148.67V_A^2 + 250.22V_A - 143 \quad (3.3)$$

where U_e is the effective cooling velocity and V_A is the output voltage of the anemometer.

3.3.4.1. Determination of the hot-wire probe position in the pipe cross-section

It is known that in steady, fully developed pipe flows there is a radial position which corresponds to the mean velocity of the flow. However this is not the case for the

unsteady flows, so that it was examined if the similar rule could be valid or not for an unsteady flow case.

In order to obtain such a general result, oscillating flows were generated with applying p_e to the tube wall while there was airflow inside it. The applicability of the hot-wire anemometer was controlled by using the cross-sectional velocity profile $u_{os} = u_{os}(r)$ (where u_{os} is the oscillating flow velocity and r is the radial position from the pipe centre) at the measurement station located at discharge pipe of the Starling resistor. The hot wire probe was moved in radial direction by means of a traverse mechanism with a dimensional sensitivity of ± 0.25 mm. The probe was traversed at equal intervals covering the radial positions of $r = \pm 12$ mm, ± 9 mm, ± 6 mm, ± 3 mm and $r = 0$ mm. The time average values of u_{os} based on instantaneous velocity data at each radial position were defined as:

$$u_{os}(r) = \frac{1}{N} \sum_{i=1}^N u_{os,i} \quad (3.4)$$

where N is the number of data. The cross sectional mean oscillating velocity, \bar{u}_{os} was later evaluated by numerical integration of u_{os} over the pipe cross section using the following equality:

$$\bar{u}_{os} = \frac{\int_0^{r'} 2\pi r u_{os}(r) dr}{\pi r'^2} \quad (3.5)$$

where r' was the limiting position ($r' = 12.0$ mm) of the hot wire probe close to the wall.

Cross sectional velocity distribution downstream of the test tubes in case of steady flow for a range of Re were appropriate with the well known velocity profiles as can be seen from the plots of Figure 3.9 and Figure 3.10 respectively. The cross sectional distribution of the mean oscillating velocity data at the measurement station for the covered cases with the tubes in a range of $7,000 \leq Re \leq 94,000$ indicated almost

symmetrical velocity profiles with respect to the pipe centreline as can be seen from the sample plot of Figure 3.11 independent the distance from the collapse position of the test tube. The velocity profiles for the covered test case were approximated by the polynomial expressions. The numerical integration of the obtained expressions according to equation (3.5) resulted in the calculation of the mean velocity \bar{u}_{os} in the field of self-excited oscillations. The position of the hot wire probe corresponding to \bar{u}_{os} was determined to be between $0.665R_0$ and $0.669R_0$ which can be approximated as $0.67R_0$ for the covered cases. This finding has been presented in [65]. In the studied ranges of Re the velocity data taken at this position can also be used to determine the oscillating flow rate as a function of time providing a tool for oscillating flow rate measurement.

3.4. DATA ACQUISITION SYSTEM

The data acquisition system utilized in the experimental set-up was composed of a computer, a plug-in data acquisition board (hardware), a standard software package compatible with the hardware, some application programs and a screw terminal accessory board. The application programs were prepared by using the software and Microsoft Visual Basic programming language. The screw terminal accessory board (Model: STA-16) manufactured by Keithley was used to connect the input and output (I/O) signals to main I/O connector of the hardware board through a shielded cable (C-1800).

The data acquisition system was processed as in the following order:

- i. The accumulation and conversion of the analog data was organized with a data accumulation control program which was prepared by using the software and Microsoft Visual Basic. The analog output signals of the pressure transducers and hot-wire anemometer were simultaneously acquired by means of the control program.
- ii. The analog to digital conversion of the data was then carried out with the hardware board. In this step analog data were converted into 12-bit digital data and stored in the computer.

iii. The stored data was processed accompanied by Microsoft Excel and a commercially available program called as Sigview.

3.4.1. Hardware of Data Acquisition System

At the centre of the data acquisition system, DAS-1602 high performance analog and digital I/O board by the manufacturer firm of Keithley was used as hardware. The DAS-1602 is a low-gain plug-in data acquisition board with a maximum analog input sampling rate of 100 kHz. The features of the hardware are given in Appendix 6. The installation, testing and calibration of the board were carried out after the installation of the software to the computer had been completed successfully. The information of testing and calibration of the hardware can be found in Appendix 7.

3.4.2. Software of Data Acquisition System

The DAS-1600 series standard software package was installed to the computer before installation of the hardware. The software to operate the hardware includes function libraries for writing application programs by using Microsoft Visual Basic, Microsoft Quick Basic or Microsoft Professional Basic. The package includes also support files, some example programs and utility programs such as the configuration utility, control utility and calibration utility.

The switch settings of the hardware were previously initialised to the software by means of a configuration file for supplying the compatibility between the hardware and the software. The configuration file, which contains the switch settings of the hardware, was created before installation of it by using the configuration utility program (CFG1600.exe) of the software. Then the DAS-1602 board was installed to the computer. After installation of the board; operation, testing and calibration of the board were conducted via the control panel program (CTL1600.exe) and the calibration utility program (CAL1600.exe) of the software.

3.5. CONTROL OF TIME DEPENDENT DATA ACQUISITION

In the present investigation the time dependent data accumulation was coordinated along-with a data acquisition control program at the centre of data accumulation system. The p_1 and p_2 data from the pressure transducers and the axial velocity data from hot-wire anemometer were accumulated. A data accumulation control program was prepared by using Microsoft Visual Basic programming language and the DAS-1600 standard software package. The time-dependent data accumulation control program is presented in Appendix 8. Three analog signals from the transducers and CTA were accumulated through this program over three analog input channels of the board with respect to the external pacer clock signal connected on two digital input channels of the board. The external pacer clock signal had controlled the rate of the data accumulation. Number of accumulated data was counted in the program owing to an internal counter of the board and the accumulation of the data could be stopped by the user. The accumulated data were stored as being counts in a dynamic memory buffer of the computer by the program. Thus the pressure data and axial velocity data stored in the memory buffer were saved as text documents to be ready for data processing.

3.6. CHECKING OF RELIABILITY OF THE MEASUREMENTS

It has been known that some noise could be present in the system and surroundings, which may affect the electronic output of the devices. Therefore the measurements were checked to verify whether these noises were effective or not. Initially the data from hot wire anemometer was acquired for a case when there is no airflow in the system and it was stored in the computer. Then a steady flow case was supplied to the system with $p_e = 0$ Pa, the data acquired and stored for this case. Subsequently an oscillating flow case was created by applying p_e into the Starling resistor while the same flow rate was present inside the collapsible tube. This oscillating flow was also measured by means of data acquisition system. The result of above-mentioned process has been plotted as shown in Figure 3.12. It can be seen from this figure that there are some differences between all of the cases. Namely, oscillating and non-oscillating flow can be easily distinguished from each other; furthermore the no-flow

case is very far from those two cases. The no-flow case has a nearly constant value of 1.6 Volts which is actually the output voltage from hot-wire anemometer. Since it is constant and there is no considerable fluctuation of the no-flow case it can be said that the measurements will not be influenced by the system's natural noise. Moreover steady flow case measurement does not change noteworthy with time and it takes approximately 2.55 Volts. However oscillating flow is highly changing with time, the output is fluctuating between 1.9 Volts and 2.7 Volts.

The frequency is also another verification of insignificance of the possible noise present in the system. So that FFT analysis of Figure 3.12 was performed and the result is shown in Figure 3.13. It is clear that frequency has no peak value with a magnitude of nearly zero in no-flow and steady flow cases, as expected. Because steady flow does not oscillate at all and any frequency value could not be stated for this condition as well as no-flow case. However oscillating flow exactly shows a peak magnitude value of 0.12 at 20 Hz, approximately in comparison to the other two cases. As a result, by referring to Figure 3.12 or Figure 3.13 it can be definitely concluded that any noise which may be present in the system does not affect the steady or unsteady flow measurements.

3.7. CONCLUSION

The experimental set-up has been described in this chapter by paying attention to its components and measuring instruments. The experimental set-up is basically composed of an airtight chamber which can be pressurized and includes a collapsible tube attached to rigid pipes at its both ends. The test tubes to be used in the experiments are presented together with their specification expressed in Table 3.1. It was found that they have been proper for the investigation, because when p_e applied into the airtight chamber the desired oscillations generated while air was flowing through the tube. Therefore the test system enables to analyse the flow in collapsible tubes in the course of self-excited oscillations which have certain significance in the investigations.

Then the basic principles of the measurements have been presented. The measurements are Q , p_e , p_1 , p_2 and u_{os} . The apparatuses to measure each of these parameters have been clearly introduced with the necessary calibration equations.

Subsequently the data acquisition system which is strongly required for obtaining the signals from the measuring instruments is explained. Finally the reliability of the measurements has been demonstrated by means of Figures 3.12 and 3.13, since these are clear indications that the measurements are not affected by the possible noise which may be present at the surrounding of the system.

CHAPTER 4

PRELIMINARY EXPERIMENTS FOR DETERMINING EXTERNAL PRESSURE INITIATING TUBE COLLAPSE

4.1. INTRODUCTION

In this chapter the preliminary experiments are introduced for determining the external pressure which causes the tube to collapse. The conventional measurement techniques have been used for the experiments as explained in the previous chapter. Once the tube has collapsed the flow may be classified as oscillating or non-oscillating flow depending on experimental conditions. The mentioned cases are explained in the following sections.

4.2. EXPERIMENTAL PROTOCOLS

The covered experimental investigation was composed of 42 experimental cases listed in Table 4.1 for the covered ranges of Q and p_e . For each specific test case a specified-original Q was produced through the test tube setting originally $p_e = 0$ Pa and Starling resistor was pressurized with the manual air pump gradually such that at each applied p_e , the pressures p_1 and p_2 and Δp were measured by an inclined-leg alcohol manometer having a sensitivity of ± 5 Pa. Therefore the method used in the study was different from the previous similar experiments which were performed at a constant p_e to investigate the flow limitation in terms of Δp variation with Q . In the presented study collapse of the test tube and related fact of flow reduction were described through the variation of Δp and Q with p_e .

Initially the tube was distended and no p_e was applied. The tube behaved as if it was a rigid tube as long as p_e was low enough not to initiate collapse. However if it was

continued to be increased it was seen that the tube was collapsed at a specific p_e which will therefore be called as external pressure at collapse, $p_{e,c}$ hereafter. This situation can be illustrated by Figure 4.1(d) which is the variation of Q versus p_e . The figure shows that initially the tube was distended and $Q = 0.0049 \text{ m}^3/\text{s}$; increasing p_e up to $p_{e,c}$ does not greatly affect the flow behaviour, but on reaching approximately $p_{e,c} = 1000 \text{ Pa}$, flow rate starts to decrease. The flow rate corresponding to that $p_{e,c}$ value will be called as flow rate at collapse, Q_c which is $0.00488 \text{ m}^3/\text{s}$. Increasing p_e beyond $p_{e,c}$ causes Q to decrease further, namely Q is decreased to $0.0047 \text{ m}^3/\text{s}$ at $p_e = 1750 \text{ Pa}$; however there were no oscillations observed during the process. This and similar observations will be called as *non-oscillating flow* case. Moreover if the self-excited oscillations developed in some cases on reaching $p_{e,c}$, these test cases will be classified as *oscillating flows*. The determination of collapse onset for both cases has also been investigated in [66]. The mentioned cases will be separately analysed and introduced in the following sections.

4.2.1. Non-oscillating Flow Case

In this part airflow through a collapsed situation of the tube but non-oscillating flow cases are explained. They are illustrated as some selected sample cases from Figure 4.1 to Figure 4.6. In these figures variation of p_1 , p_2 , Δp , Q and $p_{m,2}$ with p_e are given in order. It should be realized by observing these figures that a different tube in length and/or thickness is tested. In Figure 4.1, S_{1,L} was used for $Q = 0.0049 \text{ m}^3/\text{s}$ and p_1 is seen to be constant (Figure 4.1a) by taking a value of 180 Pa up to $p_e = p_{e,c} = 1000 \text{ Pa}$. Then p_1 increases when $p_e > p_{e,c}$, for example p_1 is 440 Pa and 900 Pa at $p_e = 1500 \text{ Pa}$ and $p_e = 1750 \text{ Pa}$, respectively.

The behaviour of p_2 is somewhat different from that of p_1 in a way that it starts to decrease for $p_e > p_{e,c}$. It is seen in Figure 4.1(b) that the variation is the same for both cases at $p_e < p_{e,c}$, that is p_2 has also a constant value as 85 Pa up to $p_{e,c}$. However p_2 is decreasing with p_e for $p_e > p_{e,c}$. The reason can be explained as the

area reduction of the tube due to collapse which occurs near the downstream end, thereby p_2 should decrease after collapse, i.e., when $p_e > p_{e,c}$. It is observed as from Figure 4.1(b) that $p_2 = 45$ Pa at $p_e = 1500$ Pa and further p_2 decreases to 10 Pa at $p_e = 1750$ Pa.

The variation of Δp with p_e is given in Figure 4.1(c). It is noted that the behaviour is the same as Figure 4.1(a): Δp is constant (5 Pa) up to $p_{e,c}$ and it increases with p_e for $p_e > p_{e,c}$; namely $\Delta p = 850$ Pa at $p_e = 1750$ Pa. The variation of Q with p_e (Figure 4.1d) is explained above to introduce some parameters as $p_{e,c}$ and Q_c .

The last and important parameter which should be mentioned is the downstream transmural pressure $p_{m,2}$ (Figure 4.1e). It can easily be said that when collapsed state is reached $p_{m,2}$ should certainly be negative. Starting from a positive value of $p_{m,2}$ (distended tube) and gradually increasing p_e causes it to be negative. In contrast to the other cases (Figure 4.1a to Figure 4.1d) it is linearly decreases with p_e even $p_e < p_{e,c}$ and this tendency also continues for $p_e > p_{e,c}$: $p_{m,2}$ is -250 Pa, -900 Pa, -1800 Pa at p_e of 350 Pa, 1000 Pa (collapsed case) and 1750 Pa, respectively.

The above-mentioned behaviour is also principally observed for $S_{3,L}$ (Figure 4.2), $S_{1,M}$ (Figure 4.3), $S_{2,M}$ (Figure 4.4), $S_{1,S}$ (Figure 4.5), and $S_{3,S}$ (Figure 4.6) tubes. In all of these cases flow is non-oscillating, however the magnitudes of flow parameters are varying in each case. The most remarkable difference of using a thicker tube is seen in the range of p_e . This can be justified by comparing Figure 4.4 ($S_{2,M}$) and Figure 4.6 ($S_{3,S}$), as an example. This comparison is reasonable since the initial Q settings are approximately at the same value of 0.0094 m³/s. In Figure 4.4 it is seen that the value of $p_{e,c}$ is 8000 Pa, however it is increased 25000 Pa in Figure 4.6. The considerable difference in $p_{e,c}$ should be due to the thickness, h of the test tubes. The thickness does not only affect $p_{e,c}$, but also it has an influence on the other measured parameters of p_1 , p_2 , Δp , and range of $p_{m,2}$. The same decision can even be thought

if the flow rate setting is not the same. For instance, initial Q value is $0.0173 \text{ m}^3/\text{s}$ and $0.0049 \text{ m}^3/\text{s}$ in Figure 4.2 and Figure 4.3, for $S_{3,L}$ and $S_{1,M}$, respectively, $p_{e,c}$ is much more greater for $S_{3,L}$ than $S_{1,M}$ although different Q values.

The figures should be further examined to find out the influence of other parameters such as length of the test tube, L as well as h . Figure 4.1 and Figure 4.5 for the same Q value can be selected as the illustrative plots for this purpose. The measured parameters display the similar trend at first view. However a careful examination points out that shorter tube will be collapsed under greater p_e . As it was previously determined that $p_{e,c}$ is approximately 1000 Pa in Figure 4.1 which is obtained by testing $S_{1,L}$, however $p_{e,c}$ has a higher value, approximately 2000 Pa, for the shorter tube $S_{1,S}$ in Figure 4.5. Since $p_{e,c}$ values are different, the range of p_1 and Δp values also changes in correspondence of $p_{e,c}$ in these two figures. This may be an indication that L should also be taken into consideration as well as h in collapsible tube flow investigations.

The higher $p_{e,c}$ requirement for the shorter tube and/or thicker tube is logical in fact. By considering a shorter tube, one can say that a short tube is more resistant than a longer tube to buckle. In other words as L decreases collapsible tubes may act like rigid tubes, therefore a higher $p_{e,c}$ is necessary for the tube to be collapsed. The thicker tube behaviour can be explained in the similar way. It should be accepted that a thicker tube is more resistant to collapse than a thinner tube under the action of p_e .

4.2.2. Oscillating Flow Case

As previously cited flow is oscillating in some cases if flow rate is high enough and applied p_e is great enough for a given collapsible tube. In this section oscillating flow cases are outlined. The related illustrations are shown from Figure 4.7 to Figure 4.12. It should be firstly determined that there is not oscillating case observed through 3mm thick silicone rubber tubes at all. On the other hand flow through Penrose tube oscillates for all flow rate values however small they may be. That is non-oscillating flow case through Penrose tube has not been observed.

As in the non-oscillating flow case there is a certain external pressure applied to start oscillations and this will be called again as $p_{e,c}$ as shown in Figure 4.7(d). This plot was obtained for the $S_{1,L}$ tube at an initial Q of $0.012 \text{ m}^3/\text{s}$. p_e has been increased gradually and there is no oscillation up to $p_e = 1250 \text{ Pa}$ for $Q = 0.012 \text{ m}^3/\text{s}$ through $S_{1,L}$ in Figure 4.7. The behaviour is almost the same as the non-oscillating flow case. Comparing Figure 4.7 with Figure 4.1 for this purpose it can easily be said that variations of p_1 , p_2 , Δp , Q and $p_{m,2}$ with p_e are almost similar. However there should be a difference between these two cases and this distinction can be clearly seen by examining Figure 4.1(d) and Figure 4.7(d) simultaneously. In oscillating case Q suddenly drops a value ($0.009 \text{ m}^3/\text{s}$) corresponding to $p_{e,c}$, namely just oscillations arise and this value is called as flow rate at collapse, Q_c . Then Q immediately increases to another value ($0.0115 \text{ m}^3/\text{s}$) as observed from alcohol level in manometer and oscillates at this level on average. The final value is called as oscillating flow rate, Q_{os} . This is the main difference between oscillating and non-oscillating cases.

In non-oscillating case Q slowly drops to Q_c at $p_{e,c}$. If p_e is increased beyond $p_{e,c}$, Q continues to drop gradually. However in oscillating case Q drops to Q_c then increases to Q_{os} at once and oscillates around Q_{os} . It can be easily concluded that there is not other remarkable difference between two cases by examining the figures for both cases. That is p_1 is constant up to $p_{e,c}$ as in the non-oscillating case, but it suddenly rises to a new value. The abrupt increase of p_1 at $p_{e,c}$ is again said to be the distinction from non-oscillating case. For example in Figure 4.1(a) of non-oscillating case there is more than one experimental data after $p_{e,c}$. On the other hand there is one experimental value after $p_{e,c}$ for oscillating case through $S_{1,L}$ tube in Figure 4.7(a). Initially p_1 is approximately 500 Pa and it is nearly constant up to $p_{e,c} = 1250 \text{ Pa}$. p_1 increases to 850 Pa unexpectedly when $p_{e,c}$ has been applied for this case. However p_1 does not increase suddenly at $p_{e,c}$ as can be observed in Figure 4.1(a). It has taken a slightly greater value beyond $p_{e,c}$. A cursory

examination of Figure 4.1(a) points out that there are 17 experimental data of p_1 for 17 different applied p_e values that are greater than $p_{e,c}$ and there is no sharp change in p_1 . This is not the case for oscillating case as shown in Figure 4.7(a) and only one p_1 value corresponds to $p_{e,c}$. The main cause of the single data after $p_{e,c}$ is the impossibility of unsteady measurement with the alcohol manometer. Only the first data which just corresponds to $p_{e,c}$ has been measured in oscillating case, therefore $p_e > p_{e,c}$ has not been measured. The unsteady flow measurements were done by using the experimental set-up as shown in Figure 3.2 which includes pressure transducers, hot-wire anemometer and data acquisition system and the results will be discussed in the next chapter.

The similar conclusion can be drawn for p_2 as shown in Figure 4.7(b). It is almost constant at 425 Pa for $0 < p_e < p_{e,c}$. Then it drops suddenly to 370 Pa when $p_{e,c} = 1250$ Pa. There is again only one p_2 value at $p_{e,c}$ as explained for p_1 in oscillating case.

Variation of Δp with p_e in Figure 4.7(c) is analogous to Figure 4.1(c). The only difference is again abrupt increase of Δp at $p_{e,c}$ for the oscillating case while a gradual change in Δp at a greater p_e above $p_{e,c}$ is valid for the non-oscillating case. In Figure 4.7(c) Δp is approximately constant and takes around 100 Pa up to $p_{e,c} = 1250$ Pa. It sharply increases to 500 Pa for $p_{e,c}$; oscillates around 500 Pa and again there is a single data point of the oscillating case at $p_{e,c}$.

Finally the variation of $p_{m,2}$ with p_e is shown in Figure 4.7(e). The trend is very similar to non-oscillating case, however there is no experimental data measured after $p_{e,c}$. Since flow oscillates and therefore alcohol level in the manometer oscillates, time-dependent measurement is not possible with this conventional measurement system. $p_{m,2}$ drops linearly with p_e in Figure 4.7(e) as in the non-oscillating case. It

is initially at 490 Pa and drops to -200 Pa at $p_e = 550$ Pa. It continues to linearly decrease with p_e . Finally it takes the value of -1000 Pa at $p_{e,c} = 1250$ Pa.

After comparing the oscillating and non-oscillating cases, firstly it is useful to analyse the effect of h for oscillating case only. The experiments indicate that although flow is oscillating at a specific Q through a given tube, it may be non-oscillating through another tube for the same Q . More clearly, although flow is oscillating as shown in Figure 4.7 through $S_{1,L}$ at $Q = 0.012$ m³/s, on the other hand it is not oscillating through $S_{2,L}$ for the same Q . Therefore a greater Q of 0.016 m³/s had been selected for $S_{2,L}$ as shown in Figure 4.8. Oscillations arise at $p_{e,c} = 7000$ Pa. The remarkable difference between $S_{1,L}$ (Figure 4.7) and $S_{2,L}$ (Figure 4.8) is the range of p_e . As it was previously concluded that p_e range increases for the thicker tubes and this consequence is also valid for the oscillating case. While only $p_{e,c}$ of 1250 Pa is enough for the oscillations to appear in Figure 4.7, but $p_{e,c}$ should be as high as 7000 Pa for arising the oscillations. This is the clear effect of h as understood from experimental results. It can be concluded from the results that flow is not oscillating for all tubes and for all Q values. Namely, flow through any collapsible tube is not necessarily be oscillating for all Q . The applied p_e and Q should be high enough for the oscillations to arise. If this is not the case, flow will not be oscillating at all as shown from Figure 4.1 to Figure 4.6.

The variation of p_1 with p_e is shown in Figure 4.8(a). It is approximately 1000 Pa for $0 < p_e < 7000$ Pa, but it increases to 2000 Pa abruptly at $p_{e,c} = 7000$. That is twofold increase of p_1 is seen for $S_{2,L}$ at $p_{e,c}$ and $Q = 0.016$ m³/s. It oscillates around this final value of 2000 Pa.

p_2 is nearly constant at 760 Pa (Figure 4.8b), it slightly decreases with p_e . When $p_{e,c}$ is applied it suddenly decreases to 685 Pa and oscillates around that value. It means that while change in p_1 is twofold, that in p_2 is not as high as in p_1 . In other words p_1 is more affected than p_2 due to presence of the oscillations through

collapsible tube flows. It should be also defined at this point that although p_1 is mostly affected than p_2 in its magnitude due to oscillations, p_2 drops while p_1 increases. The reason of drop in p_2 is the collapse near the downstream end. Constriction causes flow to accelerate and therefore decrease of pressure at downstream end.

The variation of Δp with p_e is shown in Figure 4.8(c). Δp is almost constant at 150 Pa up to $p_{e,c}$. However it sharply rises to 1500 Pa, i.e. the change of Δp is 10 times with respect to initial value of before oscillations. This is the average oscillating Δp of 1500 Pa at $p_{e,c} = 7500$ Pa. The relationship between Q and p_e is given in Figure 4.8(d). Q Suddenly drops to Q_c of $0.01 \text{ m}^3/\text{s}$, but it reaches to $0.015 \text{ m}^3/\text{s}$ of average oscillating value, Q_{os} in comparison to initial Q setting of $0.016 \text{ m}^3/\text{s}$.

The downstream transmural pressure $p_{m,2}$ linearly decreases with increasing p_e as shown in Figure 4.8(e). Initially it has a positive value of 500 Pa. Increasing p_e causes $p_{m,2}$ to decrease continuously in contrast to other parameters. It has been emphasized that p_1 , p_2 , Δp , and Q are nearly constant up to $p_{e,c}$ for both oscillating and non-oscillating cases. However, $p_{m,2}$ always decreases with p_e even if $p_e < p_{e,c}$. For instance $p_{m,2}$ is -1000 Pa, -2500 Pa and -5000 Pa for p_e which is less than $p_{e,c}$ of 1100 Pa, 2500 Pa and 4200 Pa, respectively. It is decreasing linearly with all values of p_e in other words. Finally it has a value of -7000 Pa at $p_{e,c}$.

As it has been pointed out previously that experiments with Penrose tubes have shown that there are oscillations for any Q at a specific applied $p_{e,c}$. Therefore smaller Q values can be tested through Penrose tubes. As a sample case flow through P_M is shown in Figure 4.9 at initial Q of $0.0095 \text{ m}^3/\text{s}$ in comparison to $0.016 \text{ m}^3/\text{s}$ in Figure 4.8. Another interesting finding is that $p_{e,c}$ is very small in comparison to silicone rubber tubes in Figure 4.7 or Figure 4.8. It is seen in Figure 4.9(d) that $p_{e,c}$ is approximately 290 Pa for Q of $0.0095 \text{ m}^3/\text{s}$ through P_M . It has

dropped to $0.007 \text{ m}^3/\text{s}$ and then instantly increases to $0.0082 \text{ m}^3/\text{s}$ at $p_{e,c}$. A very small $p_{e,c}$ necessary for Penrose tubes in comparison to silicone rubber tubes should be due to small h of P_M and also tube's mechanical properties.

Initially p_1 is 350 Pa in Figure 4.9(a) and it is constant up to $p_{e,c}$. When p_e is increased to be $p_{e,c} = 290 \text{ Pa}$, p_1 takes 900 Pa at once in comparison to 350 Pa. It oscillates around 900 Pa at $p_{e,c}$. In Figure 4.9(b) p_2 is initially 293 Pa and drops sharply to 283 Pa at $p_{e,c}$. This change in p_2 is not as high as that in p_1 as determined for the case in Figure 4.8(b). However Δp is greatly influenced by the oscillations. It is nearly at 50 Pa up to $p_{e,c}$ and there are no oscillations observed, but on applying $p_{e,c} = 290 \text{ Pa}$, oscillations take place and Δp quickly raises to 600 Pa and oscillates. It can be said that due to oscillations Δp has a change of 12 times with respect to initial case, i.e. before oscillations.

Another interesting property of flow through Penrose tube is $p_{m,2}$ which is shown in Figure 4.9(e). It is linearly decreasing with p_e as previously stated. Unlike silicone rubber tubes, Penrose tube may be oscillating at a much smaller value of $p_{m,2}$. It was previously indicated that $p_{m,2} = -7000 \text{ Pa}$ when oscillations started in Figure 4.8(e). Namely, a highly negative $p_{m,2}$ is necessary for flow through silicone rubber tubes to have oscillations. However $p_{m,2}$ is not as high as that for Penrose tubes as can be seen from Figure 4.9(e). It is nearly 0 Pa, i.e. external pressure is almost equal to internal pressure as compared to Figure 4.8(e).

The other oscillating flow cases through collapsible tubes of $S_{1,M}$, P_s and $S_{1,S}$ are given in Figures 4.10, 4.11 and 4.12, respectively. These figures demonstrate and support the outlined findings of Figure 4.7, Figure 4.8 and Figure 4.9. Especially, Figure 4.10 is very similar to Figure 4.7. The initial Q setting is the same; the only difference is the L of the collapsible tube. That is while $S_{1,M}$ is tested in Figure 4.10, $S_{1,L}$ is used for the experimental measurement in Figure 4.7. It can be said that L is not so effective on the results since the behaviour of these two figures is very similar.

In Figure 4.11 flow through P_S is investigated like Figure 4.9. However a smaller initial Q value of $0.005 \text{ m}^3/\text{s}$ is chosen to show the oscillations arise even at a small Q for the Penrose tube. The main findings from Figure 4.9 are realized to be valid for Figure 4.11.

The final sample diagram to explain oscillating flows is plotted as shown in Figure 4.12 for $S_{1,S}$ tube. This may be compared with Figure 4.7 and it can be determined that the behaviour is the same as $S_{1,L}$ tube. Lastly there isn't a noteworthy difference between previous figures for the silicone rubber tubes of oscillating case.

In summary there are two cases observed for the flows through collapsible tubes: non-oscillating case and oscillating case. The condition for obtaining any of these cases is highly dependent on tube characteristics, Q and $p_{e,c}$. For example flow through $S_{1,L}$ is non-oscillating for $Q = 0.005 \text{ m}^3/\text{s}$ (Figure 4.1), on the other hand it is oscillating at $Q = 0.012 \text{ m}^3/\text{s}$ for the same tube (Figure 4.7). Thickness has a certain effect on the flow, because $p_{e,c}$ is very different for $S_{1,L}$ and $S_{2,L}$ tubes for both oscillating or non-oscillating case. Moreover, 3 mm thick silicone rubber tubes do not display oscillations while $S_{1,L}$ (Figure 4.7) and $S_{2,L}$ (Figure 4.8) do show.

Another main finding is related to Penrose tube. This tube has certainly different mechanical property such as E in comparison with silicone rubber tubes. A smaller $p_{m,2}$ and/or $p_{e,c}$ is enough for the oscillations to appear for Penrose tube. Experiments with Penrose tubes do not result in non-oscillating flows as long as p_e is applied. If fluid flows through a Penrose tube, there will be a certain value of $p_{e,c}$ for the flow to be oscillating.

Length of the test tube L does not affect the flow in comparing to h , however it is seen from the figures that it has some influence on the flow. It probably affects at least $p_{e,c}$ to originate the self-excited oscillations. Flow behaviour is mostly affected due to initial flow settings, tube's mechanical and geometrical properties. These factors should be taken into consideration when these types of flows are investigated.

The oscillating (29 cases) and non-oscillating (13 cases) flows through test tubes are listed in Table 4.2 and Table 4.3 respectively. Penrose tubes exhibited oscillations for the covered Q range irrespective of how small the magnitude of p_e was. The cases through Penrose tubes were also with a variable magnitude of Q_{os} in conformity with the observations in [7]. However in the non-oscillating cases through silicone rubber tube no oscillation was observed irrespective of how large the magnitude of p_e for the covered Q range. In oscillating flow cases (Table 4.2) the test tubes were thin and thick walled ones and the magnitude of Q_c/Q varies between 25.92% and 92.98%. In non-oscillating flow cases (Table 4.3) the magnitude of Q_c/Q varied between 99.83% and 96.73%. Therefore it seems that the flow rate reduction in an oscillating case seems to be greater than the one in a non-oscillating case. These observations can be used to justify not only the importance of the test tube characteristics but also the conveying flow characteristics. Penrose tube which was the thinnest tube with $h = 0.55$ mm of different L produced oscillating test cases for the covered flow rates. Silicone rubber tube of the thickest one with $h = 3$ mm of different L produced non-oscillating cases for the covered flow rates. Therefore the governing importance of h is apparent. Meanwhile cases through silicone rubber test tubes of the same h and even L were either oscillating or non-oscillating specifying the effect of conveying Q . As an example when $Q = 0.0149$ m³/s was the amount of conveying air through $S_{1,L}$ an oscillating case was observed (Table 4.2) while change in flow rate as $Q = 0.006$ m³/s and $Q = 0.0049$ m³/s (Table 4.3) through the same test tube resulted in non-oscillating cases.

4.2.3. Analysis of Non-oscillating and Oscillating Flow Cases Simultaneously

The experimental data of preceding two sections are evaluated here. Firstly the variation of Δp with p_e is investigated for this purpose. Flow through $S_{1,L}$ tube is shown as a sample plot for a non-oscillating case (Figure 4.13a) and oscillating flow case (Figure 4.13b). There are two Q values as 0.0049 m³/s and 0.006 m³/s for non-oscillating case and the experimental data of these two cases seem to be coincided

(Figure 4.13a). Therefore the variation of Δp can be represented by a single equation fitted to the data as follows:

$$\Delta p = 0.003(p_e)^2 - 0.145(p_e) - 55.59 \quad (4.1)$$

The oscillating flow case however cannot be defined with such a single relationship as shown in Figure 4.13(b). The experimental data is measured for different Q cases and each of these displays dissimilar behaviour in Δp variation with p_e . Nevertheless Δp is almost constant for all Q for $p_e < p_{e,c}$. The scattering of data is seen for $p_e > p_{e,c}$, namely when oscillations arise.

Another noteworthy point is the $p_{e,c}$ difference for each Q . It can be said that as Q increases $p_{e,c}$ also slightly increases to initiate the oscillations. For instance $p_{e,c}$ values are 1150 Pa and 1400 Pa, which are corresponding to Q values of 0.0106 m³/s and 0.0155 m³/s, respectively in Figure 4.13(b). Lastly it should be remarked here again that Δp rises suddenly for $p_e > p_{e,c}$ of oscillating case but it has a gradual increase for each increasing p_e beyond $p_{e,c}$ for non-oscillating flow case. Actually this was a previous finding in preceding sections.

In Figure 4.14 variation of Δp with p_e is indicated for S_{2,L} tube similar to Figure 4.13. There seems to be no effect of Q on the variation for the oscillating case in Figure 4.14(a). There are two regions that may be classified as a constant variation of data before oscillation ($p_e < p_{e,c}$) and abrupt increase of Δp after oscillation ($p_e \geq p_{e,c}$). The higher $p_{e,c}$ value of 7000 Pa for S_{2,L} tube as compared to S_{1,L} tube in Figure 4.13 is noticeable. There is a certain effect of h on the flow as previously emphasized. In contrast to Figure 4.13(a) for non-oscillating case, there is an effect of Q on the flow as plotted in Figure 4.14(b). The variation of Δp cannot be defined with a single equation in this case since the data does not coincide with each other. There are two distinct $p_{e,c}$ values that are approximately as 7000 Pa and 7500 Pa for Q of 0.0094 m³/s and 0.0132 m³/s, respectively. It may therefore be stated as Q

affects $p_{e,c}$ for collapsing of the tube. The greater Q causes a higher $p_{e,c}$ to initiate the buckling of the tube.

The conclusion drawn from Figure 4.14(b) is supported with Figure 4.15 again for a non-oscillating flow case through $S_{3,L}$ tube. The behaviour for these two figures is very similar: As Q increases $p_{e,c}$ to cause the collapse also rises. There are three different variations of Δp with p_e for each Q . However, $S_{3,L}$ tube will be collapsed at substantially higher $p_{e,c}$ as high as 19000 Pa compared to $S_{1,L}$ in Figure 4.13(a) or $S_{2,L}$ in Figure 4.14(b) for non-oscillating cases.

The variation of Δp with p_e through Penrose tube, which has noticeable different characteristic as compared to silicone rubber tubes, is shown in Figure 4.16. There is no non-oscillating case for P_L . In this plot it is seen that $p_{e,c}$ is highly affected with Q . $p_{e,c}$ is approximately 50 Pa when $Q = 0.0049 \text{ m}^3/\text{s}$, but it increases up to 300 Pa for $Q = 0.012 \text{ m}^3/\text{s}$. This result was also valid for silicone tubes with only the difference that smallness of $p_{e,c}$ for Penrose tubes in comparison with silicone tube. Note that Δp strongly increases after $p_{e,c}$ for each of Q . In addition, Δp has a greater sharp increase for a higher Q . For example Δp is approximately 30 Pa for all Q and it is almost constant up to $p_{e,c}$. Then it is nearly 500 Pa for $Q = 0.006 \text{ m}^3/\text{s}$ and 1750 Pa for $Q = 0.012 \text{ m}^3/\text{s}$ when $p_{e,c}$ has been applied.

The variation of Δp with p_e is lastly illustrated in Figure 4.17. In this figure a range of Q is shown for different tubes simultaneously. The figure is useful to see different tubes in the same plot. For-example, Figure 4.17(a) is the variation of Δp with p_e for oscillating case through $S_{1,L}$, $S_{2,L}$ and P_L tubes covering a range of Q . The data for P_L is concentrated on the left of the figure due to the smallness of $p_{e,c}$ for this tube. The data is scattered for different Q values through $S_{1,L}$ tube and there is a range of $50 \text{ Pa} < p_{e,c} < 1900 \text{ Pa}$. Furthermore, the experimental data for $S_{2,L}$ seems to be on

the right of the figure for $p_e > p_{e,c}$. In addition Δp value for this tube is nearly constant at 250 Pa for $p_e < p_{e,c}$.

The effect of h for non-oscillating case through tubes of $L/D_0 = 10$ is shown in Figure 4.17(b) clearly. It is again remembered by consulting this figure that $p_{e,c}$ to start the collapse of the tube increases for the thicker tube. It can be deduced that $p_{e,c}$ is nearly 1250 Pa, 7000 Pa, and 18000 Pa for the tubes of $S_{1,L}$, $S_{2,L}$ and $S_{3,L}$, respectively. The effect of h on the flow is also demonstrated with Figure 4.18. In this figure variation of Q with $p_{e,c}$ for oscillating and non-oscillating cases together. $L/D_0 = 10$, $L/D_0 = 7.5$ and $L/D_0 = 5$ cases are indicated in Figure 4.18(a), Figure 4.18(b) and Figure 4.18(c), respectively. The explanation for the effect of h cited previously is also valid for Figure 4.18: $p_{e,c}$ increases for higher Q as shown in Figure 4.14 and Figure 4.15. It increases for thicker tube in addition as shown in Figure 4.17. In other words there is a certain $p_{e,c}$ for each of Q and/or h values.

The effect of L is specified in Figure 4.19 similar to Figure 4.18. It can be concluded by referring to the figure that it is more difficult to collapse a shorter tube; therefore a higher $p_{e,c}$ is required for the shorter tube at a given Q value. This may be verified by studying Figure 4.19(a), for example. It can be seen that $p_{e,c}$ is approximately 1100 Pa for $Q = 0.005 \text{ m}^3/\text{s}$ through $S_{1,L}$. However $p_{e,c}$ is nearly 1900 Pa corresponding to the same Q but through $S_{1,S}$ tube in this case. The difference is definitely an effect due to L . This conclusion can also be drawn by carefully observing Figure 4.19(b) and Figure 4.19(c).

The overall experimental data can be more meaningfully analysed by using dimensionless parameters such as Re and K_p . Therefore Figure 4.20 has been plotted for this aim. It is seen that variation of $Re(h/L)$ with $p_{e,c}/K_p$ which are obviously dimensionless parameters: h and L are in mm; $p_{e,c}$ and K_p are in unit of pressure, Pascal, so h/L and $p_{e,c}/K_p$ are dimensionless as well as Re . It has been aimed to include the effects of all of the parameters and therefore h/L ratio is multiplied by

Re on the axis of the ordinate of the figure and K_p also includes certain tube geometrical parameters as well as mechanical properties such as E and ν as determined previously with equation (3.1). Therefore Figure 4.20 may be a useful tool to comment on the experimental results. In Figure 4.20(a) non-oscillating case for all L and h of silicone rubber tubes is shown. It can be concluded that the data is so scattered that a single equation cannot be fitted to the experimental data. However it should easily be said that h and L certainly influence the variation of $Re(h/L)$ with $p_{e,c}/K_p$. It may also be determined that the effect of h is more dominant than L . The oscillating case is analysed in Figure 4.20(b) for the silicone rubber tubes of 1 mm and 2 mm thickness with three different lengths. A single relationship may be fitted to the data to represent the variation of parameters for the oscillating case of cited tubes. It can be defined by the following equation:

$$Re(h/L) = -2.22(p_{e,c}/K_p)^3 + 111.14(p_{e,c}/K_p)^2 - 1785.3(p_{e,c}/K_p) + 9408 \quad (4.2)$$

The data scattering from equation (4.2) is in the order of $\pm 15\%$. The flow through Penrose tube is analysed separately in Figure 4.20(c) from silicone rubber tubes in Figure 4.20(b). The variation of $Re(h/L)$ with $p_{e,c}/K_p$ for the latter is somewhat different in relative to the former. Thereby a new relationship can be fitted to the data with the following equation:

$$Re(h/L) = 9.813(p_{e,c}/K_p)^{0.73} \quad (4.3)$$

The data scattering from equation (4.3) is in the order of $\pm 15\%$. The scattering of the data in the figure is of course due to L . It is useful to remember at this point that as the tube becomes shorter, it will be more stiffer to any applied p_e for initiating the collapse.

4.3. CONCLUSION

In this chapter preliminary experimental results by using conventional measuring methods have been outlined and commented to quote the effect of flow and tube parameters such as Q , L and h . Firstly the flow may be classified as non-oscillating or oscillating case according to the experimental study. The Q , L and h parameters were realized that to affect the magnitude of the applied $p_{e,c}$ just to cause the collapse near downstream end of the tube in non-oscillating case or oscillations in oscillating case. It was comprehended that as h increases $p_{e,c}$ also substantially increases. Furthermore it was found out that $p_{e,c}$ also increases as L decreases. Moreover Penrose tube showed a certain different characteristic in comparison to silicone rubber tube and it was oscillating always at any Q value if the enough $p_{e,c}$ was applied to the tube. Another finding was that a higher Q caused a greater $p_{e,c}$ to be applied for a given tube to commence the collapse or oscillations.

It should be remembered that p_1 , p_2 , Δp , Q and $p_{tm,2}$ parameters were definitely affected when $p_{e,c}$ was applied. In oscillating cases p_1 and Δp increased suddenly, however p_2 decreased for $p_e \geq p_{e,c}$. Meanwhile, p_1 , p_2 , Δp and Q had approximately constant value up to $p_{e,c}$. The alcohol level in the manometer dropped and increased immediately to a value which was called Q_{os} lower than initial set of Q . When $p_{e,c}$ was applied $p_{tm,2}$ decreased linearly with p_e . In non-oscillating case there was no sudden increase of p_1 or Δp , but instead of this, a gradual increase was observed for $p_e > p_{e,c}$. The constant value of p_1 , p_2 and Δp was also seen up to $p_{e,c}$ for this case.

In addition, the meaningful conclusion was obtained by considering the dimensionless parameters of $Re(h/L)$ and $p_{e,c}/K_p$ as shown in Figure 4.20. Many of the parameters such as Q , $p_{e,c}$, v_f and K_p which includes E , h , L , D_0 were taken into account in this figure to show their effects in combination.

Lastly, in this section although conventional measurement methods were carried out even for the unsteady flow case, the results were very explanatory. It was concluded by consulting experimental results that Q , L and h parameters were so effective in collapsible tube flow investigations; they should therefore be carefully evaluated in the related studies. The unsteady flow measurement, i.e., oscillating flow case is the subject of next chapter.

CHAPTER 5

ANALYSIS OF THE TEST CASES AT THE ONSET OF SELF-EXCITED OSCILLATIONS

5.1. INTRODUCTION

In this chapter, the experimental measurements are presented at the onset of self-excited oscillations. Time dependent variations of pressure and velocity measurements and frequency of the oscillations are given. Moreover effect of h and L of the tubes on $p_{e,c}$ and f at a specific flow rate is shown in detail since it was found that they were influenced significantly by L and especially h . The experimental results were analysed by plotting variations of f and $p_{e,c}$ with Q for the different L and h cases in order to find out their effects on the measurements. In addition the relationships between some dimensionless parameters were determined in reference to the literature. These relationships are graphically represented in Section 5.4. The non-dimensional parameters which were also selected and used in the experimental study of reference [45] are *mean flow resistance*, *Womersley number* and *dimensionless mean oscillating velocity*. Since these parameters include almost all of the properties related to both of fluid (pressure, velocity, density, kinematic viscosity) and tube (bending stiffness concerning diameter, thickness, modulus of elasticity and Poisson's ratio), they should be useful for analysing the experimental measurements. The above-mentioned works are presented in the following sections. The method of the measurements and results of the some sample cases are explained initially. Then all of the findings which were acquired similarly to the sample cases are presented. Finally the results based on the calculations of above dimensionless parameters are designated.

5.2. UNSTEADY PRESSURE and VELOCITY MEASUREMENT RESULTS

A specific steady flow rate has been supplied to the system and the external pressure is increased gradually. The pressure and velocity measurements have been recorded to the computer by means of data acquisition system when the oscillations generated. The external pressure corresponding to that instant has been called as external pressure at collapse, $p_{e,c}$ as defined previously. Some sample results are presented as plots through Figure 5.1 to Figure 5.6. A sample test case at the onset of oscillations with $S_{1,M}$ tube for $Q = 0.01\text{m}^3/\text{s}$ has been also presented in [67].

The variation of pressure and velocity with time for the case of flow through $S_{1,M}$ tube is illustrated in Figure 5.1. The steady flow rate is $0.0172\text{ m}^3/\text{s}$ and $p_{e,c}$ is 2.33 kPa for this case. It is seen from this figure that flow is highly unsteady due to the presence of oscillations and flow parameters are frequently fluctuating over the time. The results are presented for one second to show time variation of the data in a large scale. The data-sampling rate is 120 data/second in this case. It will be useful to emphasize at this point that although the total duration of measurement is more than one second, but the data is shown in Figure 5.1 for the first one second of the total time. In other words the total time elapsed during data acquiring is 5.7 second and there will be 684 data points in this figure corresponding to the mentioned duration. It is obvious that such a figure would be so complicated that the behaviour of data may not be observed clearly. Therefore this figure is given only for the first one second to be examined easily by the reader. There are 120 data points in this figure due to the mentioned sampling rate rather than 684 points. It should be noted here that the defined sampling rate is enough to have the measurements without error. Since the maximum frequency value which has been determined in the extended study [68] is about 35 Hz, it is seen that the sampling rate of 120 data/second should be enough high for the measurements. Therefore the *Nyquist's theorem* has been satisfied with this sampling rate. Because this theorem states that an analog signal waveform may be uniquely reconstructed, without error, from samples taken at equal time intervals. The sampling rate must be equal to, or greater than, twice the highest frequency component in the analog signal. It is seen that although a sampling rate of about 70 data/second will even be adequate for the measurements, it has been

adjusted by the software as a higher value of 120 data/second to have more accuracy in measurements. Moreover as it will be expressed in the following paragraph that f is 19.6 Hz for this case, it is again obvious that the sampling rate is about 6 times of the measured f and this must be an indication of precise measurement.

In Figure 5.1, upstream pressure, p_1 is oscillating nearly between 1 kPa and 5 kPa whereas p_2 is fluctuating between -2 kPa and 3 kPa. It should be noted that p_2 has sometimes negative values, but p_1 has always positive magnitudes. The root mean square (rms) of the oscillating data has been calculated due to the fact that p_2 has negative values as well as positive values. The arithmetical time average of will not be a wise method in this case. Therefore the rms of the data should be more advisable rather than arithmetic mean while evaluating the measurements (the rms of fluctuations has been also considered in [59], for example). It can be concluded that p_2 seems to be more affected in magnitude due to oscillations. This is reasonable because of the fact that the position of collapse and oscillations is at the downstream of the tube. It is useful to show the p_1 and p_2 variations in the same graphic and this has been done in Figure 5.1. In this plot p_2 again seems to be more influenced in oscillating flow. The rms of the pressure is calculated and it is represented by \bar{p}_1 and \bar{p}_2 for the upstream and downstream pressures, respectively. It has been found that $\bar{p}_1 = 3.2$ kPa and $\bar{p}_2 = 2$ kPa. Note that $\bar{p}_2 < \bar{p}_1$ as expected, since the pressure should be decreased in the flow direction. The result of oscillating flow velocity (u_{os}) measurement is also given in Figure 5.1 as u_{os} versus t . It is clear that velocity is fluctuating similar to the pressure values. It is approximately changing between 10 m/s and 60 m/s due to highly unsteady flow. The rms value of oscillating velocity (\bar{u}_{os}) has been evaluated to be 43.93 m/s for this case.

The frequency of the oscillations, f has been determined by applying Fast Fourier Transform (FFT) to the time dependent pressure and velocity data. FFT analysis of the data in Figure 5.1 has been carried out and the result is given in Figure 5.2. It is observed that there are many frequency components in the spectral analysis in Figure 5.2. However there are distinguishable specific peak magnitudes which are approximately 1.4, 1.9 and 11 in the FFT analysis of p_1 , p_2 and u_{os} , respectively. The frequency of the oscillations is found to be 19.6 Hz corresponding to these

magnitudes. The remaining frequency components are so small with respect to that corresponds to peak magnitude and they can therefore be neglected. As a result f has been obtained from any of the pressure or velocity measurement.

Another point that should be stated by referring to Figure 5.2 is that the experimental test system's calibration has been satisfied so that the obtained results are reliable. Because FFT of pressure or velocity data provides the same f value. This finding should normally be expected since velocity and pressure data are measured simultaneously. If oscillating pressure data has a frequency of 19.6 Hz, the velocity data should have the same frequency value in the same flow condition.

Another sample result obtained from the experiment with $S_{2,S}$ tube is shown in Figure 5.3. The initial steady flow rate is $0.0147 \text{ m}^3/\text{s}$ and $p_{e,c}$ is 9.03 kPa for this case. The simultaneous variations of p_1 and p_2 with time at the onset of oscillations during 2 seconds of the measurement are plotted in this figure. The sampling rate is approximately 120 data/second, total elapsed-time during data acquisition is 7.8 seconds. It is clearly seen that p_2 is more affected during oscillations. It can be observed that p_1 is less influenced in comparison with p_2 . Namely, p_1 is oscillating nearly around 3 kPa, however p_2 is in the range between -1 kPa and 2 kPa . The rms values for the pressure fluctuations computed as $\bar{p}_1 = 3.01 \text{ kPa}$ and $\bar{p}_2 = 1.38 \text{ kPa}$. The velocity is also changing frequently with time in the range between 5 m/s and 35 m/s , approximately and \bar{u}_{os} has been calculated to be 27.84 m/s .

The frequency of the oscillations of the data in Figure 5.3 is represented in Figure 5.4. Similar to Figure 5.2, f values separately determined from pressure and velocity data coincide at a unique value which in this case is 28.89 Hz at the peak magnitude of the FFT analysis. It can be noted that f has been increased in comparison to Figure 5.2. This can be attributed due to the difference of the tube thickness which is a greater value in Figure 5.4.

The final sample measurement result is illustrated in Figure 5.5. This figure has been obtained with the flow through P_L tube. The steady flow rate and $p_{e,c}$ are $0.083 \text{ m}^3/\text{s}$ and 0.16 kPa , respectively. The result is presented during 2 seconds of the developed

oscillations and sampling rate is 130 data/second which is some higher in this case in comparison with the above two sample cases. This is done in order to show here that the sampling rate can definitely be set with respect to user desire. It may even be lowered below 120 data/second; however this should cause the result to have a less precision. The range of p_1 and p_2 are $0.5\text{kPa} < p_1 < 3\text{kPa}$ and $-2\text{kPa} < p_2 < 2\text{kPa}$. These can be seen in the graph of p_1 and p_2 variations in Figure 5.5. p_2 seems to be more influenced due to oscillations in comparison with p_1 as in Figure 5.1 and Figure 5.3. Moreover \bar{p}_1 and \bar{p}_2 are calculated to be 1.37 kPa and 1.1 kPa, respectively. The velocity is oscillating between 2.5 m/s and 27.5 m/s thereby it results as $\bar{u}_{os} = 15.27 \text{ m/s}$.

The FFT analysis of Figure 5.5 has been shown in Figure 5.6. It is again found that it does not make any difference to determine f from FFT analysis of p_1 , p_2 or u_{os} variations with time. As a result f has been obtained to be 19.06 Hz corresponding to the peak magnitudes of the FFT result in three cases of Figure 5.6.

It can be concluded by referring to the sample figures that pressure and velocity magnitudes are affected by the oscillations although p_2 is more influenced than p_1 . However, the magnitudes change with respect to the flow conditions such as flow rate and external pressure as well as the tube type. Furthermore frequency of the oscillations can definitely be determined from FFT analysis performed to the velocity or pressure data. Additionally it has been seen that f varies according to the experimental flow conditions. Therefore the effects of h , L and Q on f and $p_{e,c}$ are investigated in the following section.

5.3. THE EFFECTS OF Q , h , L PARAMETERS ON $p_{e,c}$ and f

In this section all of the effects of Q , h , L on $p_{e,c}$ and f are studied and compared in detail. All of the other experimental results are obtained similarly to that are shown from Figure 5.1 to Figure 5.6. All these findings are presented from Table 5.1 to Table 5.9. However time variations of pressure and velocity are not given for all cases since only the sample figures have been presented. The experimental measurements just corresponding to the onset of oscillations are represented as

tabular forms for the test tubes. In each of these tables Q , $p_{e,c}$, \bar{p}_1 , \bar{p}_2 , \bar{u}_{os} and f values are presented for a specific tube. It is realized by examining these tables that \bar{p}_1 , \bar{p}_2 , \bar{u}_{os} , f and $p_{e,c}$ are seriously affected by Q , L and h . Therefore these are extensively studied in the following sections in graphical form to be more clearly understood.

5.3.1. Variation of f and $p_{e,c}$ with Q

Since Q has been seen to have an influence on $p_{e,c}$ and f , its effect is investigated by the plots through Figure 5.7 to Figure 5.9 which are drawn by referring to Tables 5.1-5.9. The results with Penrose tubes of different lengths are illustrated in Figure 5.7. It is clear that as Q increases f also increases slightly. For example if flow through P_L tube in Figure 5.7 is considered, it will be found that $f = 19$ Hz at $Q = 0.0083$ m³/s. However increasing Q to 0.0213 m³/s, f has the value of nearly 22 Hz. The similar behaviour is also observed for P_M and P_S tubes. In all cases of Figure 5.7, f is approximately in the range of $18\text{Hz} < f < 22\text{Hz}$ with respect to a wide range of $0.0083\text{m}^3/\text{s} < Q < 0.0213\text{m}^3/\text{s}$. Therefore it can be said that f is nearly 20 Hz for the Penrose tubes although Q has increased to 2.5 times of 0.0213 m³/s.

Similarly, it can be said by investigating Figure 5.7 that $p_{e,c}$ increases for a greater value of Q . However increase in $p_{e,c}$ is greater in comparison with that observed in f . For instance $p_{e,c}$ is 0.25 kPa at $Q = 0.0083$ m³/s for the case of P_M . It increases to 0.8 kPa and 1.6 kPa at Q of 0.015 m³/s and 0.0213 m³/s, respectively. In other words $p_{e,c}$ has increased to 6.4 times at $Q = 0.0213$ m³/s in comparison with 0.25 kPa. The similar behaviour can also be observed from the results related to P_L and P_S tubes.

The variations of f and $p_{e,c}$ with Q are demonstrated in Figure 5.8 for the silicone rubber tubes of 1 mm thick. If flow through $S_{1,L}$ in this figure is examined, it can be said that f and $p_{e,c}$ increase with Q as determined from the flow case through Penrose tube in Figure 5.7. However f does not take a constant value. It is approximately 20 Hz for $0.0101\text{m}^3/\text{s} < Q < 0.0162\text{m}^3/\text{s}$, but it is nearly 35 Hz at $Q = 0.0213$ m³/s. On the other hand $S_{1,M}$ and $S_{1,S}$ display somehow different behaviour. Because f is

decreasing with Q for these tubes unlike $S_{1,L}$. This may be an indication of certain effect of L on the flow and this effect will be explained in the next sections. The behaviour of $p_{e,c}$ is similar to the flow cases through Penrose tube in Figure 5.7.

The results for silicone rubber tube of 2 mm thick are given in Figure 5.9. It can easily be concluded that this tube has a different behaviour. Because both of $p_{e,c}$ and f decrease as Q increases. For example $f = 30\text{Hz}$ at $Q = 0.0101\text{m}^3/\text{s}$, but it has seriously decreased to nearly 20 Hz at $Q = 0.0195\text{m}^3/\text{s}$ related with flow through $S_{2,L}$ tube. Similarly $p_{e,c}$ values are approximately 9 kPa and 7.8 kPa corresponding to the same flow rate values, respectively. However it has been found in Figure 5.7 and Figure 5.8 that $p_{e,c}$ increases with Q . Therefore this finding should be due to the effect of tube thickness which will be analysed in the next parts.

5.3.2. Determination of the effect of L

As previously stated that length of the tubes, L has some effect on the experimental results which can also be seen by studying the resulting tables, it is investigated in this section. The cases given from Table 5.1 to Table 5.9 are plotted in Figure 5.10 and Figure 5.11 to analyse the influence of L . In Figure 5.10 variation of $p_{e,c}$ with Q is plotted for all of the tube lengths. Flow measurement results through Penrose tubes having different lengths are presented in Figure 5.10(a). It can be said that L has no much significance on $p_{e,c}$. Nevertheless, $p_{e,c}$ increases as L decreases. This can be verified for $Q = 0.0213\text{m}^3/\text{s}$ case. Moreover it can also be seen in Figure 5.10(b) which is plotted for the test with silicone rubber tube of 1 mm thick. $p_{e,c}$ values are approximately 2.5 kPa, 2.75 kPa and 3.4 kPa for the tubes of $S_{1,L}$, $S_{1,M}$ and $S_{1,S}$, respectively at $Q = 0.0213\text{m}^3/\text{s}$. This is also observed for the 2 mm thick silicone rubber tube. In summary it can be concluded that L has some effect on the determination of $p_{e,c}$ and as L decreases, $p_{e,c}$ increases. Higher $p_{e,c}$ necessary for a shorter tube means that as the tube becomes shorter it will be more difficult to collapse it since it may behave like a rigid tube.

The effect of L on f is shown in Figure 5.11. There is not such a clear result which has been obtained from Figure 5.10. Its influence on f is variable in different tubes.

Such as at a given Q , the value of f increases for a shorter tube in Figure 5.11(a) which is related to flow through Penrose tube. Similar behaviour can be observed from Figure 5.11(b) which is plotted for the flow through thin-walled silicone rubber tube. On the other hand, in Figure 5.1(c) related to the thick-walled silicone rubber tube, f increases with L for a specific Q . For instance, at $Q = 0.0101 \text{ m}^3/\text{s}$, $f = 32\text{Hz}$ for $S_{2,S}$, but $f = 35\text{Hz}$ for a longer tube, $S_{2,M}$. So that it may be concluded that L has some effect on f , but it is variable with respect to the tube type and wall thickness.

5.3.3. Determination of the effect of h

In this section the effect of thickness of the test tubes, h is studied. The overall effect of h on $p_{e,c}$ is given as plots in Figure 5.12. It is easily said by examining Figure 5.12(a) that the thicker tube wall causes $p_{e,c}$ to increase at a known Q value. For instance at $Q = 0.0101 \text{ m}^3/\text{s}$, $p_{e,c}$ is approximately 0.25 kPa, 2 kPa and 9 kPa for the flow through P_L , $S_{1,L}$ and $S_{2,L}$ tubes, respectively. This behaviour is also valid at other Q values.

It is again seen from Figures 5.12 (b,c) that as h becomes greater, $p_{e,c}$ also increases seriously. Figures 5.12 (a,b,c) are combined and the result is plotted in Figure 5.12(d). This figure is more explanatory in point of view of the effect of h , since it includes all of the test tubes. It should be said that the above finding is still valid. Furthermore, $p_{e,c}$ is nearly between 0.25 kPa and 2 kPa for all flow Q values and all lengths of Penrose tubes. It is changing between 2 kPa and 3 kPa for $S_{1,L}$, $S_{1,M}$ and $S_{1,S}$ tubes. However $p_{e,c}$ range has increased seriously for 2 mm thick silicone rubber tubes as $8\text{kPa} < p_{e,c} < 10\text{kPa}$, approximately regardless of Q .

The effect of h on f is shown with the plots given in Figure 5.13. It seems that f increases with increasing h at a given Q value. For example in Figure 5.13(a) $f = 20\text{Hz}$ at $Q = 0.0101 \text{ m}^3/\text{s}$ for $S_{1,L}$ tube, however $f = 30\text{Hz}$ for $S_{2,L}$ tube. Similarly this conclusion can also be seen in Figures 5.13(b,c). Figure 5.13(d) is a combination of Figures 5.13(a-c) similar to Figure 5.12(d). It may be deduced by referring to this combined figure that f is in the range of 20 Hz, approximately for all lengths of Penrose tubes. However a range of $20\text{Hz} < f < 25\text{Hz}$ is seen for all

lengths of thin-walled silicone rubber tube. Finally it is clear that f takes values as $25\text{Hz} < f < 35\text{Hz}$ for thick-walled silicone rubber tubes of different lengths. Therefore Figure 5.13(d) is a better representation rather than separately Figures 5.13(a-c) to understand the effect of h on f .

As a summary to explain the influence of h it can be concluded that as h increases f and especially $p_{e,c}$ increase. However the functional relationship is missing.

5.4. EVALUATION OF EXPERIMENTAL RESULTS IN TERMS OF DIMENSIONLESS PARAMETERS

In this section the experimental measurement results listed through Table 5.1 to Table 5.9 were studied to express them as non-dimensional parameters. So that mean flow resistance defined as

$$\frac{(\bar{p}_1 - \bar{p}_2)A_0}{\bar{u}_{os}\rho_f\nu_f L} \quad (5.1)$$

where A_0 is the cross-sectional area of the circular tube. Equation (5.1) has been selected as a reasonable parameter which was already introduced similarly and used in [45]. However the mean flow resistance defined with (5.1) is not the same as that given in [45]. It was expressed in that study as $\frac{(\bar{p}_1 - \bar{p}_2)A_0^2}{Q_{os}\rho_f\nu_f L}$ where Q_{os} is the mean flow rate of oscillating flow and they measured it instead of \bar{u}_{os} . One can easily see that $Q_{os} = \bar{u}_{os}A_0$ since \bar{u}_{os} was actually measured by means of hot wire anemometer fixed on the downstream rigid pipe as described previously in Chapter 3. As a result equation (5.1) can be written in reference to [45].

This parameter should have significance in the point of view that it includes information about both of flow ($p_1, p_2, u_{os}, \rho_f, \nu_f$) and tube (D_0, L) so that one can get a general result on the collapsible tube flow investigations. Actually it may also be called as Reynolds number of oscillating flow although such an approach has not been defined in [45]. Since $(\bar{p}_1 - \bar{p}_2)/\rho_f$ is a parameter corresponding to square of

velocity, namely it can be regarded as $(\bar{u}_{os})^2$. The remaining parameters are written to make equation (5.1) as a dimensionless term. Then there remain only velocity times a characteristic length divided by ν_f and it may therefore be regarded as a Reynolds number of oscillating flow.

The dimensionless parameter given in equation (5.1) has been plotted versus dimensionless downstream transmural pressure as

$$(\bar{p}_2 - p_{e,c})/K_p \quad (5.2)$$

which is again selected as the second dimensionless parameter in [45] with the only difference being that p_e was present in that study instead of $p_{e,c}$ which is already the new terminology defined in the present investigation. Note that mean downstream transmural pressure has been made a non-dimensional parameter by dividing it to the circumferential bending stiffness of the tubes, K_p (equation 3.1) which is in the unit of pressure, Pascal.

In Figure 5.14 (a) the result is plotted for P_L, P_M and P_S tubes. It is interesting that there are two regions which show different behaviours. For example if the case of P_M is considered, in the first part the mean flow resistance increases with higher mean downstream transmural pressure. However, the flow resistance increases with the lower downstream transmural pressure in the second part. Namely, $\frac{(\bar{p}_1 - \bar{p}_2)A_0}{\bar{u}_{os}\rho_f\nu_f L}$ is nearly 950 and 1600 corresponding to $(\bar{p}_2 - p_{e,c})/K_p$ of 42 and 58, respectively. On the other hand the resistance values are nearly 4500 and 5500 for the $(\bar{p}_2 - p_{e,c})/K_p$ of 62 and 40, respectively. The similar trend can be observed from the variations related to P_L and P_S tubes. The highest resistance value of 15000 is seen for the shortest tube, P_S at non-dimensional mean downstream transmural pressure of 58. After all, it can be said that $(\bar{p}_2 - p_{e,c})/K_p$ values remain in the positive range for the experiments with Penrose tubes.

The similar graph has been plotted for the silicone rubber tubes in Figure 5.14(b). It is readily observable that thick-walled silicone rubber tubes show a different behaviour than thin-walled silicone rubber tubes. It is understood that mean flow resistance increases linearly with lower mean downstream transmural pressure for the flow through thick-walled silicone rubber tube. The similar behaviour had also been observed in [45] in which flow of water through a thin-walled ($h = 0.2\text{mm}$) Penrose tube was studied. For instance $(\bar{p}_1 - \bar{p}_2)A_0 / \bar{u}_{os}\rho_f\nu_f L$ values obtained from the test with $S_{2,S}$ tube are 7500 and 21500 for $(\bar{p}_2 - p_{e,c})/K_p$ values of approximately -7 and -11, respectively. Furthermore the resistance also increases with the shorter tube length. $(\bar{p}_1 - \bar{p}_2)A_0 / \bar{u}_{os}\rho_f\nu_f L$ values are in a band between 2500 and 7500 for the longest tube, $S_{2,L}$. In contrary, mean flow resistance increases with higher mean downstream transmural pressure for the experiments with the silicone rubber tubes of 1 mm thick. The cases with $S_{1,M}$ and $S_{1,S}$ tubes are very similar in behaviour, i.e. the obtained experimental data linearly increases for the test by using these tubes. The data is not linearly changing for the case of $S_{1,L}$ tube. Finally it can be concluded that $(\bar{p}_2 - p_{e,c})/K_p$ values remain in the negative range only for the tests carried out with thick-walled silicone rubber tubes. However there are both of positive and negative downstream transmural pressure ranges for the experiments with thin-walled silicone rubber tubes.

Another useful dimensionless parameter is *Womersley number* (W) which had been used also in [45] can be determined with the following equation:

$$W = \sqrt{\frac{2\pi f R_0^2}{\nu_f}} \quad (5.3)$$

This parameter has been plotted with respect to another dimensionless pressure as

$$(\bar{p}_2 - p_{e,c})/(\bar{p}_1 - \bar{p}_2) \quad (5.4)$$

and the experimental results are shown in Figure 5.15 for all of the test tubes. The result is shown for Penrose tubes in Figure 5.15(a). This figure clearly indicates that

W linearly increases as the non-dimensional pressure term defined by equation (5.4) decreases. Furthermore the behaviour seems to be not affected by the length of Penrose tubes. All of the experimental data points are nearly coinciding. For example W is 35.5 and 39 corresponding to $(\bar{p}_2 - p_{e,c})/(\bar{p}_1 - \bar{p}_2)$ values of 3.5 and 0.25, respectively regardless of L . Therefore the experimental data in Figure 5.15(a) can be represented by the following relationship:

$$W = -0.875(\bar{p}_2 - p_{e,c})/(\bar{p}_1 - \bar{p}_2) + 39 \quad (5.5)$$

Equation (5.5) is valid for the Penrose tube regardless of L and the data experimental data scattering from this equation is in the order of $\pm 2\%$.

It is remarked here that $W = 27$ in [45] based on downstream pressure fluctuations. It is seen that W is lower than the present investigation's range due to the fact that they've tested a smaller diameter Penrose tube ($D_0 = 12\text{mm}$) in comparison with the tubes used in the present investigation. Actually the authors of that study have not shown a plot similar to Figure 5.15 of this study.

If thin-walled silicone rubber tubes are considered as shown in Figure 5.15(b), it can be said that W is not affected so much by the increase or decrease of $(\bar{p}_2 - p_{e,c})/(\bar{p}_1 - \bar{p}_2)$ and it changes as $35 < W < 40$ in this figure. However there is only one experimental data which has a W of 50 related to $S_{1,L}$ tube. This should be due to the higher f value measured in the experiment. Similarly W has a value between 45 and 50 in Figure 5.15(c) related to the experiments with thick-walled silicone rubber tubes. It can be seen that since experimental data is scattered in Figures 5.15(b,c), it was not possible to fit a curve to the data like Equation (5.5).

The combined form of Figures 5.15(a-c) is shown in Figure 5.15(d). It is clear in this figure that W slightly increases as h increases. It is also understood that experimental results with Penrose tubes figures out that the dimensionless pressure parameter defined by equation (5.4) is in the positive range. However it has always negative values for the results obtained from testing of silicone rubber tubes. In addition the

effect of L on the on the variation of W with $(\bar{p}_2 - p_{e,c})/(\bar{p}_1 - \bar{p}_2)$ seems to be insignificant.

The next dimensionless term which is related to mean oscillating velocity has been selected from [45] as

$$\frac{\bar{u}_{os}}{\sqrt{K_p / \rho_f}} \quad (5.6)$$

Note that $\sqrt{K_p / \rho_f}$ has the unit of velocity and equation (5.6) is therefore dimensionless. It is necessary to emphasize that the same rule is followed here similar to writing (5.1). In their study [45] the parameter is $Q_{os} / (A_0 \sqrt{K_p / \rho_f})$. It is again remembered that since $Q_{os} = \bar{u}_{os} A_0$, the parameter in (5.6) has therefore been obtained. The variation of $Q_{os} / (A_0 \sqrt{K_p / \rho_f})$ with $(\bar{p}_2 - p_e) / K_p$ was studied in [45] and $Q_{os} / (A_0 \sqrt{K_p / \rho_f})$ was nearly constant at 0.25, approximately regardless of $(\bar{p}_2 - p_e) / K_p$.

In Figure 5.16, the dimensionless velocity has been plotted versus non-dimensional pressure term defined by equation (5.4) instead of (5.2), since dimensionless velocity defined with equation (5.6) itself already includes K_p as in the case of equation (5.2). The result obtained with the test of Penrose tubes is presented in Figure 5.16(a). A cursory survey of this figure points out that dimensionless mean oscillating velocity increases as the dimensionless mean downstream transmural pressure decreases regardless of L . There is a range of $5 < \bar{u}_{os} / \sqrt{K_p / \rho_f} < 17.5$ corresponding to dimensionless mean downstream transmural pressure range between 4 and 0.25. Moreover the following equation was obtained by fitting an exponential curve to the experimental data in Figure 5.16(a):

$$\frac{\bar{u}_{os}}{\sqrt{K_p / \rho_f}} = 9.202 \left(\frac{\bar{p}_2 - p_{e,c}}{\bar{p}_1 - \bar{p}_2} \right)^{-0.325} \quad (5.7)$$

Equation (5.7) is related to the flow through Penrose tubes regardless of L and it results in a maximum error margin of 20% .

The result obtained from experiment with thin and thick-walled silicone rubber tubes is shown in Figure 5.16(b). In contrary to Figure 5.16(a), dimensionless velocity increases with higher dimensionless transmural pressure. In this case the effect of L is also not so much important. However it is noted that the thin-walled silicone rubber tube has a greater value of dimensionless velocity. In other words, the result with thick-walled silicone rubber tube gives $0.5 < \bar{u}_{os} / \sqrt{K_p / \rho_f} < 1.5$, but it yields as $1.5 < \bar{u}_{os} / \sqrt{K_p / \rho_f} < 4$ for the experiment with thin-walled silicone rubber tubes. Although the experimental data in Figure 5.16(b) seem to be linearly changing, a curve could not be fitted to them to propose an empirical relationship due to scattering of the data.

Similarly, Figure 5.16(c) has been plotted in a combined manner to show the result obtained from the experiments with testing all of the tubes. The conclusions drawn by examining Figures 5.16(a,b) are more clearly observed in the combined figure. It should be emphasized that the dimensionless velocity values are higher for Penrose tubes in comparison with silicone rubber tubes.

5.5. CONCLUSION

In this chapter the results of experimental measurements are presented in detail. The measurements correspond to the instant at which self-excited oscillations arise due to the collapse of the tube under the applied external pressure. It has been found that pressure and velocity signals fluctuate seriously with time during oscillations. In unsteady cases, the tube is observed to inflate and collapse in harmony with the oscillating p_2 and the oscillating tube shapes remain partially collapsed at downstream of the tube. Also p_2 seems to be more affected by the oscillations (for example, see Figure 5.3). These points have already been emphasized in Section 5.2 clearly. The magnitudes which reveal this finding in reference to Figures 5.1, 5.3 and 5.5 are presented in that section. Furthermore frequency of the oscillations may be

determined by FFT analysis of velocity or pressure data (Figures 5.2, 5.4 and 5.6). It has been concluded by observing these figures that f values can be obtained by FFT analysis carried out on velocity or pressure data. This can be verified due to the fact that both of the operations result in the same f .

After presenting some sample cases of time dependent pressure and velocity measurement result, all of the other experimental results are given in tabular form and then the graphical representations of these tables are indicated by the plots from Figure 5.7 to Figure 5.13 in Section 5.3. It has been realized by examining these figures that $p_{e,c}$ and f are influenced by the tube properties such as h , L , E as well as flow rate. It is seen that f and particularly $p_{e,c}$ are much more affected by h in comparison with L . Therefore all of these parameters suggested to be carefully taken into consideration in collapsible tube flow investigations.

Moreover the relationships between some dimensionless parameters determined from [45] are presented in Section 5.4 as shown from Figure 5.14 to Figure 5.16. It is seen that these dimensionless parameters have also been affected by Q , L , h as well as the tube's material type. Meanwhile, it was found by considering equations (5.5, 5.7) that an empirical correlation could be proposed for the experimental data obtained with Penrose tube tests. On the other hand, it was not possible to fit a curve to the data related to the experiments with silicone rubber tubes. This may be a clear indication of the fact that the tube material is definitely significant for the collapsible tube flow investigations. Finally, the suggested dimensionless parameters which are defined with equations (5.1-5.4, 5.6) are significant because of the fact that they include many of the factors related to flow ($\bar{p}_1, \bar{p}_2, f, p_{e,c}, \bar{u}_{os}, \rho_f, \nu_f$) and tube (D_0, L, h, K_p). Therefore these non-dimensional terms should be useful in further studies.

CHAPTER 6

THEORETICAL CALCULATIONS OF FREQUENCY and COMPARISON WITH MEASUREMENTS AT THE ONSET OF OSCILLATIONS

6.1. INTRODUCTION

In this chapter, the experimental measured frequency values presented in Chapter 5 are studied to be determined theoretically. The basic tools in the theoretical calculations are the linear stability theory which determines the onset of oscillations and the tube law. These are expressed in the following sections.

6.2. LINEAR STABILITY THEORY

The linear stability analysis has been introduced and used in reference [13]. As an overview to the linear stability analysis, the mathematical method used to find out the critical velocity that causes onset of oscillations is to assume that waves of unknown wavelengths are travelling along the tube wall, deforming both the wall and fluid. For any wavelength, there is a fluid speed that causes the corresponding wave amplitude to grow. Those fluid speeds will have different values for the different possible wavelengths of the assumed waves. The lowest fluid speed is the critical one (u_c). Once that information is known, the corresponding frequency, f associated with u_c is obtained. The following equations have been proposed in [13]:

$$S(k) = \left[\frac{(1 + Tk^2 + Bk^4) \tanh k}{Ma^2 k^2 \tanh k + k(1-a)^2} \right]^{1/2} \quad (6.1)$$

$$\omega^*(k) = akS \quad (6.2)$$

where ω^* is the dimensionless angular frequency and k is the dimensionless wave number.

$$a = G(G + Mk \tanh k)^{-1} \quad (6.3)$$

S expressed with equation (6.1) is the speed index defined by

$$S = \frac{u_c}{c} \quad (6.4)$$

u_c is the critical oscillation velocity and c is the speed of long waves which is exactly similar to equation (2.9) and defined as

$$c = \sqrt{E_w b / \rho_f} \quad (6.5)$$

where E_w is the elastance (tube law) which can be determined by

$$E_w = \frac{dp_m}{db} \quad (6.6)$$

b is the half distance between the opposing walls of the buckled tube and ρ_f is the fluid density. In equation (6.1) T is the longitudinal tension and B is the bending stiffness to elastance ratio:

$$B = \frac{Eh^3 / 9}{E_s b^3} \quad (6.7)$$

where E is the modulus of elasticity of the tube material, h is the wall thickness and E_s is the specific elastance:

$$E_s = b \left(\frac{dp_m}{db} \right) \quad (6.8)$$

M in equation (6.1) is the wall to fluid mass ratio:

$$M = \rho_w h / \rho_f b \quad (6.9)$$

where ρ_w is the wall density. G in equation (6.3) is the ratio of fluid friction to wall damping:

$$G = \frac{R_f}{R_w} \quad (6.10)$$

where R_f is the friction factor of fluid given by

$$R_f = \frac{3v_f}{2b^2} \quad (6.11)$$

R_w is the wall damping coefficient which determines the rate at which oscillations, once started, will decay if the driving force is removed.

The graph of $S(k)$ versus k has been plotted in [13] as shown in Figure 6.1. The parameter values are $D_0 = 6.5\text{mm}$, $h = 1.9\text{mm}$, $\rho_w = 941 \text{ kg/m}^3$, $E = 1 \times 10^6 \text{ N/m}^2$, $E_w = 6 \times 10^6 \text{ N/m}^3$, $T = 0$, $R_w = 1.72/\text{s}$, $b = 0.7 \text{ mm}$, $\rho_f = 0.8 \text{ kg/m}^3$ (at -200 mm-Hg) and $v_f = 2.25 \times 10^{-5} \text{ m}^2/\text{s}$. The fluid friction is determined from (6.11) to be $R_f = 3v_f / 2b^2 = 68.9/\text{s}$. Inserting these values into the above equations it has been found that $M = 3193$, $B = 529$ and $G = 40$.

In Figure 6.1 all velocities above the curve are unstable for the enclosed band of wave numbers. In any flow situations, the speed starts from zero and increases to the desired level. As S increases from zero, the first reached instability is at the minimum of the curve $S(k)$. The minimum occurs in Figure 6.1 at the critical wave number $k = 0.1$. The dimensionless critical oscillation velocity has been calculated as $S = 0.3$. This calculated k and S values are then inserted into equation (6.2) and the dimensionless critical oscillation frequency has been determined as

$\omega^* = akS = 0.0179$. Note that a is calculated from (6.3) as $a = 0.557$. c is computed as 72.5 m/s from equation (6.5). Subsequently u_c can be found from equation (6.4) as $u_c = 21.7$ m/s. The dimensional equivalent of ω^* is the angular velocity (ω) which is determined by

$$\omega = \frac{\omega^* c}{b} \quad (6.12)$$

The dimensional counterpart of ω is the oscillation frequency which can be obtained with

$$f = \frac{\omega}{2\pi} \quad (6.13)$$

Therefore inserting the values of ω^* , c and b into equation (6.12), ω has been determined in [13] as 1854 rad/s. Then f can be calculated from equation (6.13) to be 295 Hz. These predictions agree well with the measurements of airflow through a thick-walled latex tube in reference [8] when the tube initiated oscillations.

It has been noted that for all S lower than minimum of S in Figure 6.1, the system is stable according to the linear stability theory, so it has been seen that it takes a large enough fluid velocity to cause flutter.

In this chapter predictions of the linear stability theory are compared with experimental data taken immediately at the onset of oscillations (Chapter 5), that is the data represent initial oscillations. The curves similar to Figure 6.1 have been plotted for the test tubes. In the calculations wall-damping coefficient R_w has been selected as 3.5/s, 2/s and 0.5/s for the thick-walled silicone rubber tube, thin-walled silicone rubber tube and Penrose tube, respectively. Actually these could not be measured so that they have been determined with reference to the study [8] in which $R_w = 1.72$ /s for the 1.9 mm-thick latex tube. In the present investigation $h = 0.55$ mm for Penrose tube (latex) and R_w is reasonably taken as 0.5/s. In reference [8] $R_w = 3.48$ /s for 1.9 mm-thick silicone rubber tubes, thereby R_w parameters are

evaluated as 3.5/s for 2 mm-thick silicone rubber tubes and 2/s for 1 mm-thick silicone rubber tubes.

Another point related to equation (6.5) is the determination of E_w , representing the tube law which is a non-linear relationship between transmural pressure across the tube wall and cross-sectional area of the tube. Since it has not been measured experimentally in this study, a generalized tube law by Jaekle [69] has been used. So that the tube law calculations are explained in the next section.

6.3. TUBE LAW CALCULATIONS

A generalized tube law derived in [69] is utilized in this investigation. The relation he derived is given by the equation:

$$P(\alpha) = -8.1494 - 0.00468\alpha^{-3.6797} + 2.526\alpha^{73.75} + 4.9944\alpha - 0.3917\alpha^{-1.5} \quad (6.14)$$

where $\alpha = A/A_0$ is the dimensionless area ratio. This tube law relation is assumed to hold true for any tube of tapered thickness. The relation had been also used in the experimental study [7] in which a tapered tube was tested for the investigation of air flow through it. Jaekle [69] has calculated tube law defined in equation (6.14) by fitting a curve to the data from several different tubes. $P(\alpha)$ is the dimensionless tube law which is expressed by

$$P(\alpha) = \frac{p_{tm}}{K_p} \quad (6.15)$$

The tube law obtained according to equations (6.14 and 6.15) is given separately for silicone rubber tubes and Penrose tubes in Figure 6.2. It is understood by examining the graphical representation of tube law results in Figure 6.2 that there is a region in which a small decrease in p_{tm} causes a large decrease in A . The tube is highly deformable in this region. For example consider the case for silicone rubber tube of 1 mm thick in Figure 6.2. p_{tm} is -650 Pa at $A = 3 \times 10^{-4} \text{ m}^2$, but decreasing p_{tm} to -850 Pa causes A to be $2 \times 10^{-4} \text{ m}^2$. It is seen that there is a change in A of $1 \times 10^{-4} \text{ m}^2$

corresponding to decrease in p_{tm} of 200 Pa only. Namely A has been decreased by 33% as comparable to a small change in p_{tm} .

However, there is not such behaviour in some part of the tube law graphics in Figure 6.2. The tube is stiffer in such cases. For instance $A = 6.13 \times 10^{-5} \text{ m}^2$ at $p_{tm} = -3000$ Pa for the 1 mm-thick silicone rubber tube, but lowering p_{tm} to -4000 Pa, A can be determined as $5.37 \times 10^{-5} \text{ m}^2$. It means that there is a contraction of area about 12.4% for a decrease in p_{tm} of 1 kPa. Therefore these two regions are comparable to each other with respect to the above numerical explanations. The similar conclusions can be drawn by studying the other two plots in Figure 6.2.

Although the test tubes in the present investigation are not tapered, i.e. they have uniform wall-thickness; equation (6.14) has been used in the calculations. Therefore it may be satisfied that whether Jaekle's tube law can also be valid for the tubes of uniform thickness.

There seems to be a difficulty related to equation (6.6) which indicates that it is necessary to know $p_{tm} = p_{tm}(b)$. However it is clearly seen from equation (6.15) that $p_{tm} = p_{tm}(\alpha)$. Thus the relationship between A and b should be known to have $p_{tm} = p_{tm}(b)$. Actually A and b parameters have not been measured in the present study. Therefore it has been tried to be derived from reference [8]. There are two tables in that study (Table 2 and Table 3 of [8]) which list A values corresponding to b values as well as some flow parameters. These can be made dimensionless as A/A_0 and b/D_0 . In reference [8] D_0 is 6.5 mm and A_0 is thereby 33.18 mm^2 . The experimental relationship between A/A_0 and b/D_0 which is obtained from [8] has been plotted and presented in Figure 6.3. Therefore the following relationship may be proposed as an approximation by fitting a curve to the data of Figure 6.3 in the following exponential form:

$$\frac{A}{A_0} = 0.36e^{4.80(b/D_0)} \quad (6.16)$$

It is now proper to write equation (6.15) as $p_{im} = K_p P(\alpha)$. Here $P(\alpha)$ is defined with equation (6.14), but in this case equation (6.16) which represents dimensionless area ratio is inserted in place of α . As a result the obtained relation is given by

$$p_{im} = K_p \left[\begin{array}{l} -8.1494 - 0.00468 \left(0.36 e^{4.80 \frac{b}{D_0}} \right)^{-3.6797} + 2.526 \left(0.36 e^{4.80 \frac{b}{D_0}} \right)^{73.75} \\ + 4.9944 \left(0.36 e^{4.80 \frac{b}{D_0}} \right) - 0.3917 \left(0.36 e^{4.80 \frac{b}{D_0}} \right)^{-1.5} \end{array} \right] \quad (6.17)$$

Note that D_0 is 0.0254 m in this study. Finally, $E_w = \frac{dp_{im}}{db}$ can be obtained:

$$\frac{dp_{im}}{db} = K_p \left(\begin{array}{l} 139.62 e^{-695.06b} + 6.664 \times 10^{-29} e^{13930.62b} \\ + 339.62 e^{188.89b} + 513.81 e^{-283.34b} \end{array} \right) \quad (6.18)$$

Once having the information of K_p , equation (6.18) can be computed and thereby E_w has been determined corresponding to a given b value.

6.4. CALCULATIONS OF f & u_c BY USING LINEAR STABILITY THEORY and COMPARISON WITH EXPERIMENTAL DATA

The functional form of equation (6.1) is graphically represented for all test tubes used in this study by evaluating the necessary parameters outlined in Section 6.2. The variations of S with k are given in Figure 6.4 for Penrose tube, thin-walled silicone rubber and thick-walled silicone rubber tubes. It is clear in equation (6.18) that E_w has not a constant value, but it changes with respect to the b value. Figure (6.1) has been plotted in [13] for the case of $b = 0.7$ mm, namely $b/D_0 = 0.108$ can be found in the account of $D_0 = 6.5$ mm. Therefore b is selected as 0.0027 m as an initial step for the calculations ($D_0 = 0.0254$ m in this study) by considering $b/D_0 = 0.108$ in reference [13]. As a result Figure 6.4 has been plotted as a sample representation regarding $b = 0.0027$ m. Then frequencies at the onset of oscillations are calculated

for a range of b value, similarly to the procedure explained in the linear stability theory (Section 6.2).

It is seen in Figure 6.4 that minimum value of S is 0.772 at $k = 0.19$ for Penrose tube which has a density of $\rho_w = 1020 \text{ kg/m}^3$. In this case wall-damping coefficient, R_w is 0.5/s which has been already explained in Section 6.2. E_w is calculated to be 8715 N/m^3 with $b = 0.0027 \text{ m}$. Then the following parameters are calculated to be $a = 0.49$, $c = 4.43 \text{ m/s}$, $\omega^* = akS = 0.072$, $\omega = 118.84 \text{ rad/s}$, $f = 18.91 \text{ Hz}$ and $u_c = 3.42 \text{ m/s}$. Note that this calculated frequency value well remains in the range of experimental findings in Chapter 5.

Results with thin-walled silicone rubber tube ($\rho_w = 1200 \text{ kg/m}^3$) can be examined similarly from Figure 6.4. It has been found that the minimum of the curve occurs at $k = 0.17$ and $S = 1.052$. The parameters used in the calculations are $R_w = 2/s$ for 1 mm thick silicone rubber tube and $b = 0.0027 \text{ m}$. Thereby $E_w = 8.86 \times 10^4 \text{ N/m}^3$, $c = 14.12 \text{ m/s}$, $u_c = 14.86 \text{ m/s}$, $a = 0.124$, $\omega^* = 0.022$, $\omega = 116.4 \text{ rad/s}$ and $f = 18.53 \text{ Hz}$. This predicted f value is also in the range of experimental measurements presented in Chapter 5.

The next result with testing of silicone rubber tube ($\rho_w = 1200 \text{ kg/m}^3$) of 2 mm thick is seen in Figure 6.4. It is seen in the relationship between S and k that S has a minimum value of 1.037 corresponding for $k = 0.16$. R_w is 3.5/s in this case. Similarly the parameters calculated are $a = 0.044$, $E_w = 7.09 \times 10^5 \text{ N/m}^3$, $c = 39.94 \text{ m/s}$, $u_c = 41.44 \text{ m/s}$, $\omega^* = 0.0073$, $\omega = 107.5 \text{ rad/s}$ and so that f is predicted to be 17.12 Hz at the onset of oscillations. It should be remembered here that b is chosen to be 0.0027 m for these calculations.

It is understood that the frequency values are in the band of experimental measurements and it can be concluded that the selected $b/D_0 = 0.108$ is a good approximation to start the calculations for determining some parameters at the onset of oscillations.

After the mentioned calculations, the relationship between b and f has been studied to obtain it. For a range of b including $b=0.0027$ m, f values at the onset of oscillations have been computed similarly. It should be noted that E_w changes at each b value, therefore S and the other parameters in linear stability calculations change as well as f . As a result Figure 6.5 has been obtained for this purpose by using the theoretical method outlined in this chapter. This figure shows the variation of f with b for the test tubes at the oscillations onset. In all three cases of this figure it is so clear that f is obviously influenced by the change of b , namely f increases with decreasing of b regardless of the tube type. However, effect of b seems to be more prominent for the silicone rubber tubes in comparison with Penrose tube. The behaviour of the trend related to Penrose tube is not as sharp as that related to silicone rubber tubes. In summary, as the distance between walls is decreased, a higher oscillation frequency should be expected at the onset of oscillations.

After having the information of relation between b and f , it is desired to know $\alpha = A/A_0$ at the onset of oscillations. This can be obtained easily since previously the relationship between A/A_0 and b/D_0 has been found as illustrated in Figure 6.3. Once f is known, b may be predicted from Figure 6.5, thereby α is determined from Figure 6.3. Furthermore S , c and u_c values can be computed in accordance with the b value. These calculations have been done and the results are given in Table 6.1, Table 6.2 and Table 6.3 for the test tubes. These tables indicate the flow rate Q and steady mean flow velocity \bar{u} as well as measured frequencies at the onset of oscillations. Meanwhile b values are predicted by considering the measured f and by referring to Figure 6.5. The oscillation frequencies are also calculated for the predicted b value by linear stability theory and computed f values are also given in these tables for comparison. A/A_0 ratios are found from Figure 6.3 with respect to the selected b value and the predictions for the dimensionless area ratio are presented in the tables. Finally, c and minimum value of S which causes the oscillations to develop are calculated according to the b value; so that the velocity which corresponds to the oscillations onset, u_c are given in these tables.

Table 6.1 is related to Penrose tubes. It can be said that b is approximately accepted as an average value of 0.0021m. Then it may be understood that A/A_0 can be regarded as 0.54 for the covered test cases. It is interesting that since $u_c < c$, S values are less than one for the test with Penrose tubes. S is nearly 0.7 for the cases. If $S = 1$ case is the critical case as cited widely in the literature, then $S < 1$ case can be regarded as sub-critical. Therefore it can be concluded that the oscillations arise for the Penrose tube even flow is sub-critical similar to the reference [13]. Another point which is worthy to state that critical oscillation velocities are lower than measured velocities $u_c < \bar{u}$, so that oscillations may well have been generated. It is certainly known that the oscillations have already developed and the data in the table is obtained at the onset of oscillations.

In Table 6.2 the results related to thin-walled silicone rubber tube are presented. The b value has an average of 0.0025 m and A/A_0 is approximately 0.59 for the covered cases. In this case oscillations develop at some greater value of A/A_0 in comparison to Penrose tube. Furthermore S values are seen to be slightly greater than unity, i.e. oscillations originate for supercritical condition ($S > 1$). Therefore it can be said that the properties of the tube is important while determining the case that whether oscillations generate at sub-critical or supercritical flow condition. As in Table 6.1, here $u_c < \bar{u}$ also, that is it can be expected that oscillations may have been arisen in the flow.

The next one is Table 6.3 which is associated with the results obtained by testing of thick-walled silicone rubber tube. In the covered range b is nearly 0.0022 m which can be expressed in terms of A/A_0 as 0.56. Therefore it may be said by referring these three tables that oscillations will be generated when $0.55 < A/A_0 < 0.6$, approximately. S is also greater than unity in Table 6.3 similarly to Table 6.2. Therefore silicone rubber tubes have a different effect in comparison with Penrose tubes. Meanwhile it is noticeable from Table 6.3 that oscillations have been present even $u_c > \bar{u}$ for some cases such as flow through $S_{2,S}$ tube at $Q = 0.0147 \text{ m}^3/\text{s}$, $\bar{u} = 29.01 \text{ m/s}$, but u_c has been predicted to be 37.17 m/s. It is known that if $u_c < \bar{u}$, oscillations may have developed and otherwise they cannot be expected to be

present. However all of the cases in Table 6.3 are absolutely related to the oscillations onset. The reason of this situation may be attributed to the properties of the tube. It should be noted by referring to the last three tables that calculated frequencies in accordance with the reference b values are in conformity of the experimental measurements. Furthermore the indicated b values are reasonable in magnitude accompanying the reference [8].

6.5. CONCLUSION

The experimental measurements presented in Chapter 5 are studied to be determined theoretically. It has been found first of all that the dimensionless tube law derived by Jaekle in equation (6.14) is proper to be used for the calculations. Although it has been obtained from testing of tubes which have tapered wall thickness, it is realized that this correlation may even be utilized for tubes of uniform wall thickness as used in this present study.

Furthermore, the linear stability theory is apparently a valuable tool for the collapsible tube flow investigations. However there is a difficulty to determine R_w and b parameters which will be used in the calculations. Actually they are not easy to be measured and especially there is a lack of information on R_w in the literature except for the studies given in references [8,13]. In the calculations of this chapter these two parameters have therefore been selected by referring to these papers. Nevertheless the theoretical predictions have been seen to remain in the range of experimental measurements of this study. Therefore it can be concluded that the linear stability theory should be a strong tool to predict some parameters such as f , S and u_c at the onset of oscillations generated frequently in the flow through collapsible tubes.

CHAPTER 7

CONCLUSION AND SUGGESTIONS FOR FURTHER INVESTIGATIONS

In this chapter general conclusions drawn from the experimental study of airflow through collapsible tubes are presented and the necessary works for the related future investigations are suggested.

Literature survey has pointed out that the subject is significant due to its relevance to physiological flows and biomechanical applications. Therefore related studies are continuing. The self-excited oscillations which often generate for the flow case through soft walled elastic tubes make flow complex due to highly fluid-structure interaction. Therefore these oscillations and their basic mechanism have been studied in the experimental and theoretical investigations.

An experimental set-up as shown in Figures 3.2 was constructed by referring to the available literature to investigate airflow through collapsible elastic tubes. In the previous experimental studies on collapsible tube flows water was preferred as fluid. There is a lack of experimental study with air. Another contribution of this study is that several tube types such as Penrose tube and silicone rubber tube were tested. The silicone rubber tubes had 1 mm 2 mm and 3 mm thickness while Penrose tube was 0.55 mm thick. Furthermore their lengths were changed for three cases as ratio of length to inside diameter were 10, 7.5 and 5. However in the available literature, the properties of the tube have been constant, such that only one type of tube was tested, in general. Therefore much more behaviour of the collapsible tube flows should be emerged by testing tubes with a wide range.

One advantage of the investigation may be the applicability of hot wire anemometer to measure the oscillating flow velocity. In the previous collapsible tube flow studies almost no investigators have used hot wire anemometer. The constructed

experimental set-up was verified to be proper for the collapsible tube flow research by referring to the obtained results. It was seen that oscillations generated according to flow rate magnitude and tube type. The 3 mm thick silicone rubber did not show oscillating flow case at all. On the other hand Penrose tube had shown oscillatory flow cases regardless of Q , if the necessary $p_{e,c}$ had been applied. In addition silicone rubber tube of 1 mm and 2 mm resulted in oscillating case or non-oscillating case depending on the flow rate and external pressure magnitude. All these clearly explained that as well as flow conditions even the tube itself can determine that whether flow will be oscillating or not. As a result the thickness, diameter, length and material type are very important factors in the related investigations.

A set of experimental test case had been formed and these data actually corresponded to the onset of oscillations. It was shown that upstream and downstream pressures as well as flow velocity seriously fluctuated during the oscillations. Also p_2 was seen more affected in comparison to p_1 . The FFT analysis of these measurements revealed the frequency of the oscillations. The relationship between f , $p_{e,c}$, Q , h , L for each of the tube type was studied to be determined.

Some theoretical calculations related to linear stability theory according to reference [13] had also been done to compare with the experimental data. The calculated frequency values were in the range of measured frequency at the onset of oscillations. Therefore, this matching had emphasized importance of the experimental results in point of view of their reliabilities. By the way, the applicability of Jaekle's universal tube law in equation (6.14) for tapered wall thickness tubes had been used to know that whether it could be also used for tubes of uniform wall thickness. The calculations seemed to satisfy this condition by paying attention to the obtained results of the present study in which tubes of uniform wall thickness had been tested. However this point remains a gap and needs to be checked in further studies.

As a result this extensive range experimental study should be useful for the future investigations with respect to its presented results. The investigation will continue by using a *mass flow rate controller system* adapted to the experimental set-up.

In the future studies the followings can be suggested to have much more information about such a complex flow:

1. The pressure-flow behaviour of collapsible tube flows with air should be researched. In this study, actually the system did not enable to observe this since upstream transmural pressure could not be fixed. In the literature it is cited that much more information can be obtained from such a characteristic curve. In water flows this can be easily achieved in comparison with airflow.
2. The flow limitation case should be studied since it has been considered to be main cause of the oscillations. However this has not been the only case of unsteady flow generation.
3. The exact mechanisms of the oscillations should be determined clearly since this has been a gap in the literature.
4. Tube law should be determined experimentally for tube of uniform thickness to check that whether tube law in [69] for tapered wall thickness can be used also for the tubes of uniform wall thickness.
5. Studies directing to flow field measurements should be concentrated.
6. The theoretical investigations should be made to model the self-excited oscillations.

REFERENCES

1. Conrad, W.A. (1969). Pressure–flow relationships in collapsible tubes. *IEEE Transactions on Biomedical Engineering*, **BME-16**, 284–295.
2. Kamm, R.D. and Pedley, T.J. (1989). Flow in collapsible tubes: a brief review. *Transactions of the ASME Journal of Biomechanical Engineering*, **111**, 177–179.
3. Bertram, C.D. (2003). Experimental studies of collapsible tubes. In *Flow Past Highly Compliant Boundaries and in Collapsible Tubes*, P.W. Carpenter and T.J. Pedley (Eds.), Kluwer Academic Publishers, 51–65.
4. Grotberg, J.B. and Jensen, O.E. (2004). Biofluid mechanics in flexible tubes. *Annual Review of Fluid Mechanics*, **36**, 121–147.
5. Bertram, C.D. (2004). Flow phenomena in floppy tubes. *Contemporary Physics*, **45**, 45–60.
6. Heil, M. and Jensen, O.E. (2003). Flows in deformable tubes and channels: Theoretical models and biological applications. In *Flow Past Highly Compliant Boundaries and in Collapsible Tubes*, P.W. Carpenter and T.J. Pedley (Eds.), Kluwer Academic Publishers, 15–49.
7. Patel, N.R. (1993). *A study of flow limitation and flow induced oscillations during airflow through collapsible tubing*. B.S. Thesis, Massachusetts Institute of Technology.
8. Gavriely, N., Shee, T.R., Cugell, D.W. and Grotberg, J.B. (1989). Flutter in flow limited collapsible tubes: a mechanism for generation of wheezes. *Journal of Applied Physiology*, **66**, 2251–2261.
9. Knowlton, F.P. and Starling, E.H. (1912). The influence of variations in temperature and blood pressure on the performance of the isolated mammalian heart. *Journal of Physiology*, **44**, 206–219.

10. Bertram, C.D. and Raymond, C.J. (1991). Measurements of wave speed and compliance in a collapsible tube during self-excited oscillations: a test of the choking hypothesis. *Medical and Biological Engineering and Computing*, **29**, 493–500.
11. Luo, X.Y. and Pedley, T.J. (2000). Multiple solutions and flow limitation in collapsible channel flows. *Journal of Fluid Mechanics*, **420**, 301–324.
12. Gavriely, N., Palti, Y., Alroy, G. and Grotberg J.B. (1984). Measurement and theory of wheezing breath sounds. *Journal of Applied Physiology*, **57**, 481–492.
13. Grotberg J.B. and Gavriely, N. (1989). Flutter in collapsible tubes: a theoretical model of wheezes. *Journal of Applied Physiology*, **66**, 2262–2273.
14. Lambert, R.K. (1989). A new computational model for expiratory flow from nonhomogeneous human lungs. *Transactions of the ASME Journal of Biomechanical Engineering*, **111**, 200–205.
15. Guyton, A.C. (1963). Venous Return. *Handbook of Physiology*, Section 2, *Circulation*, Vol.II W.F. Hamilton and P. Dow (Eds.), American Physiological Society, Washington, D.C.
16. Griffiths, D.J. (1971). Hydrodynamics of male micturition. Part I: theory of steady flow through elastic-walled tubes. *Medical and Biological Engineering and Computing*, **9**, 581–588.
17. Jensen, O.E. and Pedley, T.J. (1989). The existence of steady flow in a collapsed tube. *Journal of Fluid Mechanics*, **206**, 339–374.
18. Shimizu, M. (1985). Characteristics of pressure-wave propagation in a compliant tube with a fully collapsed segment, *Journal of Fluid Mechanics*, **158**, 113–135.
19. Morgan, P. and Parker, K.H. (1989). A mathematical model of flow through a collapsible tube—I. model and steady flow results. *Journal of Biomechanics*, **22**, 1263–1270.
20. Pedley, T.J. and Luo, X.Y. (1998). Modelling flow and oscillations in collapsible tubes. *Theoretical and Computational Fluid Dynamics*, **10**, 277–294.

21. Young, T. (1808). Hydraulic investigations, subservient to an intended Croonian lecture on the motion of the blood. *Philosophical Transactions of the Royal Society*, **98**, 164-186.
22. Shapiro, A.H. (1977). Steady flow in collapsible tubes. *Transactions of the ASME Journal of Biomechanical Engineering*, **99**, 126-147.
23. Brower, R.W. and Scholten, C. (1975). Experimental evidence on the mechanism for the instability of flow in collapsible vessels. *Medical and Biological Engineering*, **13**, 839-845.
24. Elliot, E.A. and Dawson, S.V. (1977). Test of wave-speed theory of flow limitation in elastic tubes. *Journal of Applied Physiology*, **43**, 516-522.
25. Kececioglu, I., McClurken, M.E., Kamm, R.D and Shapiro, A.H. (1981). Steady, supercritical flow in collapsible tubes. Part I: experimental observations. *Journal of Fluid Mechanics*, **109**, 367-389.
26. Bertram, C.D. and Pedley, T.J. (1982). A mathematical model of unsteady collapsible tube behaviour. *Journal of Biomechanics*, **15**, 39-50.
27. Conrad, W.A., Cohen, M.L. and McQueen, D.M. (1978). Note on the oscillations of collapsible tubes. *Medical and Biological Engineering and Computing*, **16**, 211-214.
28. Katz, A.I., Chen, Y. and Moreno, A.H. (1969). Flow through a collapsible tube. Experimental analysis and mathematical model. *Biophysical Journal*, **9**, 1261-1279.
29. Cancelli, C. and Chiocchia, G. (1979). On the onset of self-excited oscillations in a collapsible tube flow with sonic index values less than one: mathematical model and numerical results. *Accademia Nazionale Dei Lincei, Memorie Sc. Fisiche, sez. I*, **15**, 317-352.
30. Schoendorfer, D.W. and Shapiro, A.H. (1977). The collapsible tube as a prosthetic vocal source. *Proceedings San Diego Biomedical Symposium*, **16**, 349-356.

31. Holmberg, J.L. and Wilson, T.A. (1970). Mechanics of the flow in an elastic tube extending from an orifice into a pressure vessel. *Transactions of the ASME Journal of Applied Mechanics*, **37**, 812–816.
32. Hayashi, S., Hayase, T., Miura, Y. and Imura, I. (1999). Dynamic characteristics of collapsible tube flow. *JSME International Journal, Series C*, **42**, 689–696.
33. Jensen, O.E. (1992). Chaotic oscillations in a simple collapsible-tube model. *Transactions of the ASME Journal of Biomechanical Engineering*, **114**, 55–59.
34. Bertram, C.D., Raymond, C.J. and Pedley, T.J. (1990). Mapping of instabilities for flow through collapsed tubes of differing length. *Journal of Fluids and Structures*, **4**, 125–153.
35. Cancelli, C. and Pedley, T.J. (1985). A separated flow model for collapsible tube oscillations. *Journal of Fluid Mechanics*, **157**, 375–404.
36. Pedley, T.J. (1980). *The fluid mechanics of large blood vessels*. Cambridge University Press, UK, 301–362.
37. Hayashi, S., Hayase, T. and Kawamura, H. (1998). Numerical analysis for stability and self-excited oscillation in collapsible tube flow. *Transactions of the ASME Journal of Biomechanical Engineering*, **120**, 468–475.
38. Pedley, T.J. (1992). Longitudinal tension variation in collapsible channels: A new mechanism for the breakdown of steady flow. *Transactions of the ASME Journal of Biomechanical Engineering*, **114**, 60–67.
39. Heil, M. (1995). *Large deformations of cylindrical shells conveying viscous flow*. PhD thesis, University of Leeds, Leeds.
40. Heil, M. (1997). Stokes flow in collapsible tubes: computation and experiment. *Journal of Fluid Mechanics*, **353**, 285–312.
41. Elad, D., Sahar, M., Avidor, J.M. and Einav, S. (1992). Steady flow through collapsible tubes: measurements of flow and geometry. *Transactions of the ASME Journal of Biomechanical Engineering*, **114**, 84–91.

42. Holt, J.P. (1969). Flow through collapsible tubes and through in situ veins. *IEEE Transactions on Biomedical Engineering*, **BME-16**, 274–283.
43. Nishiyama, H., Okajima, A., Nagayama, E. and Suzuki, T. (1997). Flow characteristics and tube deformation on collapsible tube flow. *Fifth Triennial International Symposium on Fluid Control, Measurement and Visualization*, Hayama, Japan, 625–630.
44. Low, H.T. and Chew, Y.T. (1991). Pressure-flow relationships in collapsible tubes: effects of upstream pressure fluctuations. *Medical and Biological Engineering and Computing*, **29**, 217–221.
45. Low, H.T., Chew, Y.T., Winoto, S.H. and Chin, R. (1995). Pressure-flow behaviour in collapsible tube subjected to forced downstream pressure fluctuations. *Medical and Biological Engineering and Computing*, **33**, 545–550.
46. Bertram, C.D. and Castles, R.J. (1999). Flow limitation in uniform thick-walled collapsible tubes. *Journal of Fluids and Structures*, **13**, 399–418.
47. Griffiths, D.J. (1969). Urethral elasticity and micturition hydrodynamics in females. *Medical and Biological Engineering*, **7**, 201–215.
48. Matsuzaki, Y. and Matsumoto, T. (1989). Flow in a two-dimensional collapsible channel with rigid inlet and outlet. *Transactions of the ASME Journal of Biomechanical Engineering*, **111**, 180–184.
49. Griffiths, D.J. (1977). Oscillations in the outflow from a collapsible tube. *Medical and Biological Engineering and Computing*, **15**, 357–362.
50. Conrad, W.A., McQueen, D.M., and Yellin, E.L. (1980). Steady pressure flow relations in compressed arteries: possible origin of Korotkoff sounds. *Medical and Biological Engineering and Computing*, **18**, 419–426.
51. Griffiths, D.J. (1971). Steady fluid flow through veins and collapsible tubes. *Medical and Biological Engineering and Computing*, **9**, 597–602.
52. Shimizu, M. and Tanida, Y. (1983). On the mechanism of Korotkoff sound generation at diastole. *Journal of Fluid Mechanics*, **127**, 315–339.

53. Ohba, K., Yoneyama, N., Shimanaka, Y. and Maeda, H. (1984). Self-excited oscillation of flow in collapsible tube. *Technology Reports of Kansai University*, **25**, 1–13.
54. Sakurai, A. and Ohba, K. (1986). Self-excited oscillation of flow in collapsible tube. III (A resonant oscillation of air flow). *Technology Reports of Kansai University*, **28**, 41–48.
55. Bertram, C.D. (1986). Unstable equilibrium behaviour in collapsible tubes. *Journal of Biomechanics*, **19**, 61–69.
56. Barclay, W.H. and Thalayasingam, S. (1986). Self-excited oscillations in thin-walled collapsible tubes. *Medical and Biological Engineering and Computing*, **24**, 482–487.
57. Yamane, T. and Orita, T. (1992). Self-excited oscillations with and without supercritical flow in collapsible tubes. *7th International Conference on Biomedical Engineering*, Singapore, 502–504.
58. Yamane, T. and Orita, T. (1994). Relationship of pressure wave velocity to self-excited oscillation of collapsible tube flow. *JSME International Journal, Series A*, **37**, 71–78.
59. Kounanis, K. and Mathioulakis, D.S. (1999). Experimental flow study within a self oscillating collapsible tube. *Journal of Fluids and Structures*, **13**, 61–73.
60. Oruç, V. and Çarpınlioğlu, M.Ö. (2006). Elastik tüplerdeki akışların araştırılmasına yönelik bir deney düzeneğinin tanıtımı. *GAP V. Mühendislik Kongresi Bildiriler Kitabı*, Şanlıurfa, 305-310.
61. Oruç, V. and Çarpınlioğlu, M.Ö. A test rig for the investigation of airflow through collapsible tubes. *Proceedings of the Institution of Mechanical Engineers, Part C: Journal of Mechanical Engineering Science (In press)*.
62. Douglas, J.F., Gasiorek, J.M. and Swaffield, J.A. (1995). *Fluid Mechanics* (3rd ed.). Longman.
63. BS 903-Part A2. (1995). *Physical testing of rubber: Method for determination of tensile stress-strain properties*.

64. Bertram, C.D. (1987). The effects of wall thickness, axial strain and end proximity on the pressure-area relation of collapsible tubes. *Journal of Biomechanics*, **20**, 863–876.
65. Çarpınlioğlu, M.Ö., Oruç, V., Kutlar, A.İ. and Gündoğdu, M.Y. A practice with hot-wire anemometry in the field of self-excited oscillations. *Proceedings of the Institution of Mechanical Engineers, Part C: Journal of Mechanical Engineering Science* (in reviewing process).
66. Çarpınlioğlu, M.Ö. and Oruç, V. An approach for the determination of collapse onset in elastic tube flows. *Proceedings of the Institution of Mechanical Engineers, Part C: Journal of Mechanical Engineering Science* (in reviewing process).
67. Çarpınlioğlu, M.Ö. and Oruç, V. Presentation of a sample test case on the self-excited oscillations in collapsible tube flows. *Proceedings of ILSA'06, 31st International Lung Sounds Association Conference*, Halkidiki, Greece, September 8-9, Session I: Airflow, Asthma, Wheeze, pp. 5-6.
68. Oruç, V. and Çarpınlioğlu, M.Ö. (2006). Elastik tüplerdeki akıslarda kendiliğinden oluşan salınımların analizine yönelik deneysel bir araştırma. *III. Ulusal Biomekanik Kongresi*, İTÜ, 1-2 Aralık.
69. Jaekle, D.E. JR. (1987). *Critical transitions associated with steady flow in collapsible tubes with varying wall stiffness*. S.M. thesis, Massachusetts Institute of Technology.

TABLES

Table 3.1. Properties of the test tubes

Material	Tube Code	L (mm)	D_0 (mm)	L/D_0	H (mm)	R_0/h	Classification	E (Pa)	ν	K_p (Pa)
Latex (Penrose Tube)	P _L	254	25.4	10	0.55	23.09	thin-walled	1.20E+06	0.48	10.55
	P _M	190.5		7.5						
	P _S	127		5						
Silicone Rubber	S _{1,L}	254	25.4	10	1	12.7	thin-walled	2.03E+06	0.48	107.31
	S _{1,M}	190.5		7.5						
	S _{1,S}	127		5						
	S _{2,L}	254	25.4	10	2	6.35	thick-walled	2.03E+06	0.48	858.48
	S _{2,M}	190.5		7.5						
	S _{2,S}	127		5						
	S _{3,L}	254	25.4	10	3	4.23	thick-walled	2.03E+06	0.48	2897.36
	S _{3,M}	190.5		7.5						
	S _{3,S}	127		5						

Table 4.1. Specification of the experimental test cases

Tube Symbol	Covered Q range	Range of p_e
$P_{L,M,S}$	$0.0049 \text{ m}^3/\text{s} \leq Q \leq 0.0120 \text{ m}^3/\text{s}$	$0 \text{ Pa} \leq p_e \leq 468 \text{ Pa}$
$S_{1,L,M,S}$	$0.0061 \text{ m}^3/\text{s} \leq Q \leq 0.0175 \text{ m}^3/\text{s}$	$0 \text{ Pa} \leq p_e \leq 4047 \text{ Pa}$
$S_{2,L,M,S}$	$0.0094 \text{ m}^3/\text{s} \leq Q \leq 0.0205 \text{ m}^3/\text{s}$	$0 \text{ Pa} \leq p_e \leq 8549 \text{ Pa}$
$S_{3,L,M,S}$	$0.0094 \text{ m}^3/\text{s} \leq Q \leq 0.0175 \text{ m}^3/\text{s}$	$0 \text{ Pa} \leq p_e \leq 24821 \text{ Pa}$

Table 4.2. Oscillating test cases

Tube Code	Q (m^3/s)	$p_{e,c}$ (Pa)	Q_c	Q_c / Q (%)	Q_{os}
P_L	0.0049	55.2	0.0030	60.5	variable (*)
P_L	0.0060	75.8	0.0031	51.6	
P_L	0.0094	220.6	0.0054	57.2	
P_L	0.0120	324.1	0.0090	74.5	
P_M	0.0049	124.1	0.0013	25.9	
P_M	0.0061	137.9	0.0040	65.9	
P_M	0.0094	289.6	0.0069	73.5	
P_M	0.0120	468.8	0.0080	66.7	
P_S	0.0049	151.7	0.0033	68.2	
P_S	0.0061	144.8	0.0049	80.9	
P_S	0.0094	282.7	0.0040	42.5	
P_S	0.0120	448.2	0.0063	52.6	
$S_{1,L}$	0.0149	1241.1	0.0092	61.5	
$S_{1,L}$	0.0146	1254.8	0.0100	68.7	0.0135
$S_{1,L}$	0.0155	1392.7	0.0106	68.1	0.0145
$S_{1,L}$	0.0120	1247.9	0.0092	76.6	0.0116
$S_{1,M}$	0.0120	1709.9	0.0102	85.0	0.0117
$S_{1,M}$	0.0149	1792.6	0.0133	89.0	0.0144
$S_{1,M}$	0.0155	1827.1	0.0144	93.0	0.0153
$S_{1,S}$	0.0106	1861.6	0.0094	88.3	0.0104
$S_{1,S}$	0.0120	1827.1	0.0098	81.7	0.0117
$S_{1,S}$	0.0149	1965.0	0.0127	84.8	0.0144
$S_{1,S}$	0.0155	2040.8	0.0139	89.3	0.0150
$S_{2,L}$	0.0205	7122.3	0.0167	81.3	0.0196
$S_{2,L}$	0.0159	7446.3	0.0106	66.7	0.0153
$S_{2,L}$	0.0200	7067.1	0.0163	81.5	0.0191
$S_{2,L}$	0.0168	7046.4	0.0115	68.2	0.0159
$S_{2,M}$	0.0159	7377.4	0.0123	77.6	0.0153
$S_{2,M}$	0.0168	7377.4	0.0139	82.4	0.0160

(*) In conformity with Patel's [7] observation.

Table 4.3. Non-oscillating test cases

Tube Code	Q (m ³ /s)	$p_{e,c}$ (Pa)	Q_c (m ³ /s)	Q_c / Q (%)
S _{1,L}	0.00602	1241.1	0.00599	99.5
S _{1,L}	0.00491	1144.5	0.00487	99.2
S _{1,M}	0.00490	1868.5	0.00474	96.7
S _{1,S}	0.00490	2013.3	0.00474	96.7
S _{2,L}	0.00941	7515.3	0.00933	99.2
S _{2,L}	0.01320	6805.1	0.01287	97.5
S _{2,M}	0.00939	8384.0	0.00935	99.6
S _{3,L}	0.00941	14341.1	0.00935	99.4
S _{3,L}	0.01311	17650.5	0.01307	99.7
S _{3,L}	0.01730	16788.7	0.01721	99.5
S _{3,S}	0.00939	22442.4	0.00930	99.0
S _{3,S}	0.01319	21339.2	0.01316	99.8
S _{3,S}	0.01729	19898.2	0.01726	99.8

Table 5.1. The experimental data for flow through P_L tube at the onset of oscillations

Q (m ³ /s)	$p_{e,c}$ (kPa)	\bar{p}_1 (kPa)	\bar{p}_2 (kPa)	\bar{u}_{os} (m/s)	f (Hz)
0.0083	0.16	1.37	1.10	15.27	19.06
0.0101	0.28	1.85	1.27	19.76	20.06
0.0150	0.69	3.6	1.52	28.84	21.46
0.0213	1.38	5.09	2.1	41.62	22.08

Table 5.2. The experimental data for flow through P_M tube at the onset of oscillations

Q (m ³ /s)	$p_{e,c}$ (kPa)	\bar{p}_1 (kPa)	\bar{p}_2 (kPa)	\bar{u}_{os} (m/s)	f (Hz)
0.0083	0.26	0.83	0.70	20.59	18.37
0.0101	0.31	1.16	0.92	23.08	18.72
0.0150	0.78	2.43	1.42	34.79	21.42
0.0213	1.62	3.94	2.05	51.29	21.90

Table 5.3. The experimental data for flow through P_S tube at the onset of oscillations

Q (m ³ /s)	$p_{e,c}$ (kPa)	\bar{p}_1 (kPa)	\bar{p}_2 (kPa)	\bar{u}_{os} (m/s)	f (Hz)
0.0083	0.23	1.34	1.11	18.75	19.13
0.0101	0.39	2.22	1.51	23.53	20.15
0.0150	0.83	3.77	1.93	32.6	21.44
0.0213	1.65	5.3	2.26	47.87	22.05

Table 5.4. The experimental data for flow through $S_{1,L}$ tube at the onset of oscillations

Q (m ³ /s)	$p_{e,c}$ (kPa)	\bar{p}_1 (kPa)	\bar{p}_2 (kPa)	\bar{u}_{os} (m/s)	f (Hz)
0.0101	1.93	1.18	0.85	19.42	19.20
0.0130	2.34	2.99	1.69	22.52	20.33
0.0162	2.52	3.90	2.26	31.22	20.43
0.0213	3.38	10.68	3.24	33.37	34.88

Table 5.5. The experimental data for flow through $S_{1,M}$ tube at the onset of oscillations

Q (m ³ /s)	$p_{e,c}$ (kPa)	\bar{p}_1 (kPa)	\bar{p}_2 (kPa)	\bar{u}_{os} (m/s)	f (Hz)
0.0101	2.00	1.03	0.61	23.25	20.92
0.0130	2.14	1.51	0.98	30.84	20.53
0.0172	2.33	3.20	2.00	43.93	19.60
0.0213	2.83	5.51	3.05	49.58	20.41

Table 5.6. The experimental data for flow through $S_{1,S}$ tube at the onset of oscillations

Q (m ³ /s)	$p_{e,c}$ (kPa)	\bar{p}_1 (kPa)	\bar{p}_2 (kPa)	\bar{u}_{os} (m/s)	f (Hz)
0.0101	2.34	1.74	1.06	20.81	25.55
0.0130	1.79	1.59	1.03	29.61	21.91
0.0172	1.93	3.23	1.97	39.32	20.17
0.0213	2.48	6.34	3.08	44.02	21.80

Table 5.7. The experimental data for flow through $S_{2,L}$ tube at the onset of oscillations

Q (m ³ /s)	$p_{e,c}$ (kPa)	\bar{p}_1 (kPa)	\bar{p}_2 (kPa)	\bar{u}_{os} (m/s)	f (Hz)
0.0101	8.96	1.75	0.42	19.26	30.47
0.0135	8.27	2.24	0.92	25.99	28.71
0.0195	8.27	3.01	1.70	43.89	19.01

Table 5.8. The experimental data for flow through $S_{2,M}$ tube at the onset of oscillations

Q (m ³ /s)	$p_{e,c}$ (kPa)	\bar{p}_1 (kPa)	\bar{p}_2 (kPa)	\bar{u}_{os} (m/s)	f (Hz)
0.0116	9.79	2.56	0.43	25.64	34.97
0.0184	8.69	3.52	1.60	41.07	29.11
0.0213	8.49	4.01	2.06	49.98	27.15

Table 5.9. The experimental data for flow through $S_{2,S}$ tube at the onset of oscillations

Q (m ³ /s)	$p_{e,c}$ (kPa)	\bar{p}_1 (kPa)	\bar{p}_2 (kPa)	\bar{u}_{os} (m/s)	f (Hz)
0.0116	10.27	2.84	0.91	21.43	32.43
0.0147	9.03	3.01	1.38	27.84	28.89
0.0184	8.76	3.66	1.80	38.15	26.92
0.0214	8.48	4.04	2.15	47.01	26.98

Table 6.1. Calculations of some parameters based on [13] in reference to the experimental measurements at the onset of oscillations for the flow through Penrose tube

Tube Code	Q (m ³ /s)	\bar{u} (m/s)	f_{meas} (Hz)	b (m) (Fig. 6.5)	f_{calc} (Hz)	A/A_0 (Fig. 6.3)	c (m/s)	S_{min}	u_c (m/s)
P _L	0.0083	16.38	19.06	0.0025	19.29	0.59	4.28	0.74	3.16
	0.0101	19.93	20.06	0.0022	20.05	0.56	3.99	0.68	2.71
	0.0150	29.60	21.46	0.0018	21.42	0.52	3.60	0.60	2.18
	0.0213	42.04	22.08	0.0016	21.99	0.50	3.42	0.58	1.98
P _M	0.0083	16.38	18.37	0.0028	18.75	0.61	4.48	0.78	3.51
	0.0101	19.93	18.72	0.0026	19.03	0.60	4.38	0.76	3.33
	0.0150	29.60	21.42	0.0018	21.36	0.52	3.61	0.61	2.19
	0.0213	42.04	21.90	0.0017	21.68	0.50	3.48	0.59	2.04
P _S	0.0083	16.38	19.13	0.0025	19.35	0.59	4.26	0.73	3.13
	0.0101	19.93	20.15	0.0022	20.13	0.56	3.97	0.67	2.67
	0.0150	29.60	21.44	0.0018	21.39	0.52	3.60	0.61	2.18
	0.0213	42.04	22.05	0.0016	21.94	0.50	3.43	0.58	1.99

Table 6.2. Calculations of some parameters based on [13] in reference to the experimental measurements at the onset of oscillations for the flow through silicone rubber tube ($h=1$ mm)

Tube Code	Q (m ³ /s)	\bar{u} (m/s)	f_{meas} (Hz)	b (m) (Fig. 6.5)	f_{calc} (Hz)	A/A_0 (Fig. 6.3)	c (m/s)	S_{min}	u_c (m/s)
S _{1,L}	0.0101	19.93	19.20	0.0027	18.70	0.60	14.07	1.052	14.79
	0.0130	25.66	20.33	0.0026	20.22	0.59	13.86	1.049	14.55
	0.0162	31.97	20.43	0.0026	20.28	0.59	13.84	1.049	14.53
	0.0213	42.04	34.88	0.0018	34.70	0.52	11.60	0.934	10.84
S _{1,M}	0.0101	19.93	20.92	0.0026	20.58	0.59	13.76	1.048	14.41
	0.0130	25.66	20.53	0.0026	20.35	0.59	13.83	1.049	14.50
	0.0172	33.94	19.60	0.0027	18.93	0.60	14.00	1.051	14.71
	0.0213	42.04	20.41	0.0026	20.27	0.59	13.85	1.049	14.53
S _{1,S}	0.0101	19.93	25.55	0.0023	25.56	0.57	12.97	1.027	13.32
	0.0130	25.66	21.91	0.0025	21.20	0.59	13.58	1.045	14.19
	0.0172	33.94	20.17	0.0026	19.27	0.60	13.89	1.050	14.58
	0.0213	42.04	21.8	0.0025	21.13	0.59	13.60	1.045	14.22

Table 6.3. Calculations of some parameters based on [13] in reference to the experimental measurements at the onset of oscillations for the flow through silicone rubber tube ($h=2$ mm)

Tube Code	Q (m ³ /s)	\bar{u} (m/s)	f_{meas} (Hz)	b (m) (Fig. 6.5)	f_{calc} (Hz)	A/A_0 (Fig. 6.3)	c (m/s)	S_{min}	u_c (m/s)
S _{2,L}	0.0101	19.93	30.47	0.0021	29.13	0.55	35.25	1.042	36.74
	0.0135	26.64	28.71	0.0022	28.08	0.56	35.71	1.043	37.23
	0.0195	38.48	19.01	0.0026	19.12	0.59	39.18	1.039	40.71
S _{2,M}	0.0116	22.89	34.97	0.0020	33.78	0.54	34.22	1.039	35.56
	0.0184	36.31	29.11	0.0022	28.32	0.55	35.60	1.042	37.11
	0.0213	42.04	27.15	0.0022	27.12	0.56	36.15	1.043	37.69
S _{2,S}	0.0116	22.89	32.43	0.0021	32.29	0.54	34.78	1.041	36.20
	0.0147	29.01	28.89	0.0022	28.19	0.55	35.66	1.043	37.17
	0.0184	36.31	26.92	0.0022	26.97	0.56	36.21	1.043	37.77
	0.0214	42.23	26.98	0.0022	27.01	0.56	36.20	1.043	37.75

FIGURES

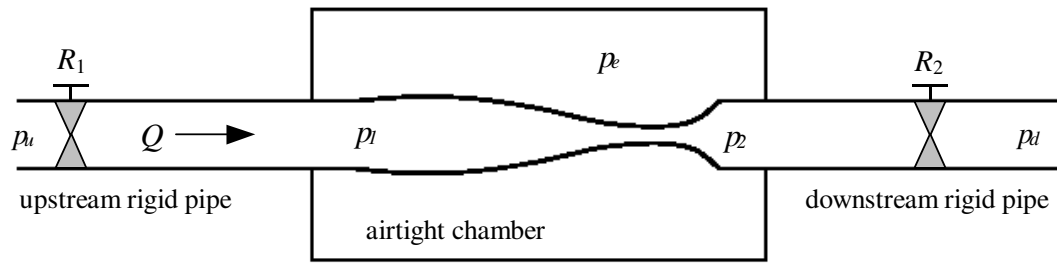


Figure 2.1. A schematic representation of Starling resistor

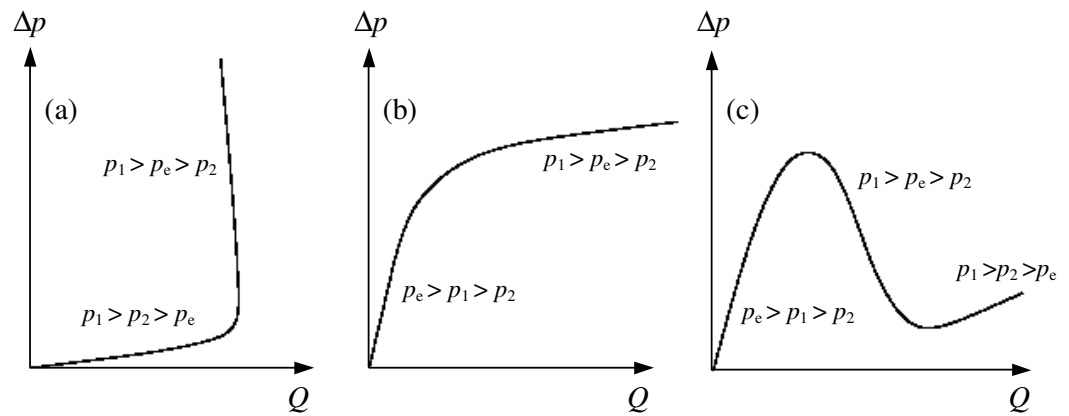


Figure 2.2. A sketch for Δp versus Q with (a) $p_{m,1}$ fixed (flow limitation), (b) $p_{m,2}$ fixed (pressure-drop limitation), (c) Conrad's [1] protocol

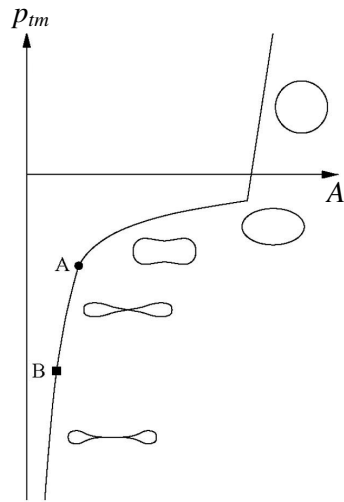


Figure 2.3. A schematic relation between p_m and A (tube law) showing typical tube cross-sections

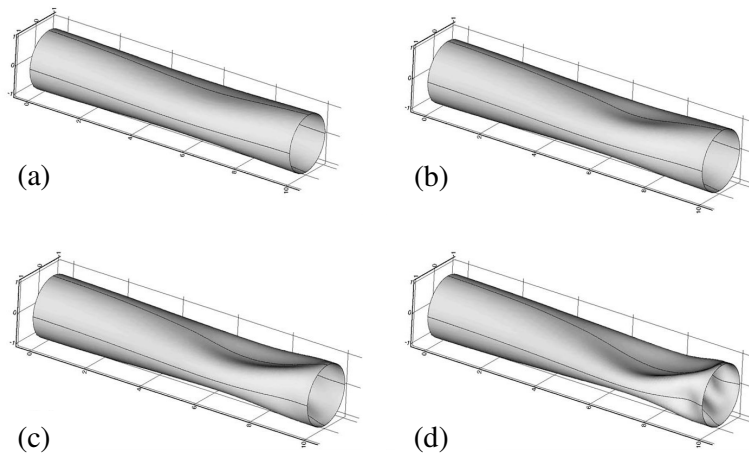
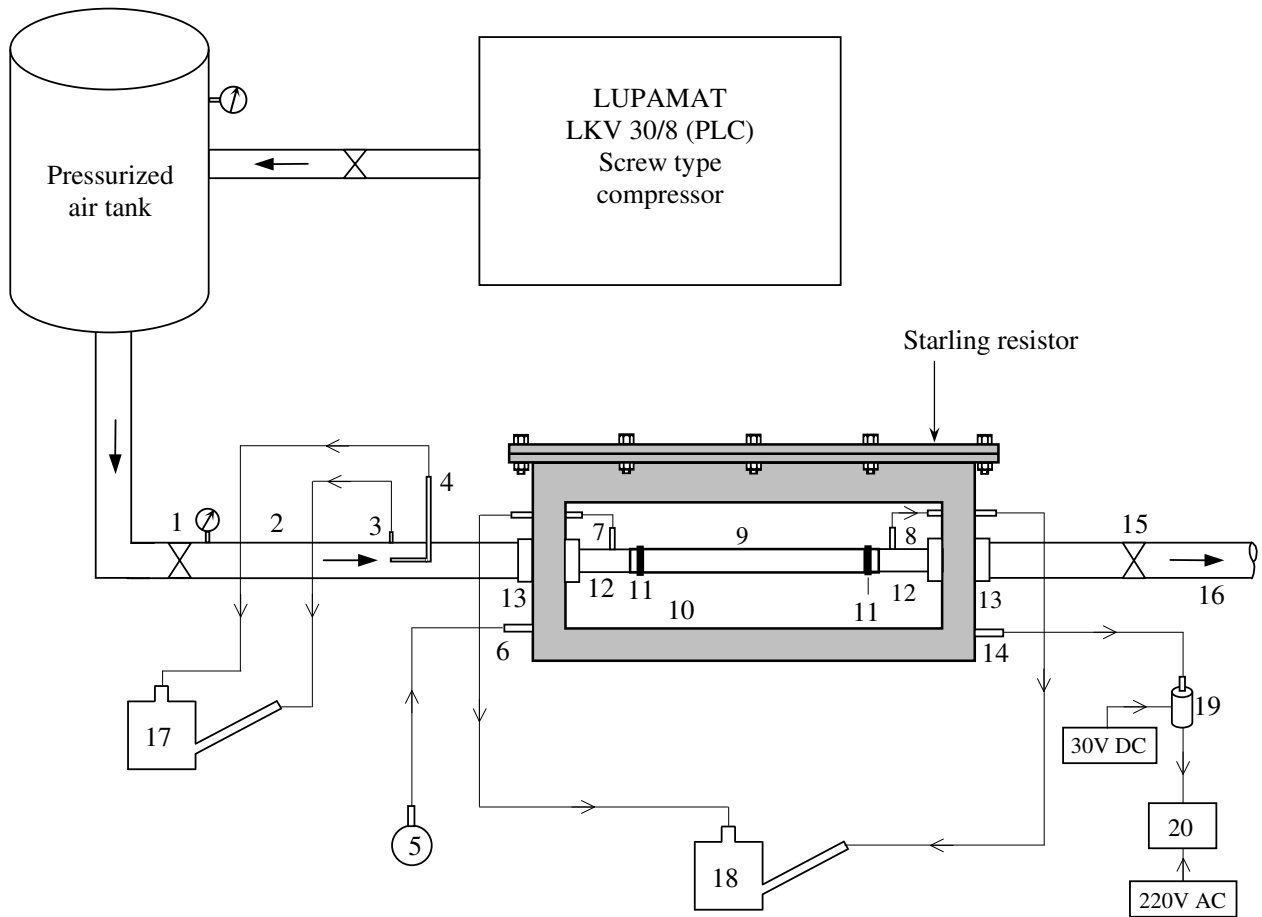
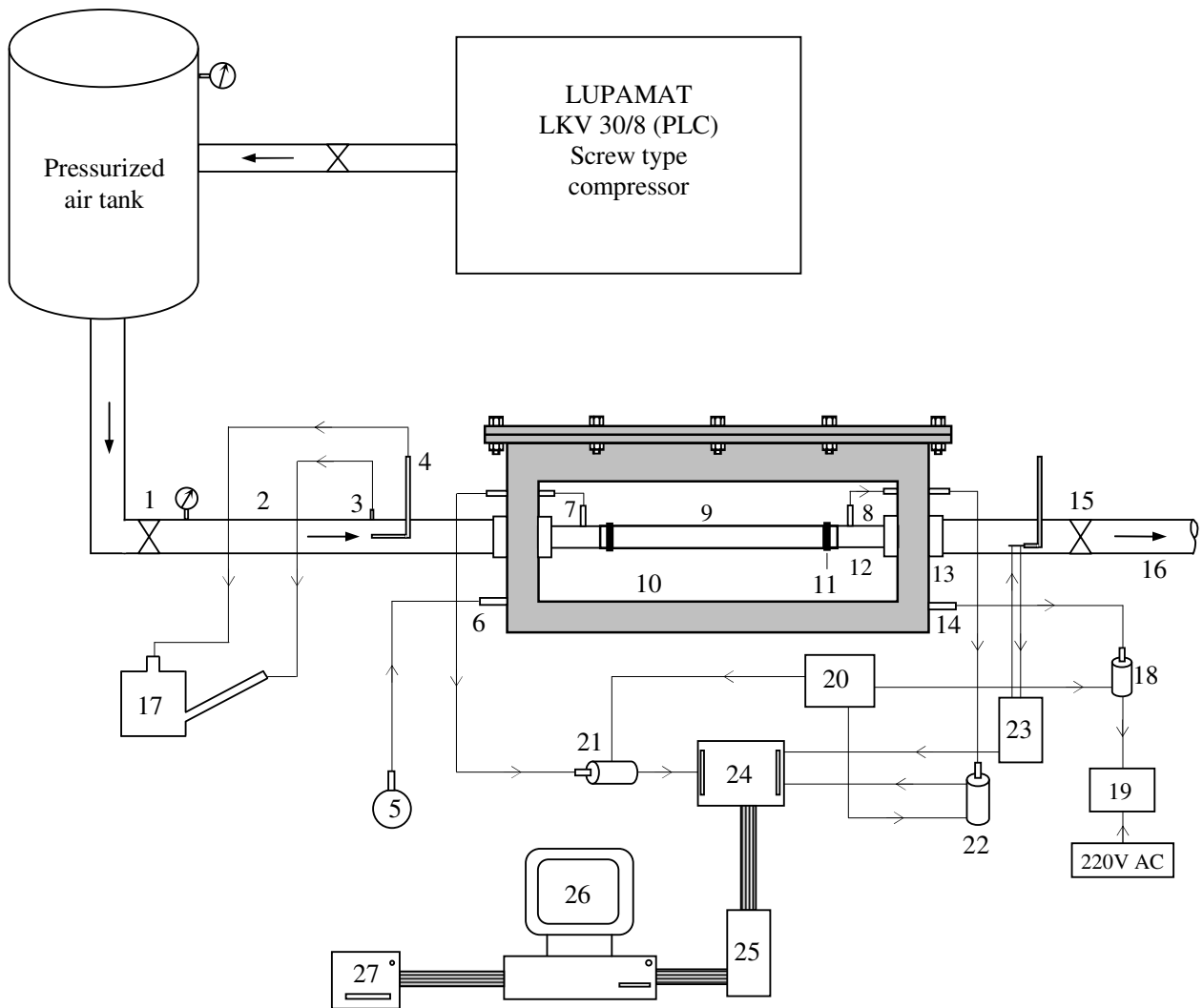


Figure 2.4. Computations from [40] demonstrating 3D buckling and collapse of a tube held open at each end, supporting an internal flow; external compression increases from panel (a) to panel (d)



- | | |
|--|---|
| 1. pressure regulator | 12. rigid attachments |
| 2. upstream rigid pipe (2m length) | 13. connection parts with O-ring |
| 3. static pressure tapping | 14. static pressure tapping for measuring p_e |
| 4. pitot tube | 15. downstream valve |
| 5. manual air pump | 16. downstream rigid pipe (2m length) |
| 6. valve for pressurizing Starling resistor | 17. inclined-leg alcohol manometer for measuring Q |
| 7. static pressure tapping for measuring p_1 | 18. inclined-leg alcohol manometer for measuring Δp |
| 8. static pressure tapping for measuring p_2 | 19. pressure transmitter |
| 9. test tube | 20. digital process controller |
| 10. observation window | |
| 11. clamps | |

Figure 3.1. A schematic representation of the experimental set-up without data acquisition system



- | | |
|---|--|
| 1. pressure regulator | 16. downstream rigid pipe |
| 2. upstream rigid pipe | 17. inclined-leg alcohol manometer for measuring Q |
| 3. static pressure tapping | 18. pressure transmitter |
| 4. pitot tube | 19. digital process controller |
| 5. manual air pump | 20. DC power supply |
| 6. valve for pressurizing the Starling resistor | 21. pressure transducer for measuring p_1 |
| 7. tapping for measuring p_1 | 22. pressure transducer for measuring p_2 |
| 8. tapping for measuring p_2 | 23. CTA Hot wire anemometer |
| 9. elastic tube | 24. STA-16 Screw terminal accessory board |
| 10. observation window | 25. DAS-1602 Hardware board |
| 11. clamps | 26. computer |
| 12. rigid attachments | 27. printer |
| 13. connection parts with O-ring | |
| 14. tapping for measuring p_c | |
| 15. downstream valve | |

Figure 3.2. A schematic representation of the experimental set-up together with its data acquisition system and measuring devices

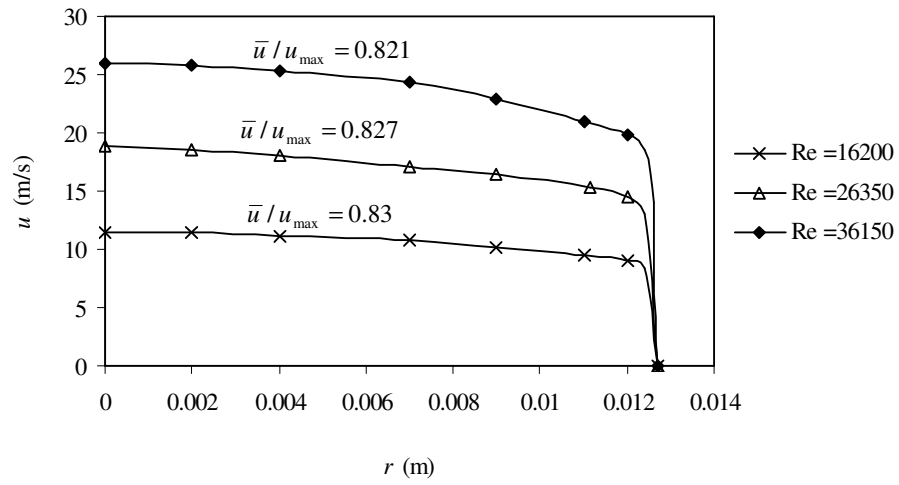


Figure 3.3. Steady turbulent flow measurements with Pitot tube at three different Re in order to show that flow is fully developed before entering to the test section

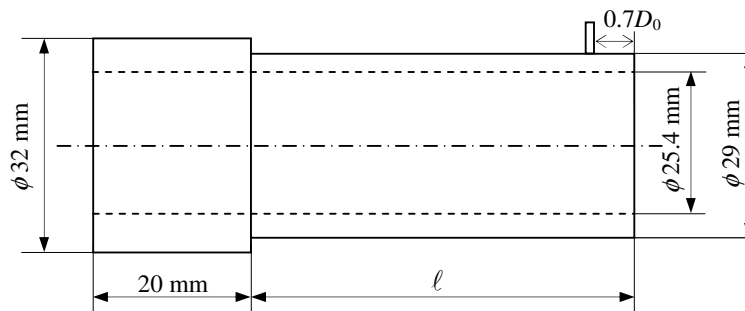


Figure 3.4. Dimensions of the rigid attachment

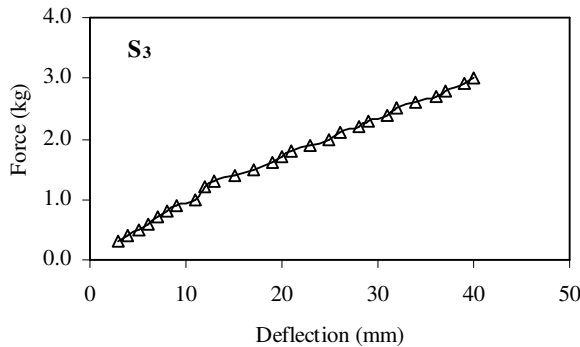
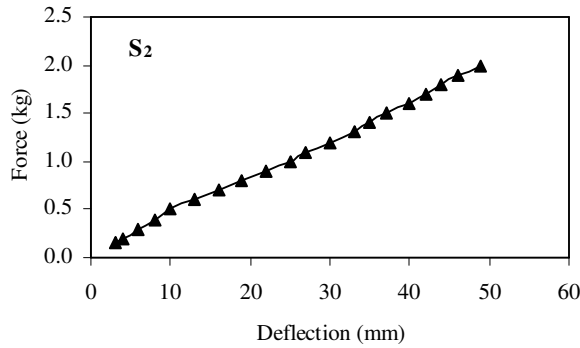
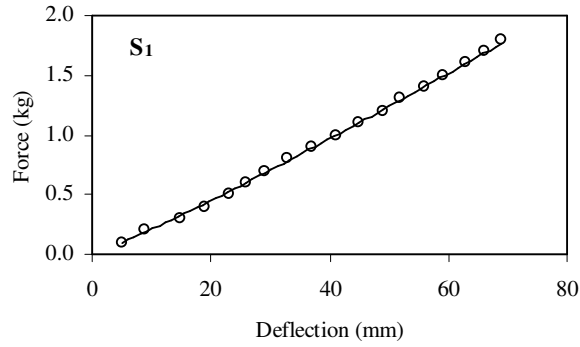
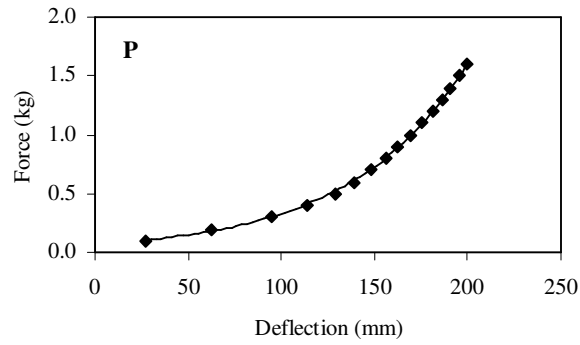


Figure 3.5. Axial force-deflection test applied to the sample of test tubes (P, S₁, S₂, S₃) for the determination of E

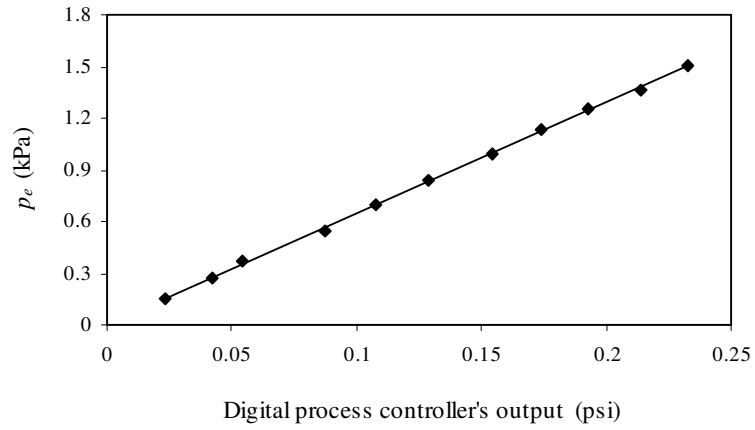


Figure 3.6. Calibration curve of pressure transmitter (E913) and digital process controller (M1-3000) combination

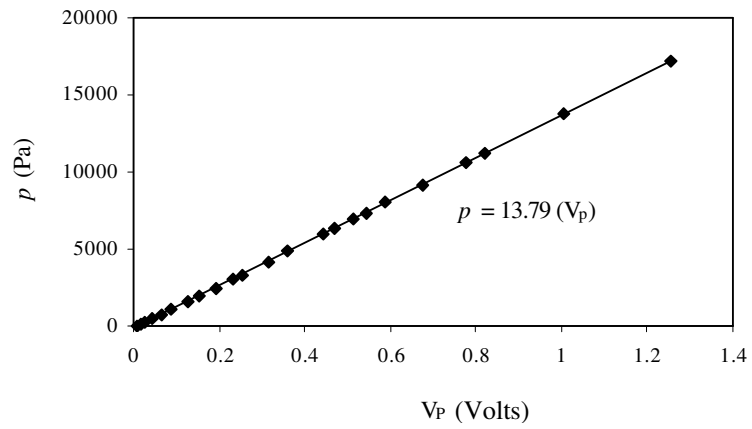


Figure 3.7. Calibration curve of Omega pressure transducer (PX951-010G5V)

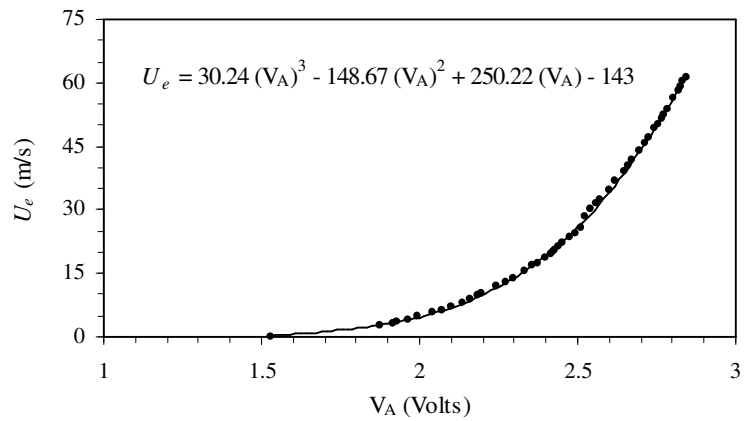


Figure 3.8. Calibration of hot-wire anemometer probe

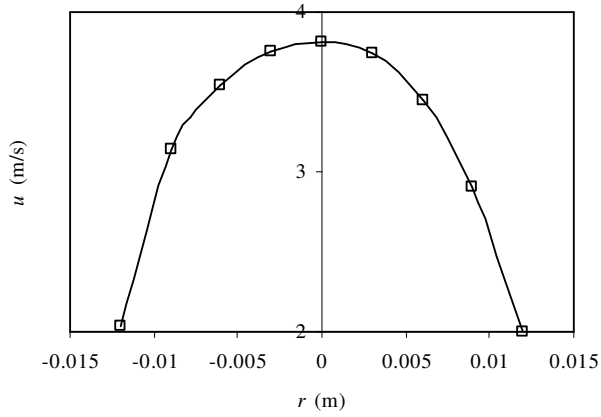


Figure 3.9. Cross-sectional velocity distribution at $5.12D_0$ downstream of $S_{1,L}$ in steady flow for $Re = 5,300$ with $p_e = 0$

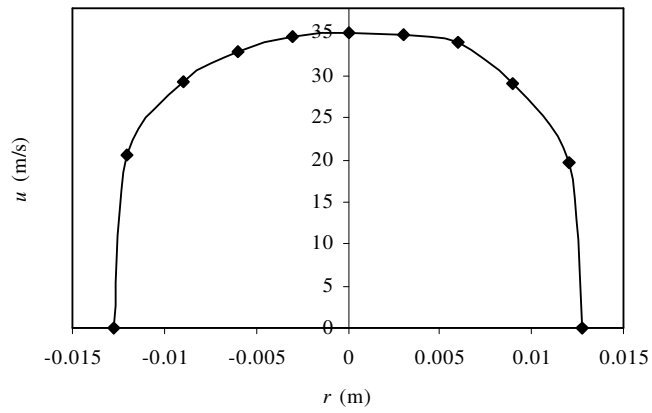


Figure 3.10. Cross-sectional velocity distribution at $5.12D_0$ downstream of $S_{1,L}$ in steady flow for $Re = 51,000$ with $p_e = 0$

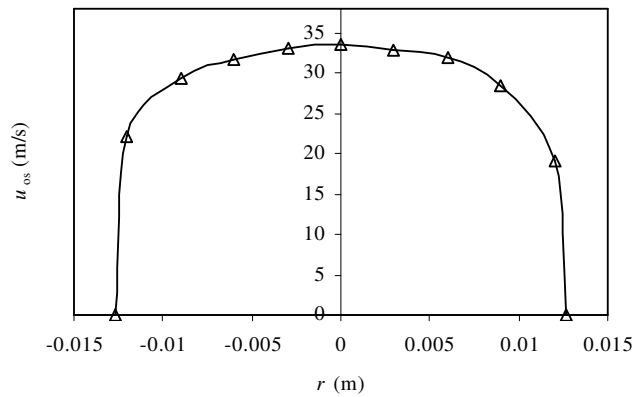


Figure 3.11. Velocity distribution at $6.3D_0$ downstream of $S_{1,M}$ in oscillating flow for $Re = 61,000$ with $p_e = 2.12$ kPa

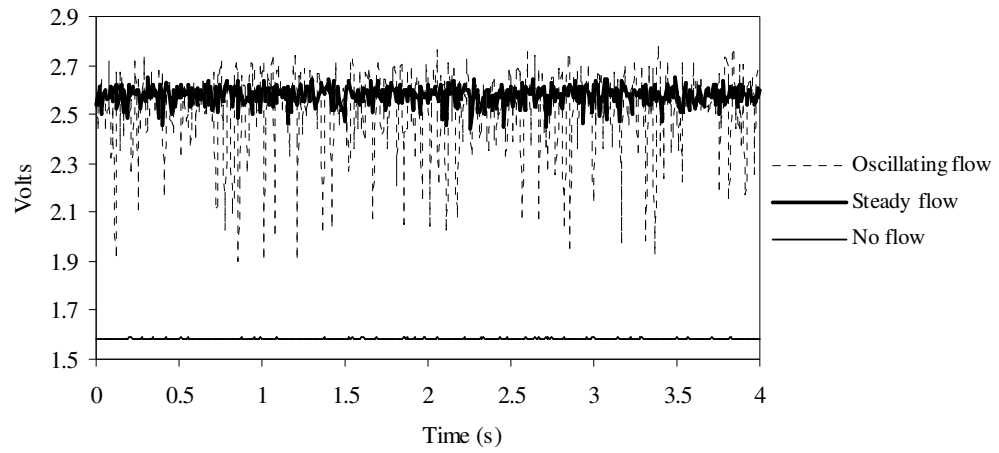


Figure 3.12. Sample measurement cases with hot wire anemometer to check the accuracy of the measurements

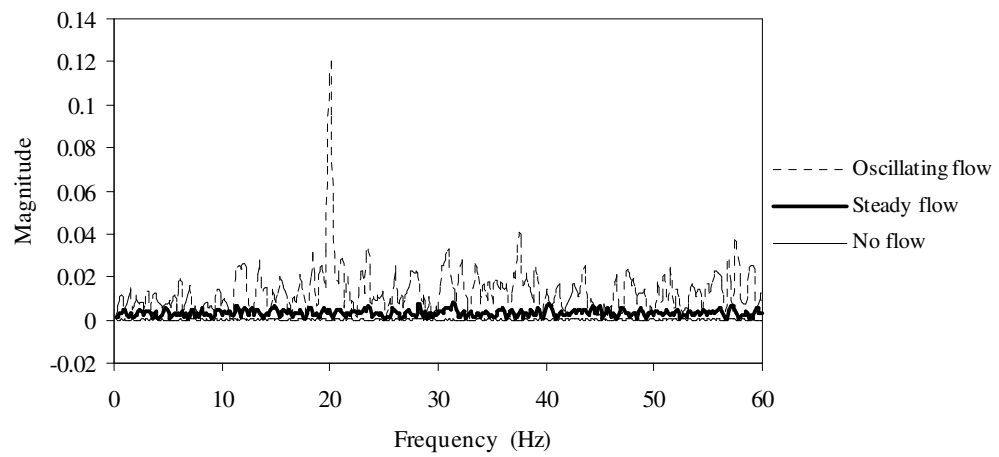


Figure 3.13. FFT analysis of Figure 3.12

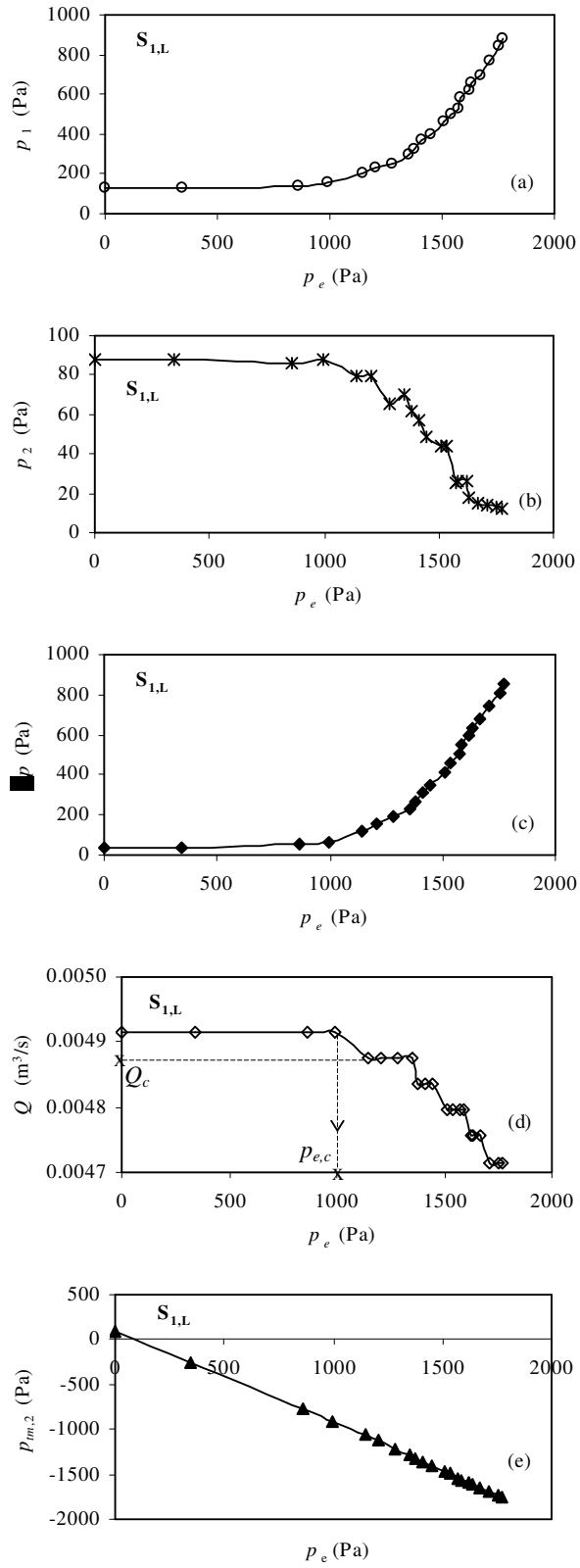


Figure 4.1. Variation of p_1 , p_2 , Δp , Q and $p_{m,2}$ with p_e for a non-oscillating case through $S_{1,L}$

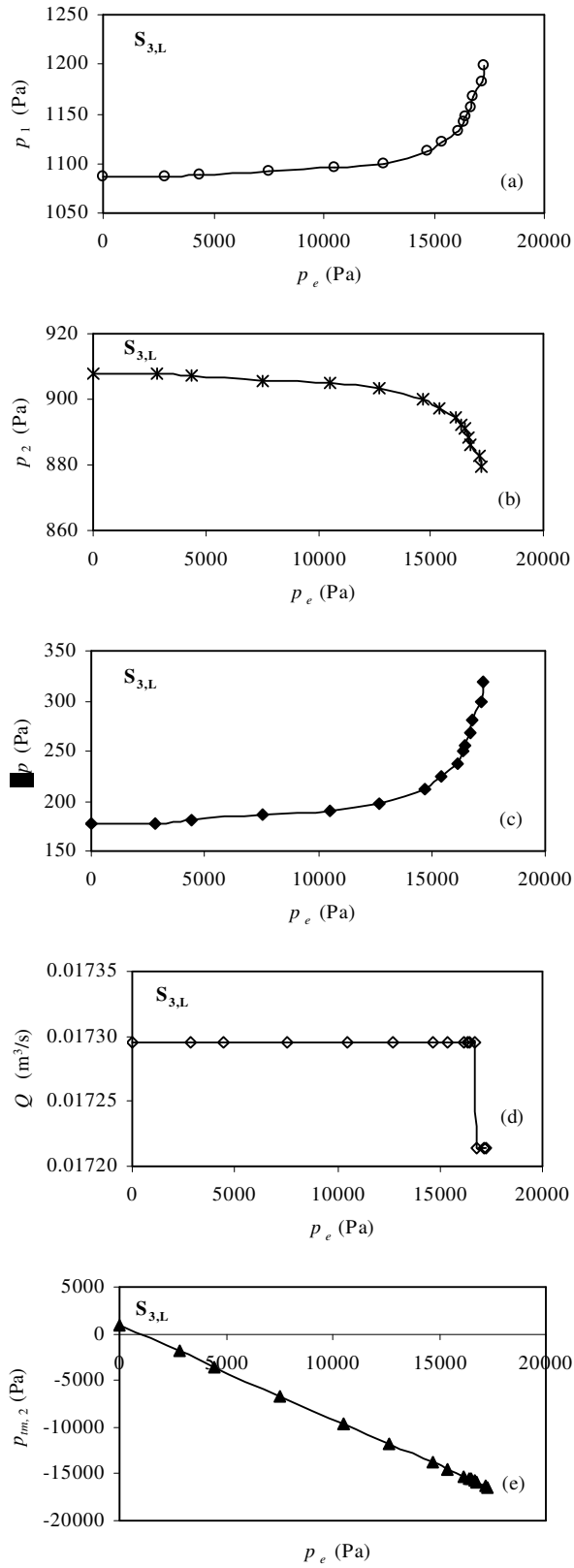


Figure 4.2. Variation of p_1 , p_2 , Δp , Q and $p_{tm,2}$ with p_e for a non-oscillating case through $S_{3,L}$

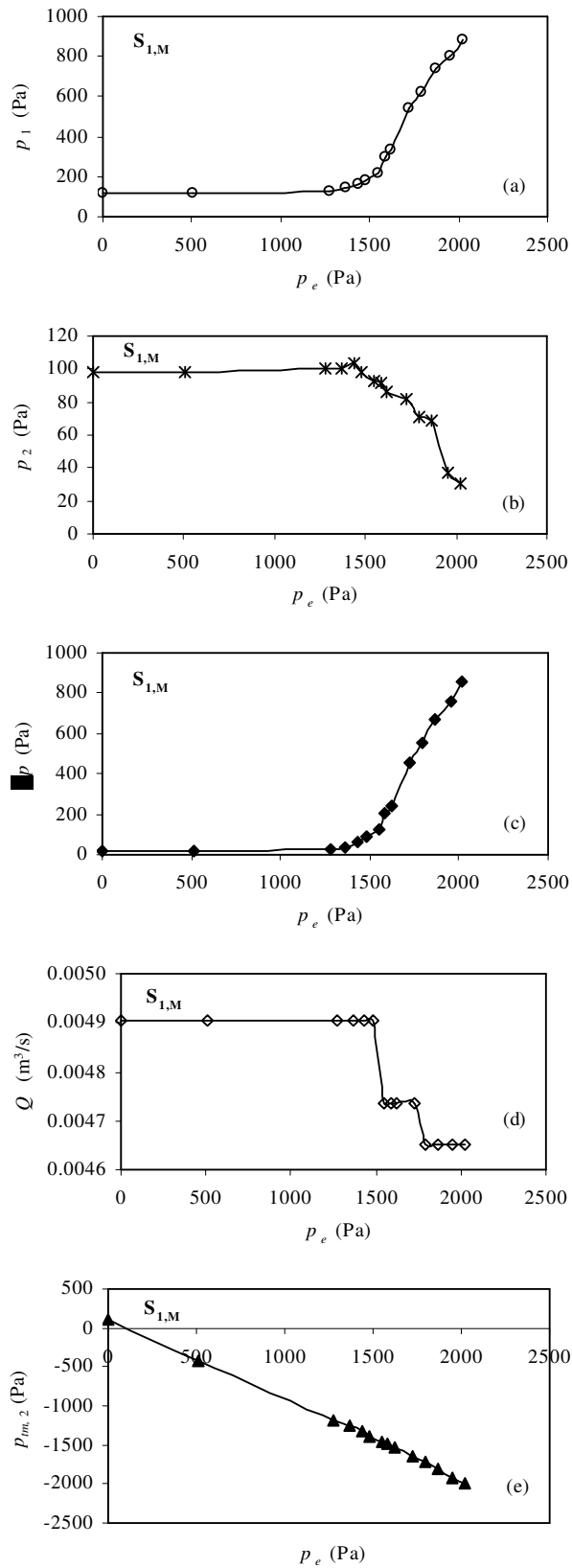


Figure 4.3. Variation of p_1 , p_2 , Δp , Q and $p_{tm,2}$ with p_e for a non-oscillating case through $S_{1,M}$

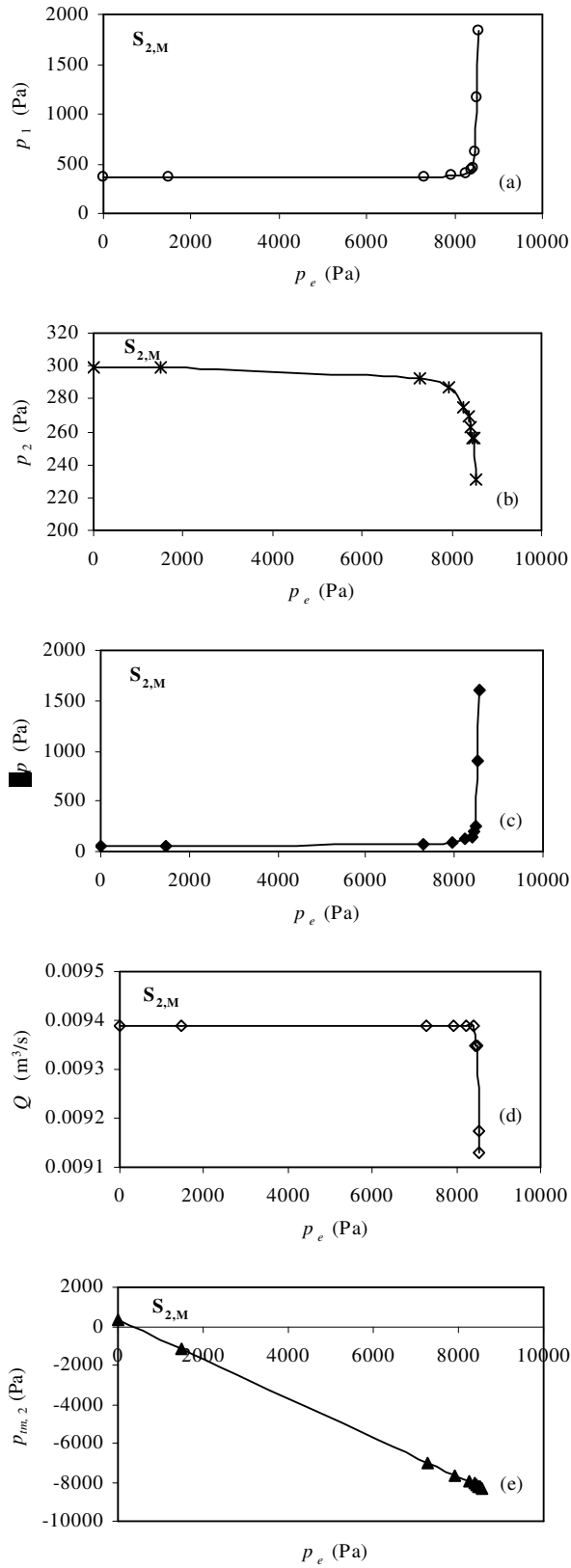


Figure 4.4. Variation of p_1 , p_2 , Δp , Q and $p_{tm,2}$ with p_e for a non-oscillating case through $S_{2,M}$

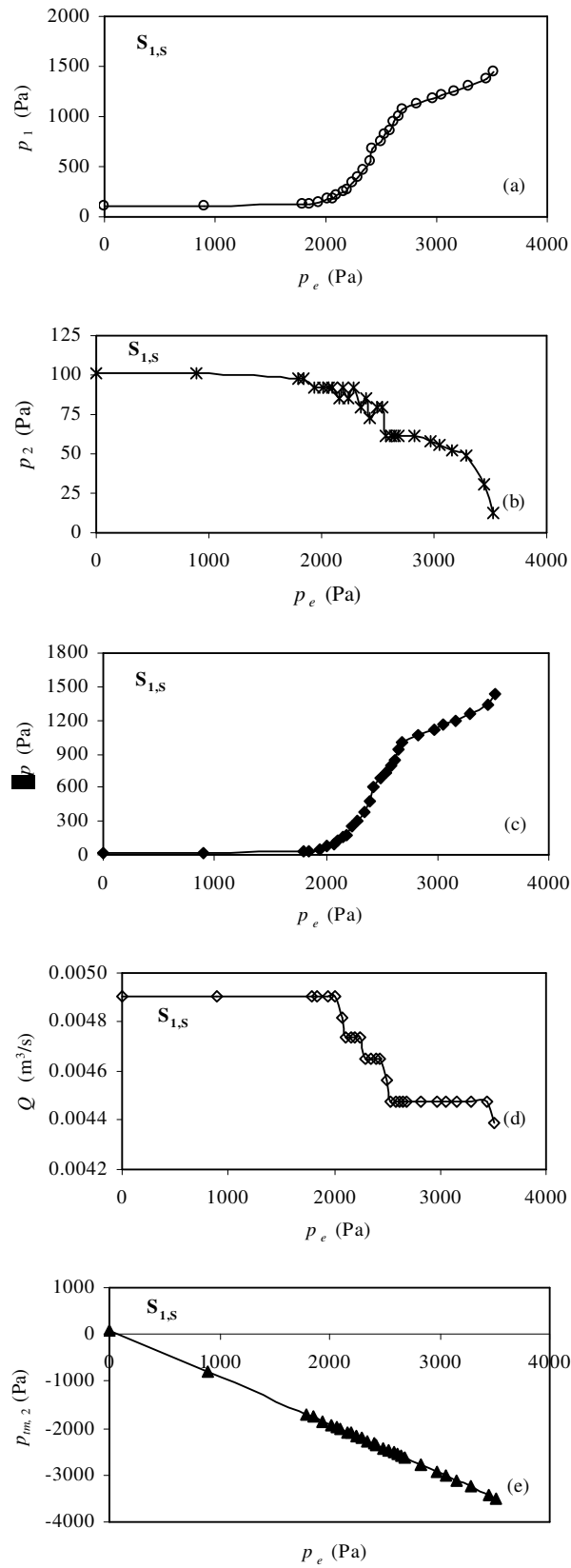


Figure 4.5. Variation of p_1 , p_2 , Δp , Q and $p_{tm,2}$ with p_e for a non-oscillating case through $S_{1,s}$

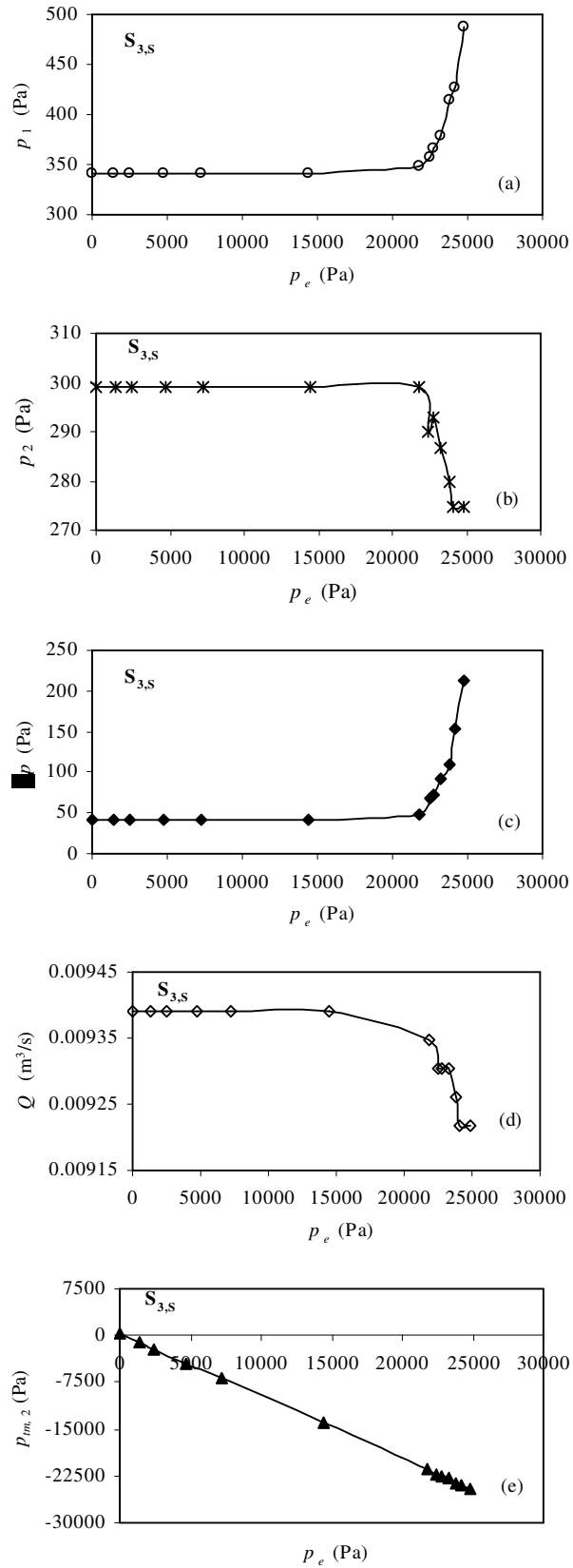


Figure 4.6. Variation of p_1 , p_2 , Δp , Q and $p_{tm,2}$ with p_e for a non-oscillating case through $S_{3,s}$

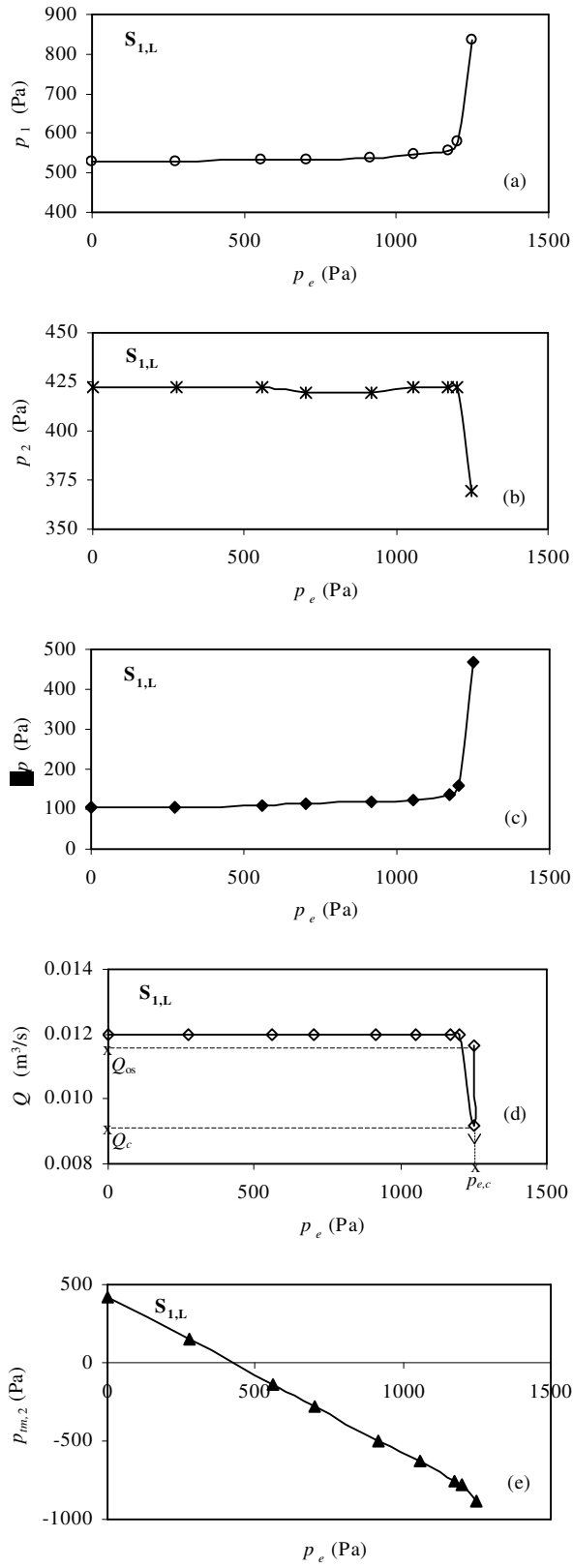


Figure 4.7. Variation of p_1 , p_2 , Δp , Q and $p_{tm,2}$ with p_e for an oscillating case through $S_{1,L}$

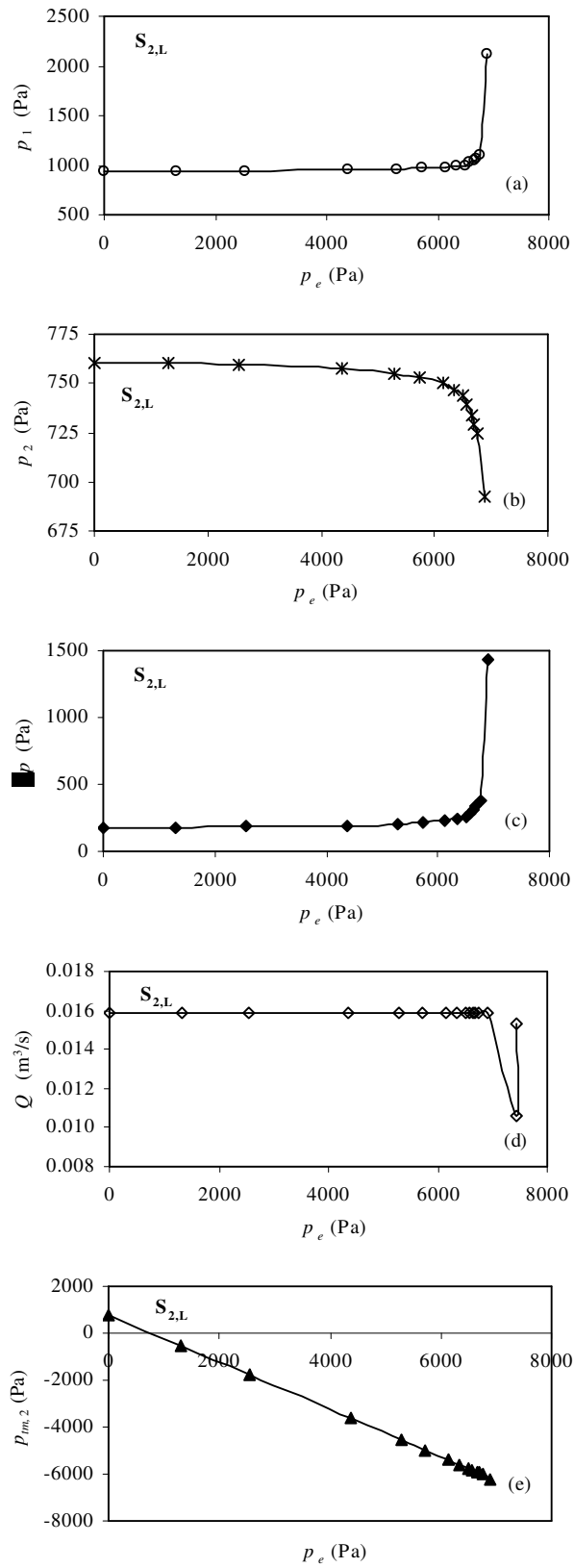


Figure 4.8. Variation of p_1 , p_2 , Δp , Q and $p_{tm,2}$ with p_e for an oscillating case through $S_{2,L}$

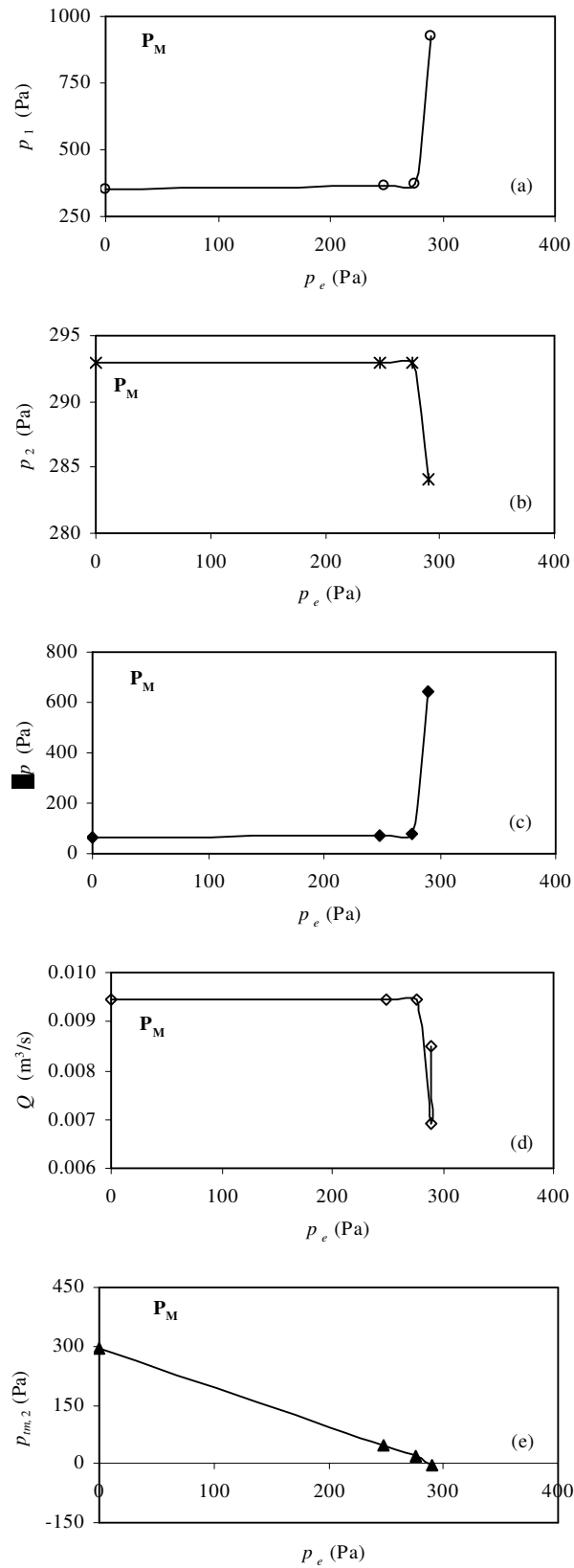


Figure 4.9. Variation of p_1 , p_2 , Δp , Q and $p_{m,2}$ with p_e for an oscillating case through P_M

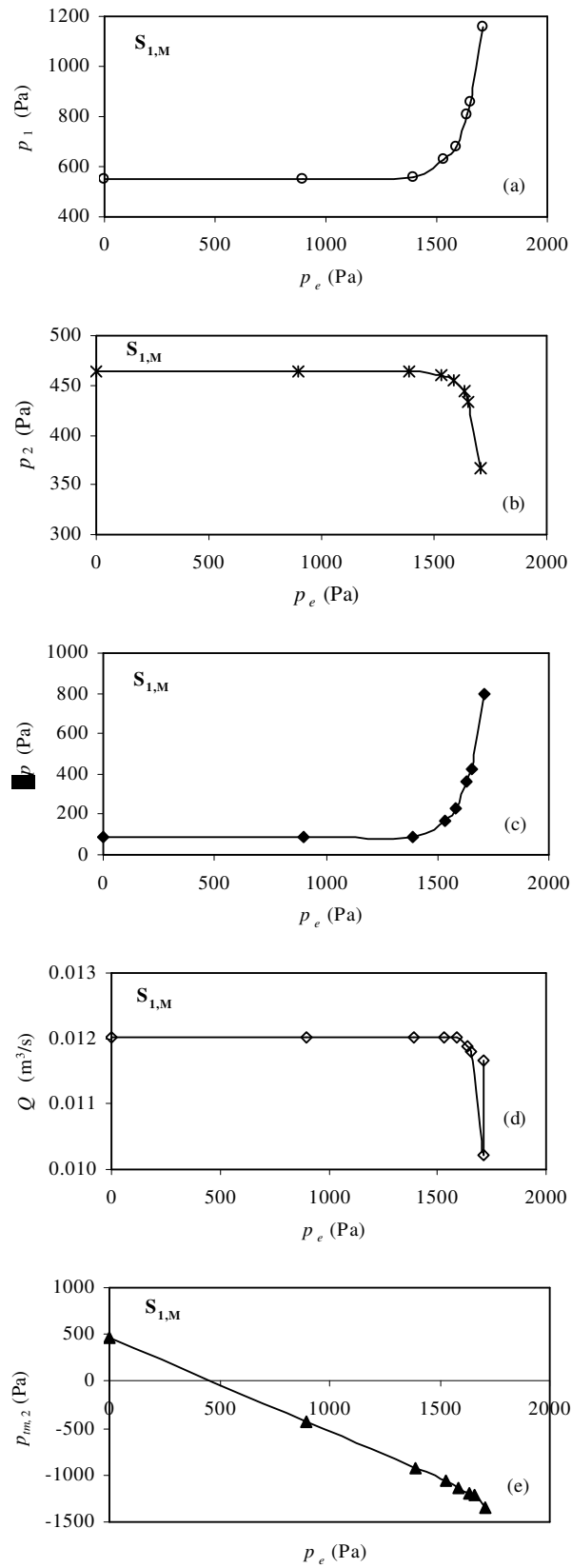


Figure 4.10. Variation of p_1 , p_2 , Δp , Q and $p_{tm,2}$ with p_e for an oscillating case through $S_{1,M}$

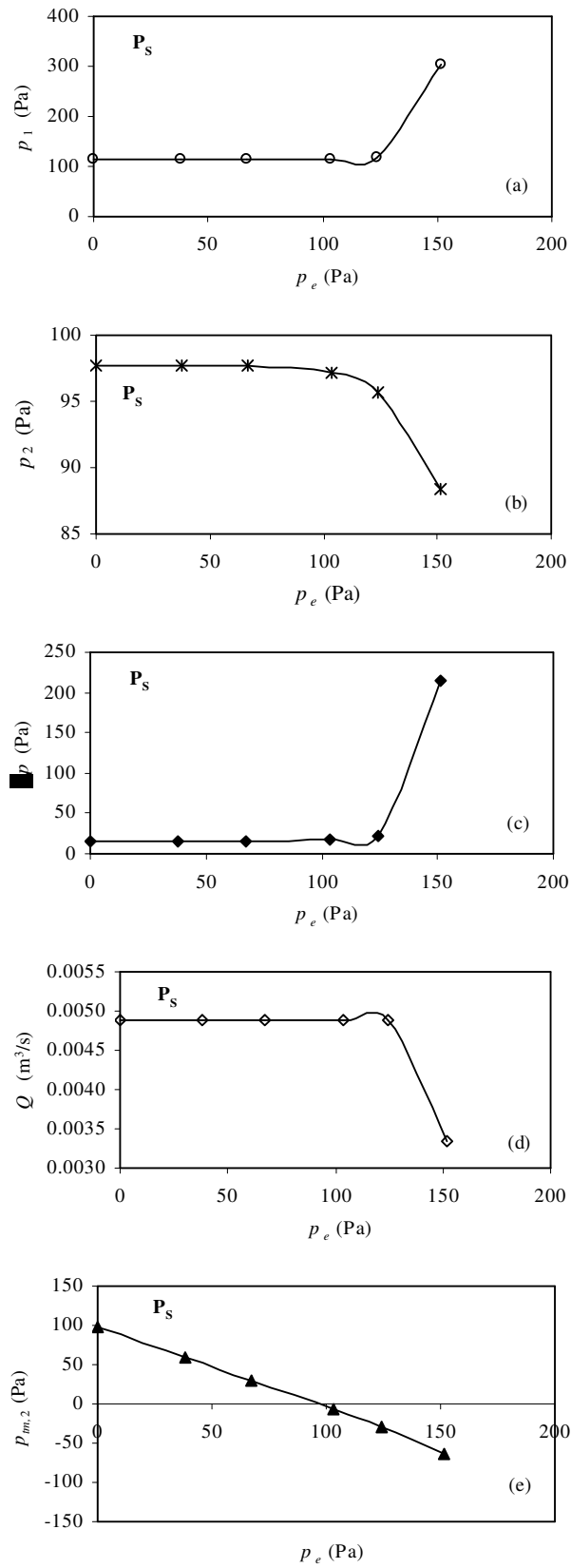


Figure 4.11. Variation of p_1 , p_2 , Δp , Q and $p_{tm,2}$ with p_e for an oscillating case through P_s

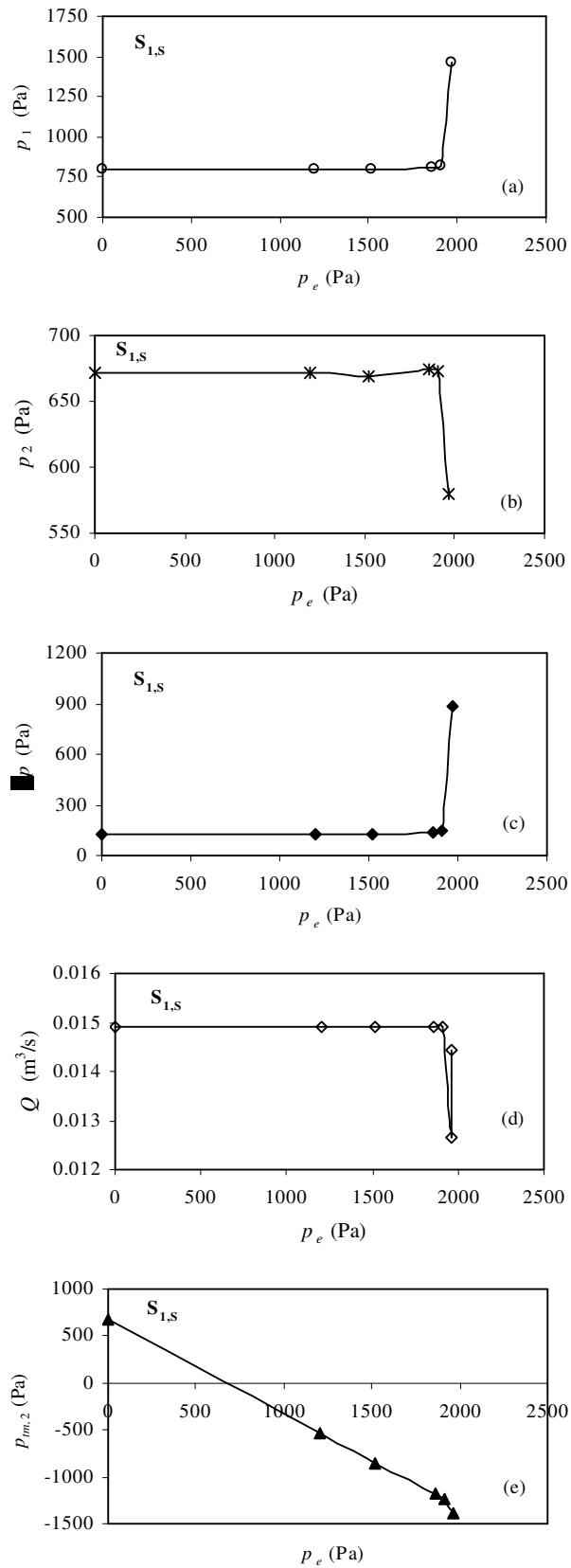


Figure 4.12. Variation of p_1 , p_2 , Δp , Q and $p_{tm,2}$ with p_e for an oscillating case through $S_{1,s}$

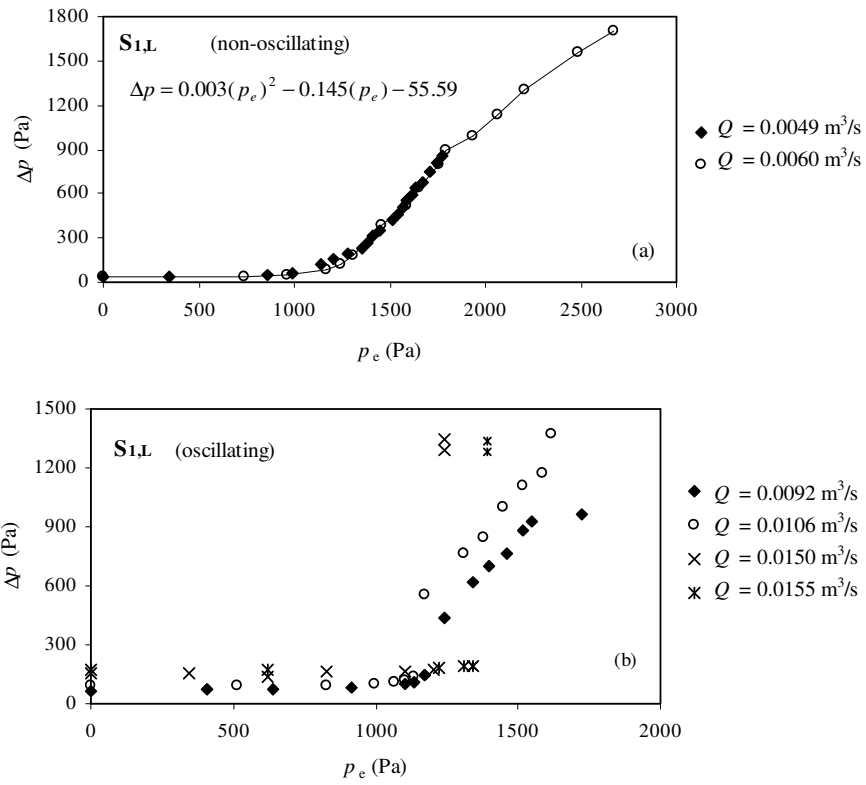


Figure 4.13. Variation of Δp with p_e through $S_{1,L}$ tube for a range of Q

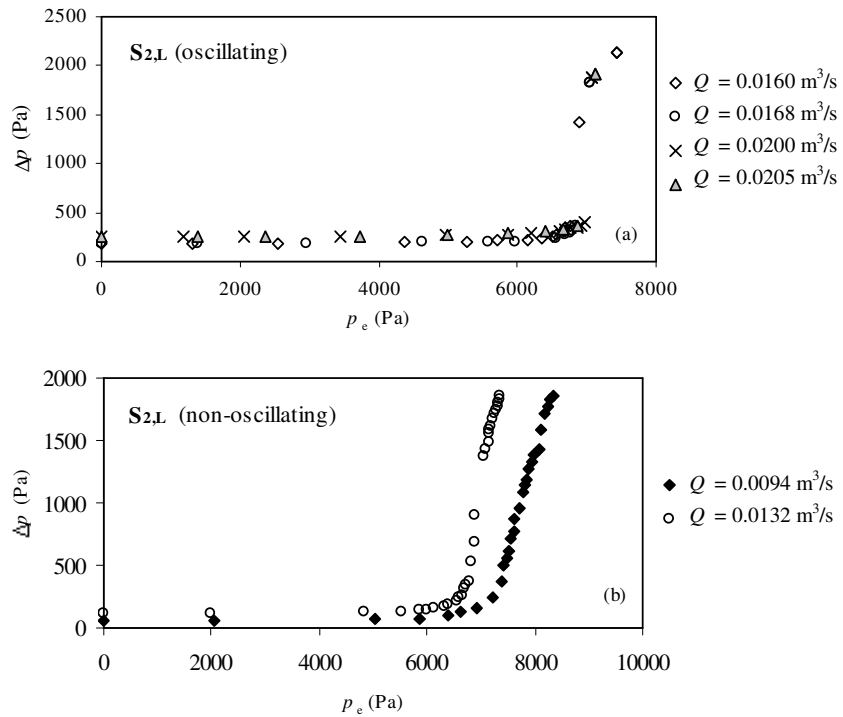


Figure 4.14. Variation of Δp with p_e through $S_{2,L}$ tube for a range of Q

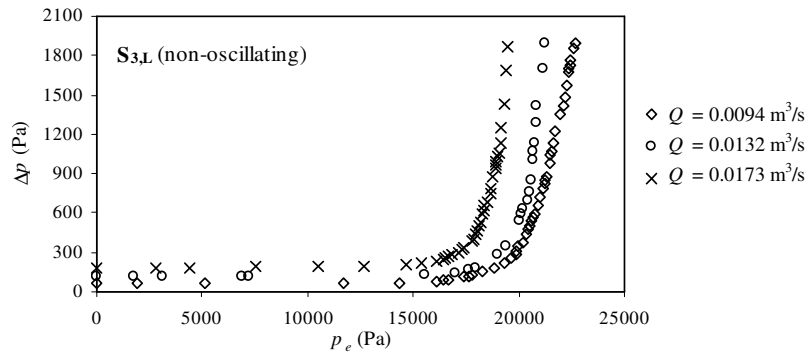


Figure 4.15. Variation of Δp with p_e through $S_{3,L}$ tube for a range of Q

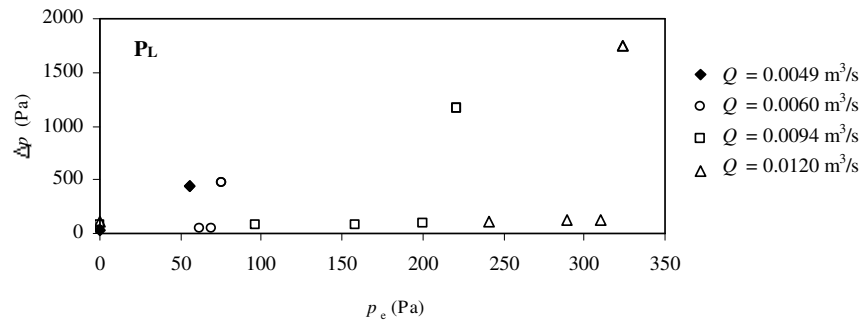


Figure 4.16. Variation of Δp with p_e through P_L tube for a range of Q

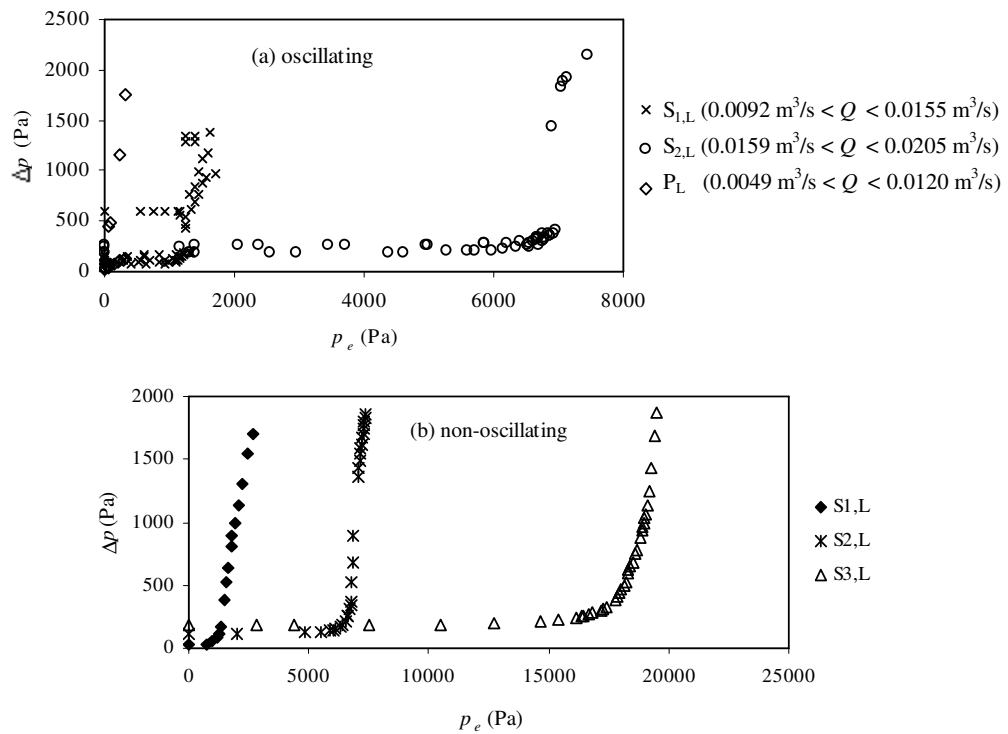


Figure 4.17. Variation of Δp with p_e for the tubes of $L/D_0 = 10$

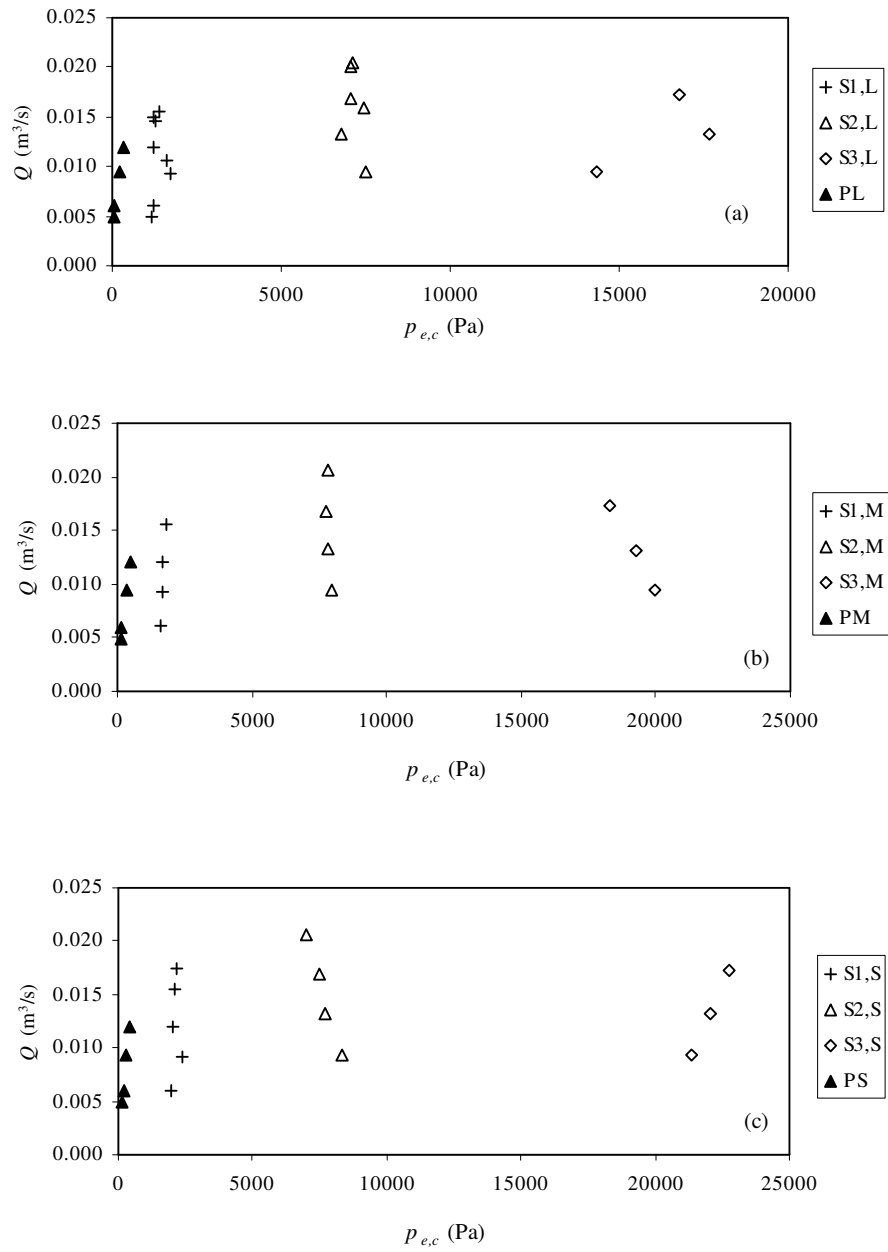


Figure 4.18. Variation of Q with $p_{e,c}$ for indicating the effect of h

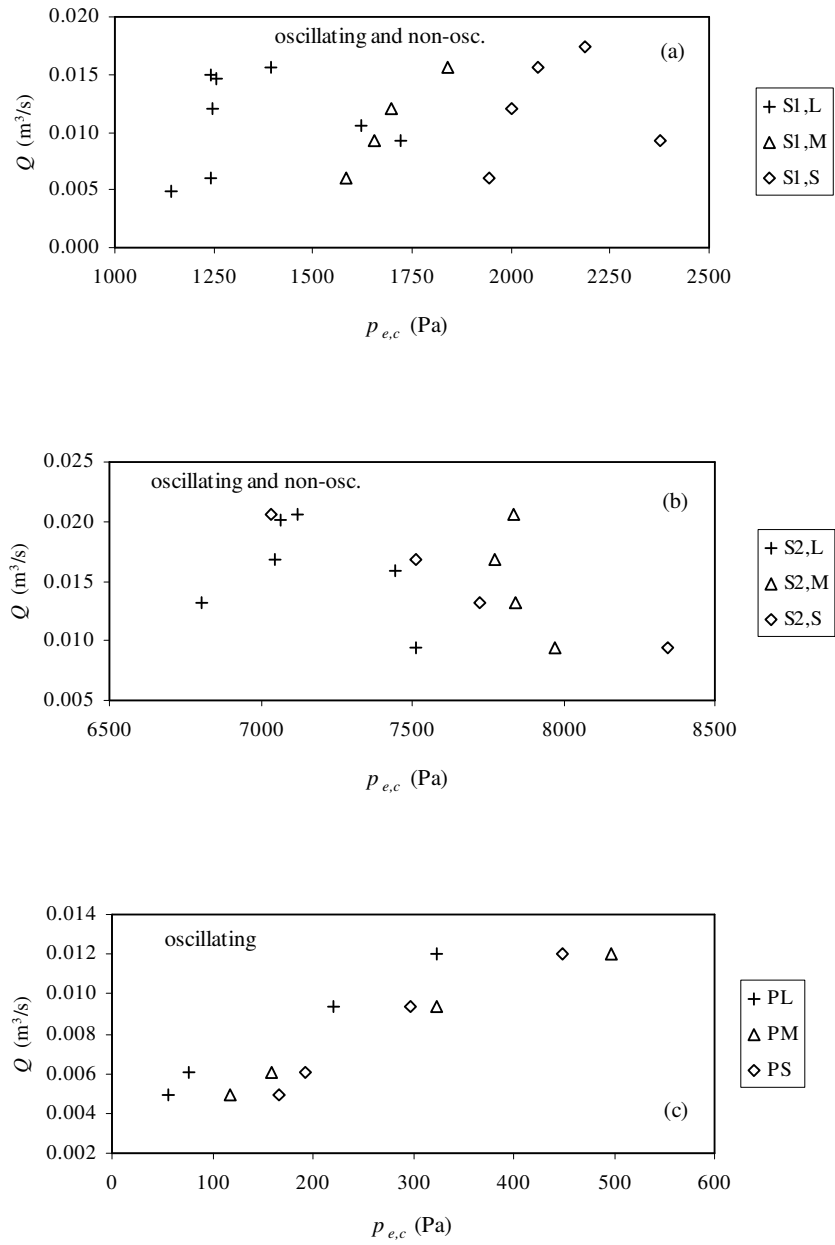


Figure 4.19. Variation of Q with $p_{e,c}$ for indicating the effect of L

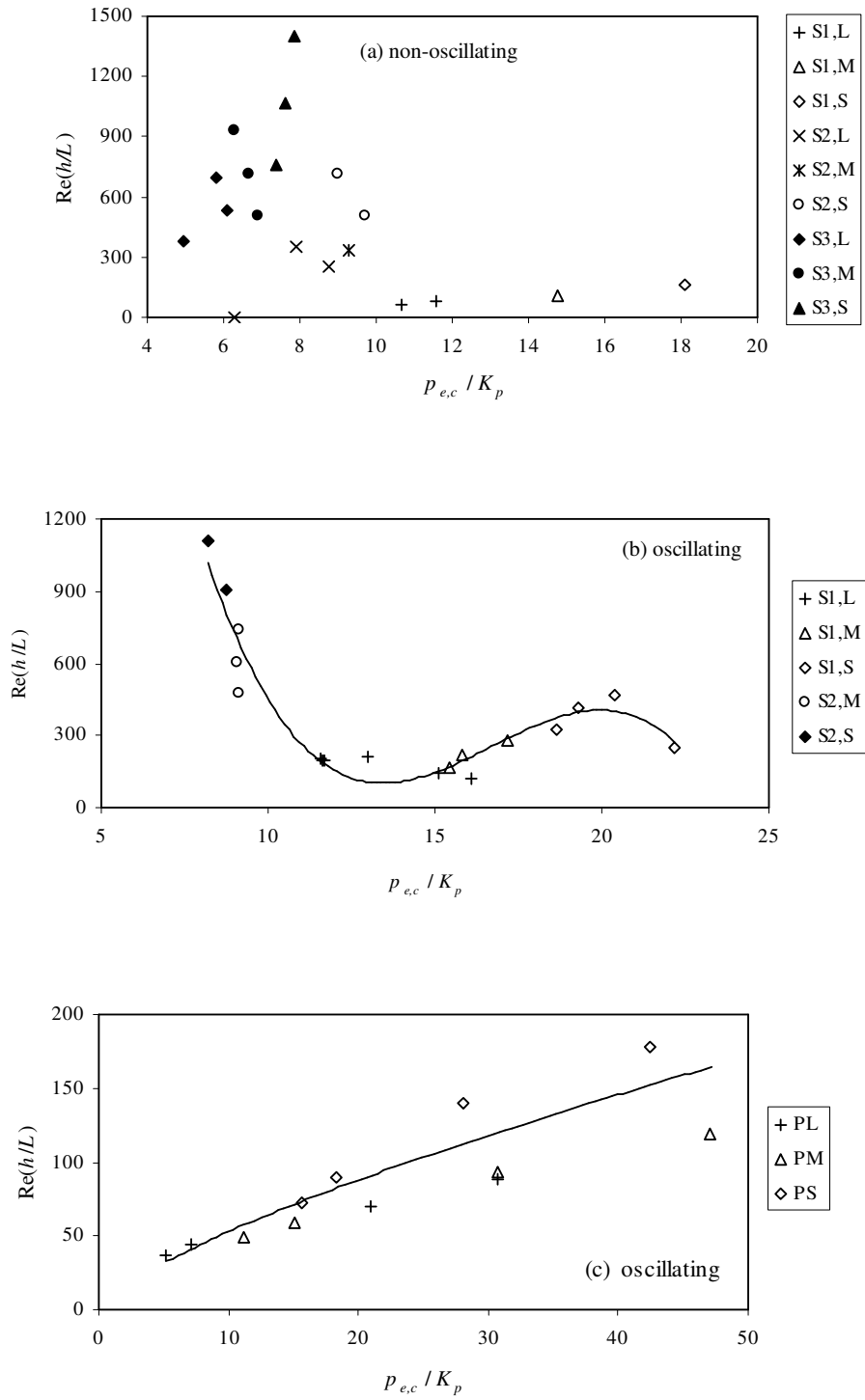


Figure 4.20. Variation of $Re(h/L)$ with $p_{e,c}/K_p$

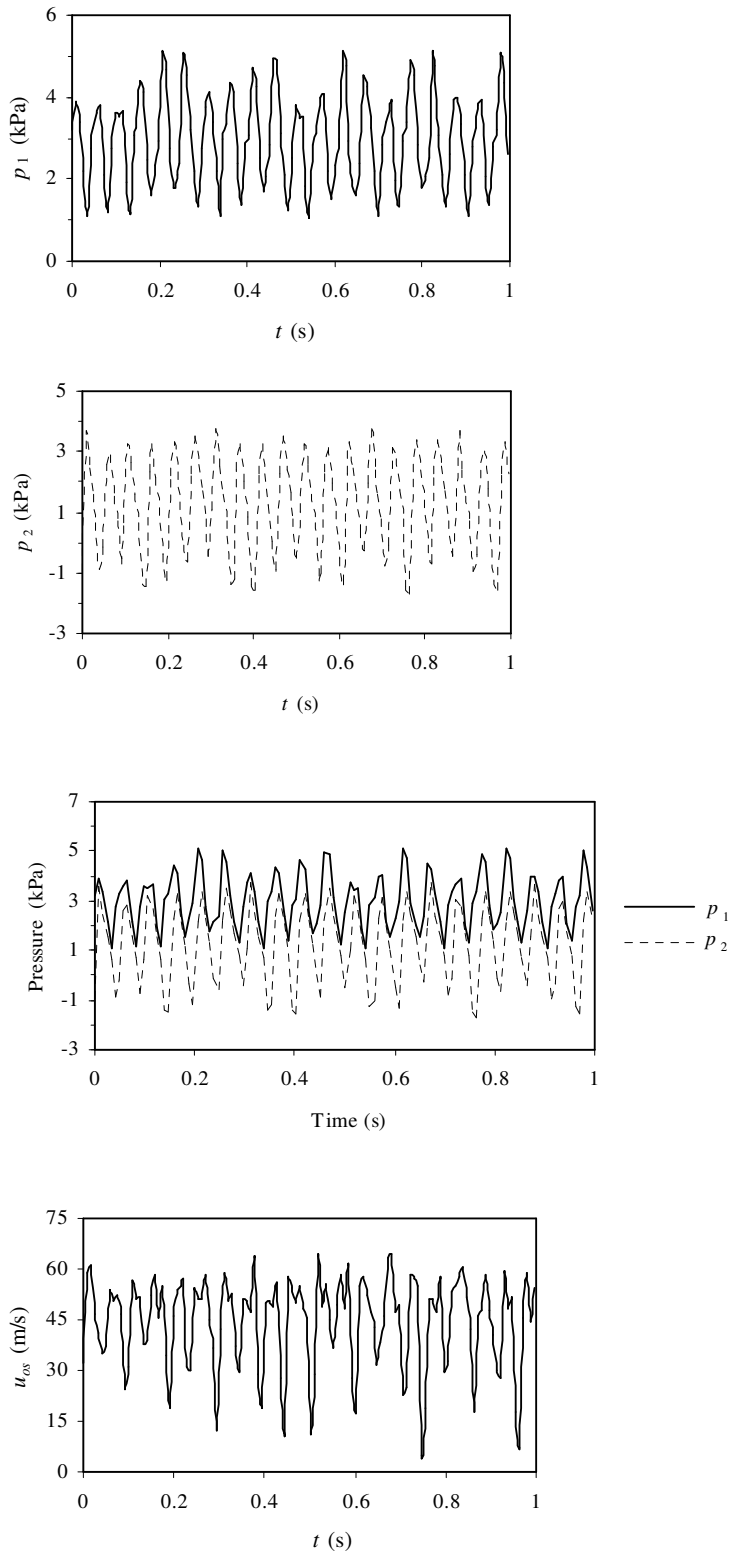


Figure 5.1. Variation of pressure and velocity with time at the onset of oscillations for the flow through $S_{1,M}$ tube ($\bar{p}_1 = 3.2$ kPa, $\bar{p}_2 = 2$ kPa, $\bar{u}_{os} = 43.93$ m/s)

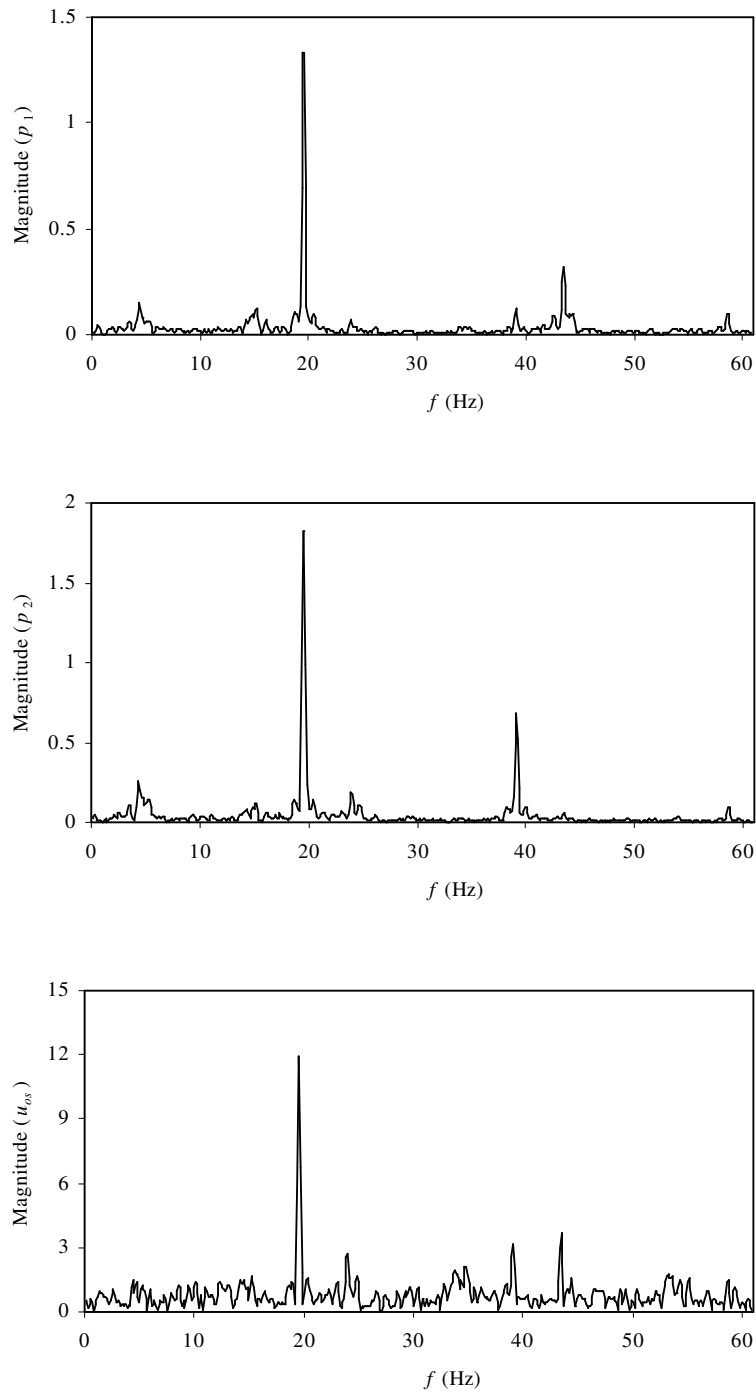


Figure 5.2. FFT analysis of Figure 5.1 (at the peak, $f = 19.60$ Hz for the three cases)

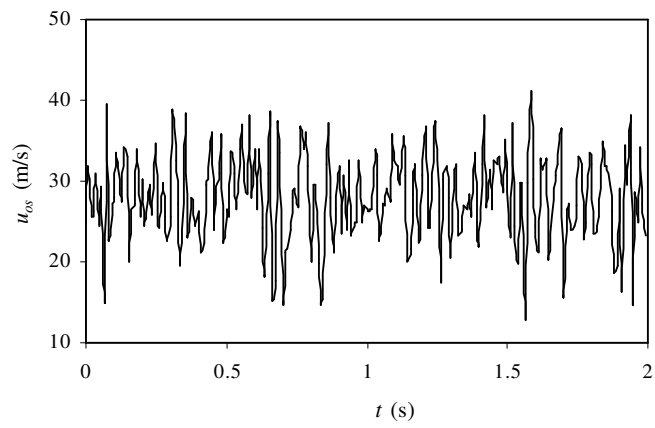
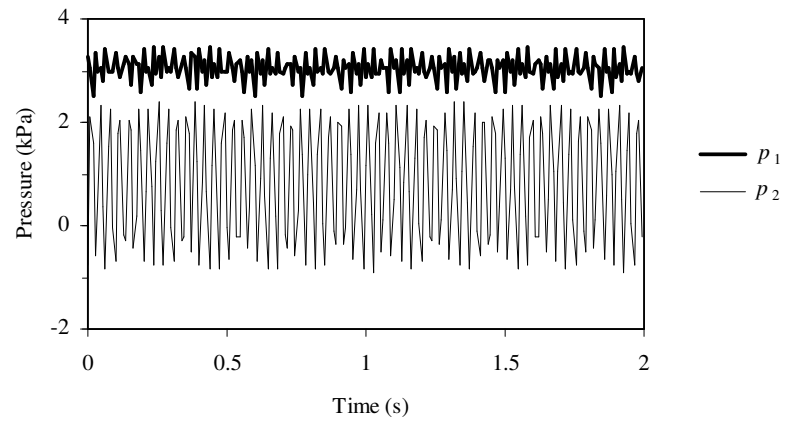


Figure 5.3. Variation of pressure and velocity with time at the onset of oscillations for the flow through $S_{2,s}$ tube ($\bar{p}_1 = 3.01$ kPa, $\bar{p}_2 = 1.38$ kPa, $\bar{u}_{os} = 27.84$ m/s)

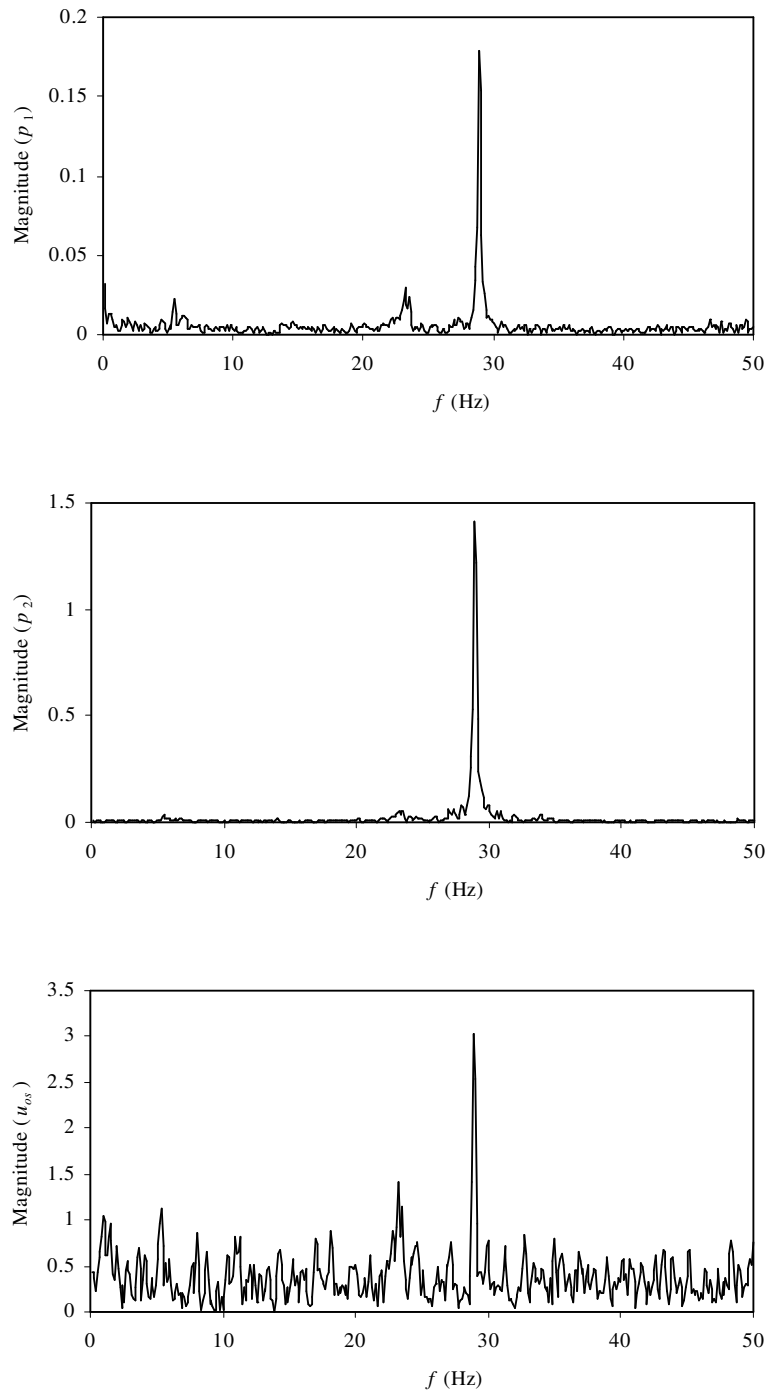


Figure 5.4. FFT analysis of Figure 5.3 (at the peak, $f = 28.89$ Hz for the three cases)

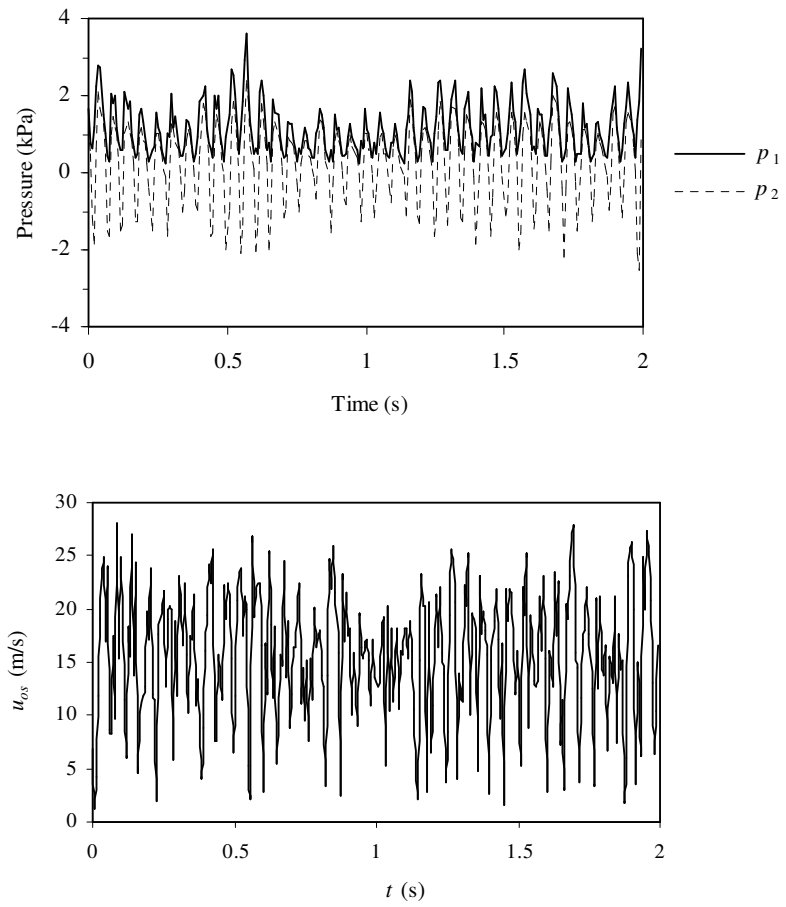


Figure 5.5. Variation of pressure and velocity with time at the onset of oscillations for the flow through P_L tube ($\bar{p}_1 = 1.37$ kPa, $\bar{p}_2 = 1.1$ kPa, $\bar{u}_{os} = 15.27$ m/s)

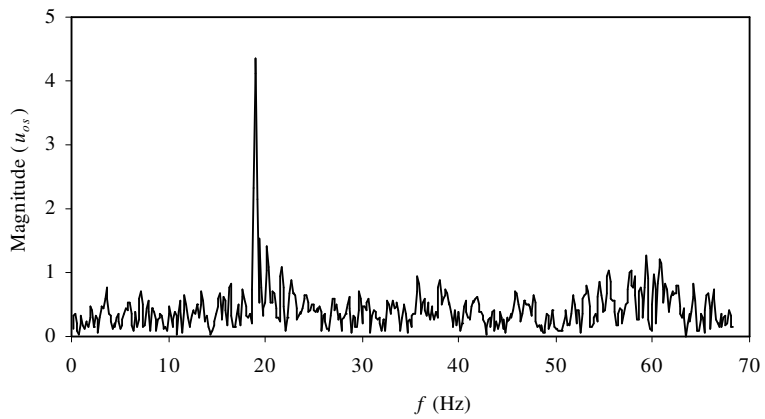
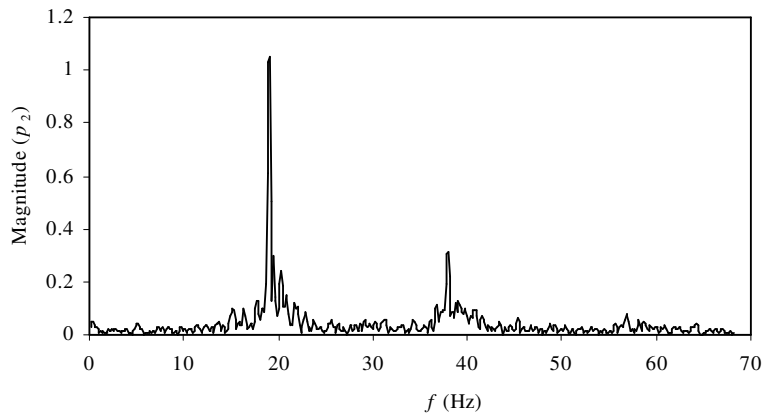
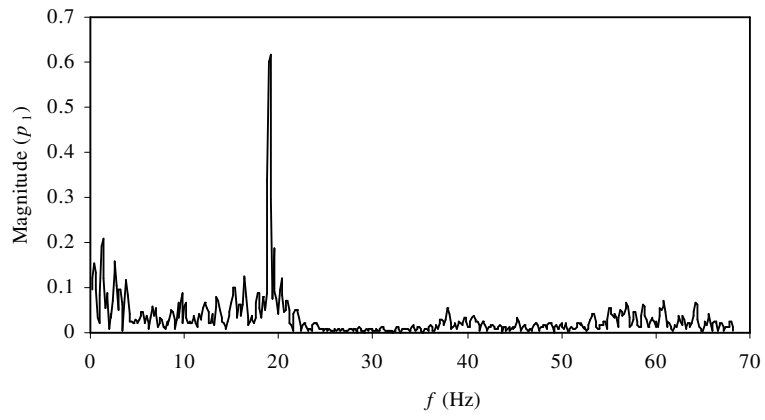


Figure 5.6. FFT analysis of Figure 5.5 (at the peak, $f = 19.06$ Hz for the three cases)

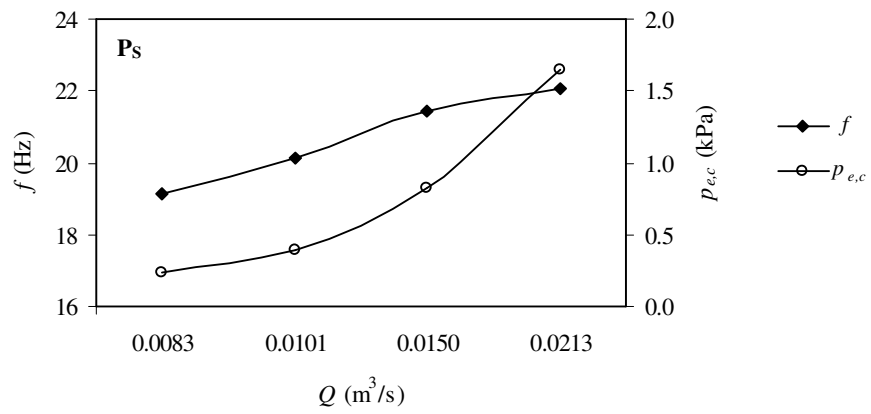
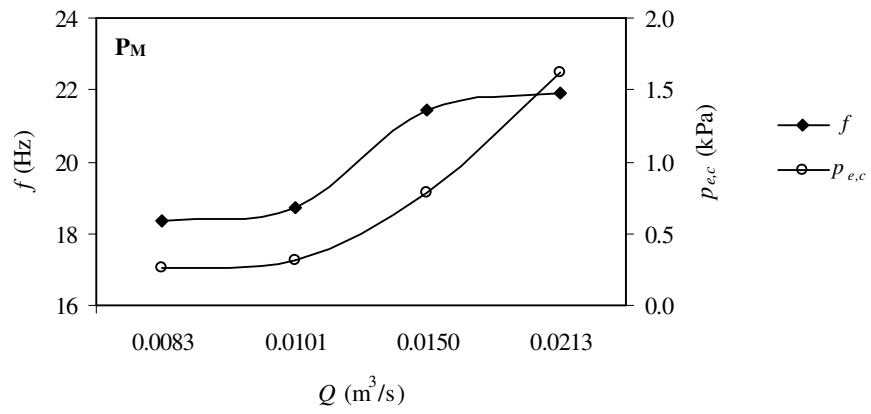
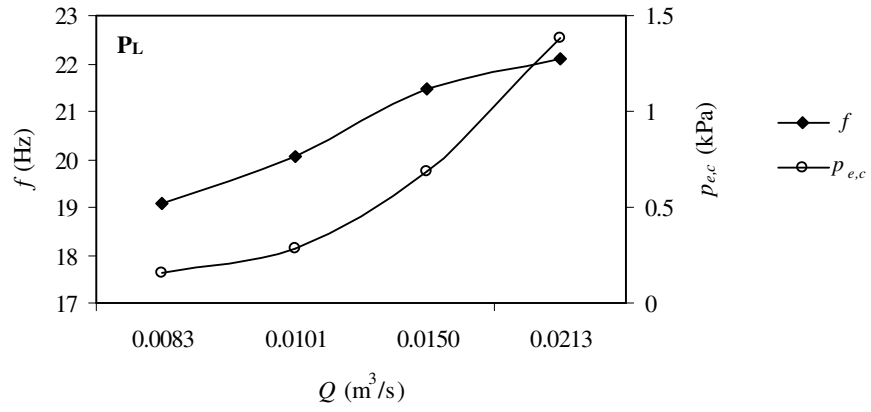


Figure 5.7. Variation of f and $p_{e,c}$ with Q at the onset of oscillations for the flow through P_L, P_M and P_S tubes

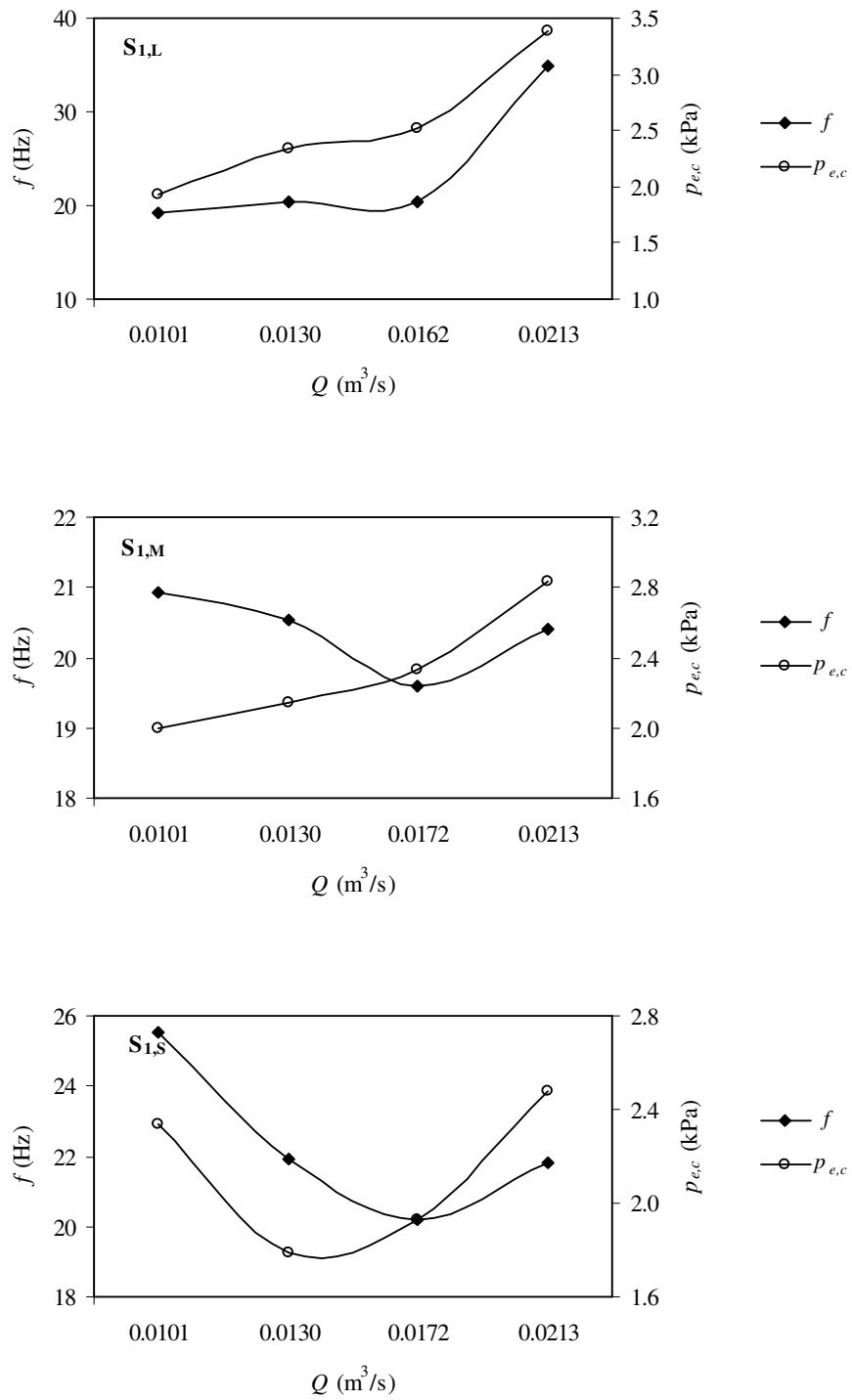


Figure 5.8. Variation of f and $p_{e,c}$ with Q at the onset of oscillations for the flow through S_{1,L}, S_{1,M}, and S_{1,S} tubes

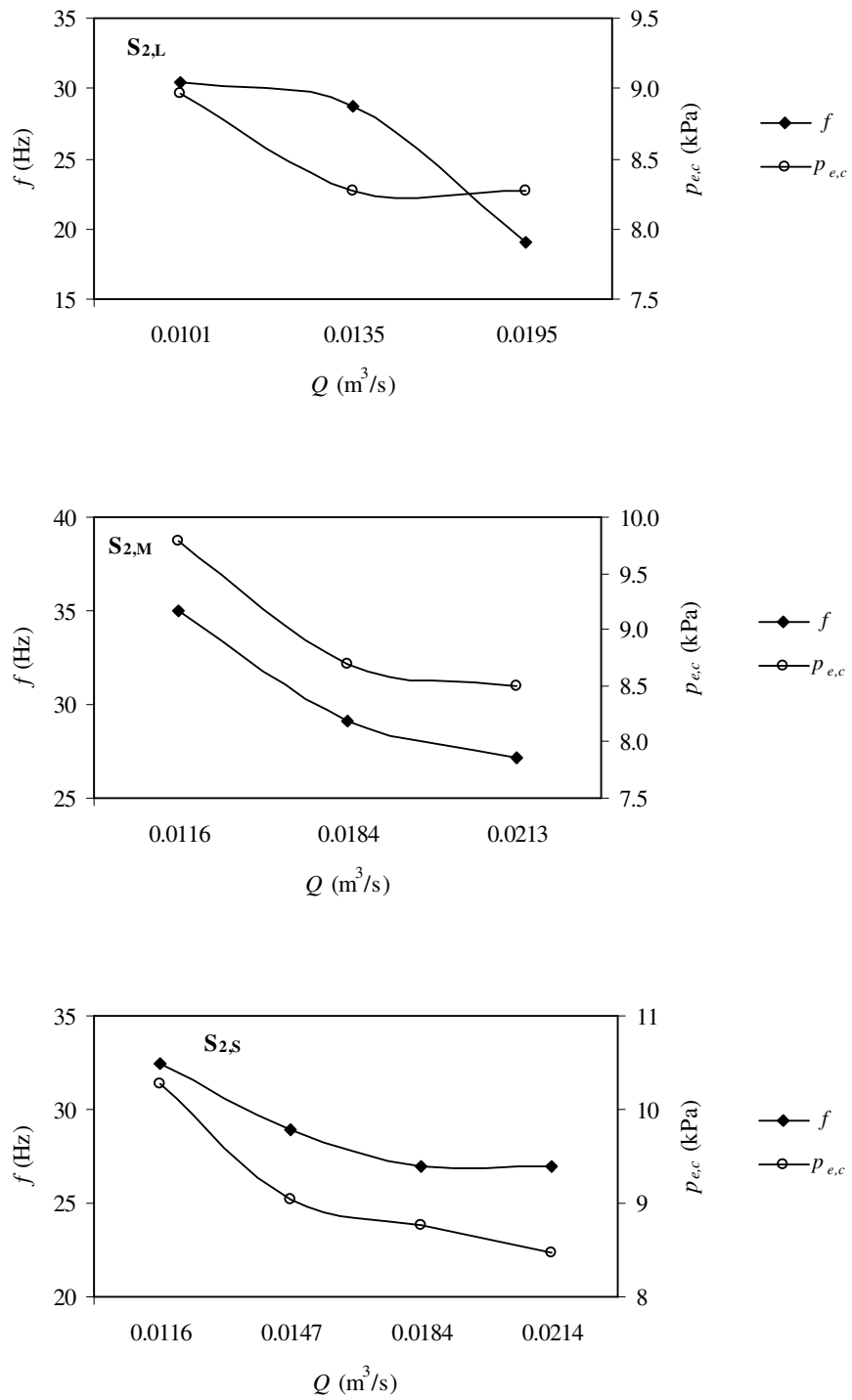


Figure 5.9. Variation of f and $p_{e,c}$ with Q at the onset of oscillations for the flow through S_{2,L}, S_{2,M}, and S_{2,S} tubes

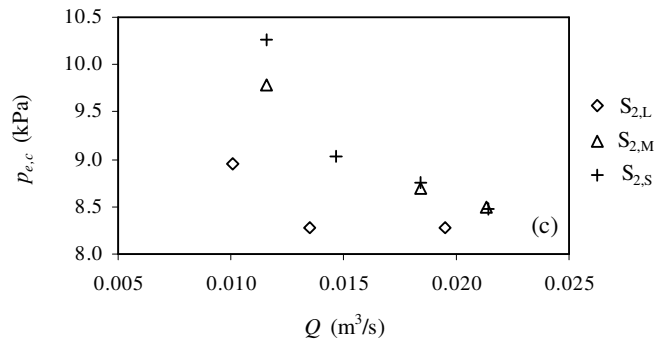
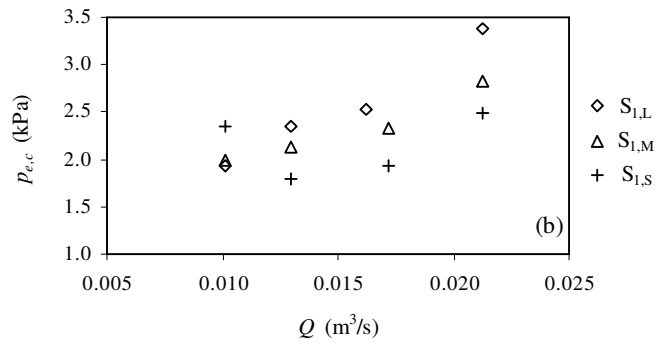
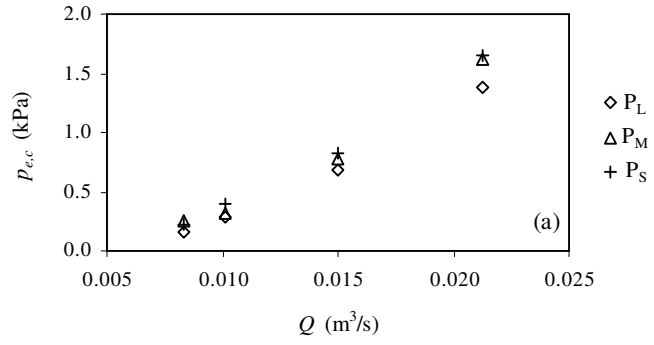


Figure 5.10. Variation of $p_{e,c}$ with Q to show the effect of length of the test tubes at the onset of oscillations

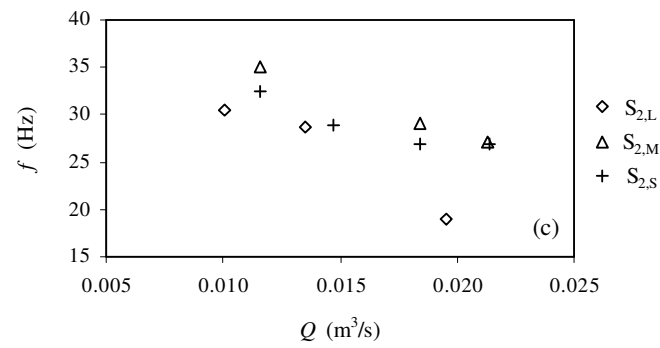
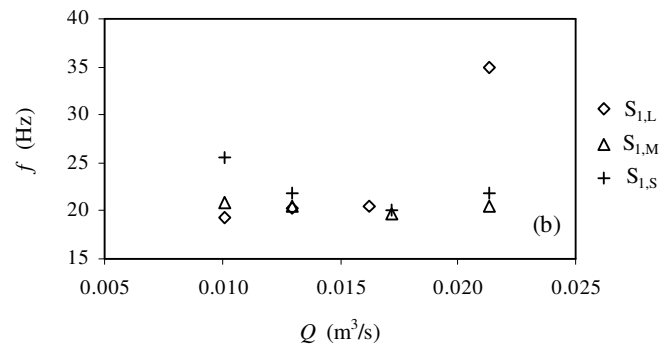
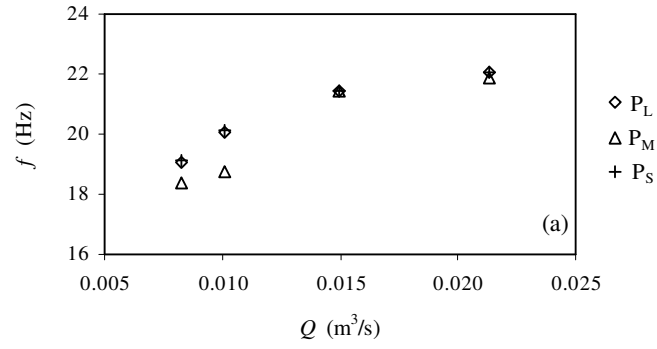


Figure 5.11. Variation of f with Q to show the effect of length of the test tubes at the onset of oscillations

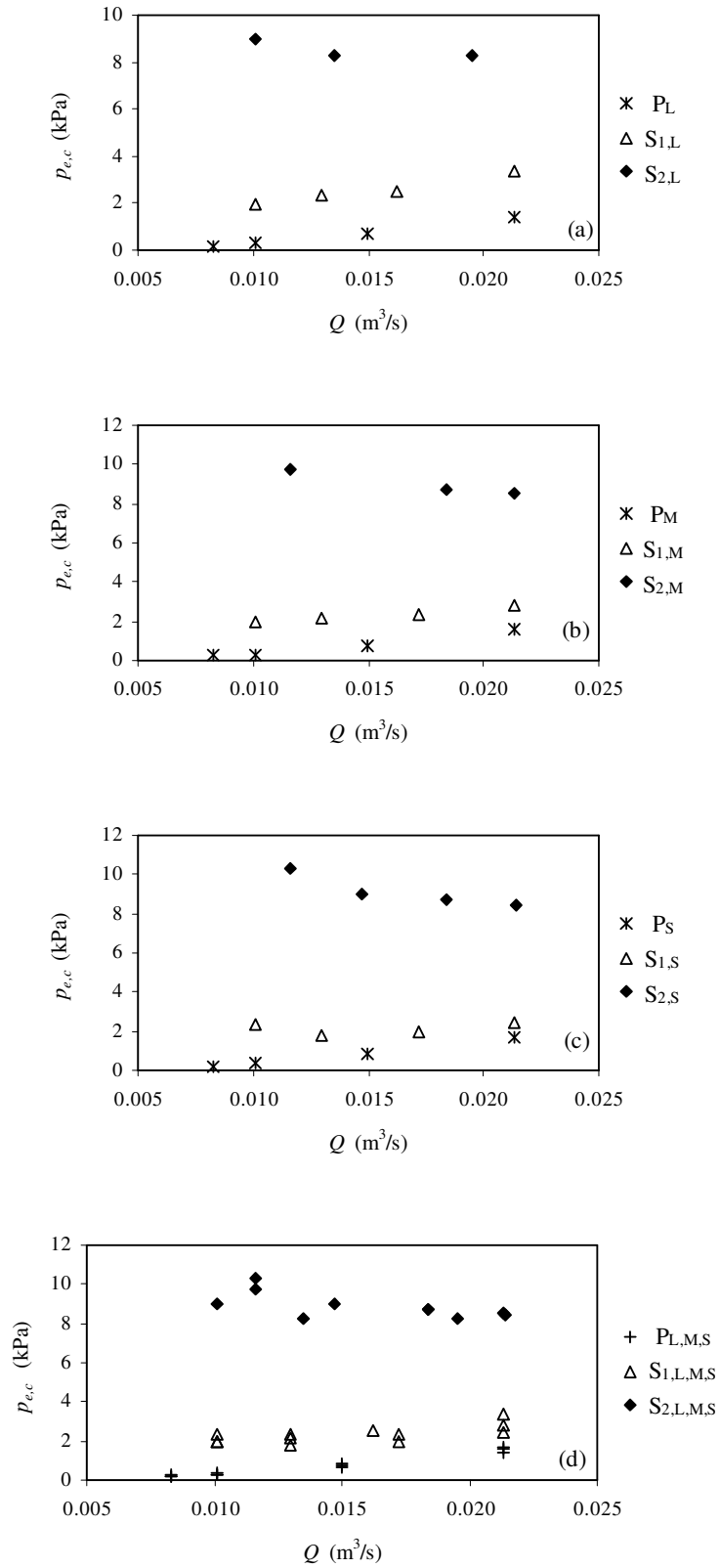


Figure 5.12. Variation of $p_{e,c}$ with Q to show the effect of thickness of the test tubes at the onset of oscillations

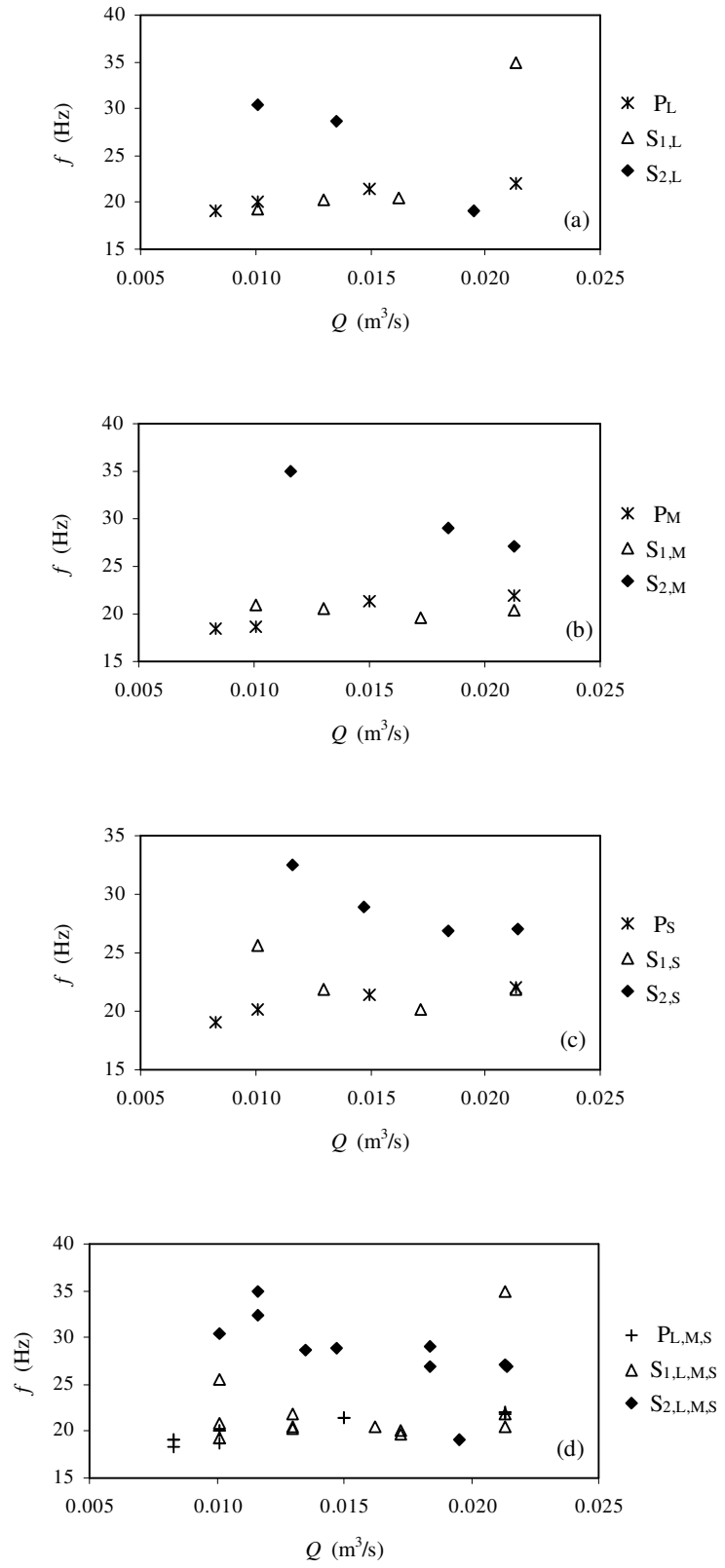


Figure 5.13. Variation of f with Q to show the effect of thickness of the test tubes at the onset of oscillations

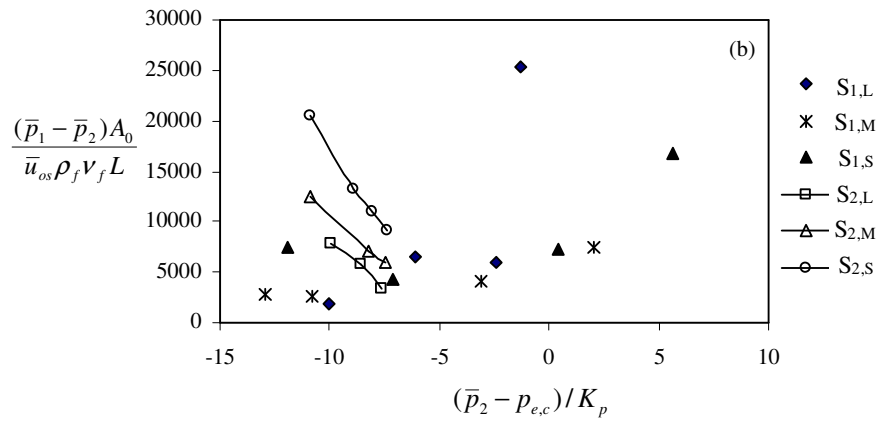
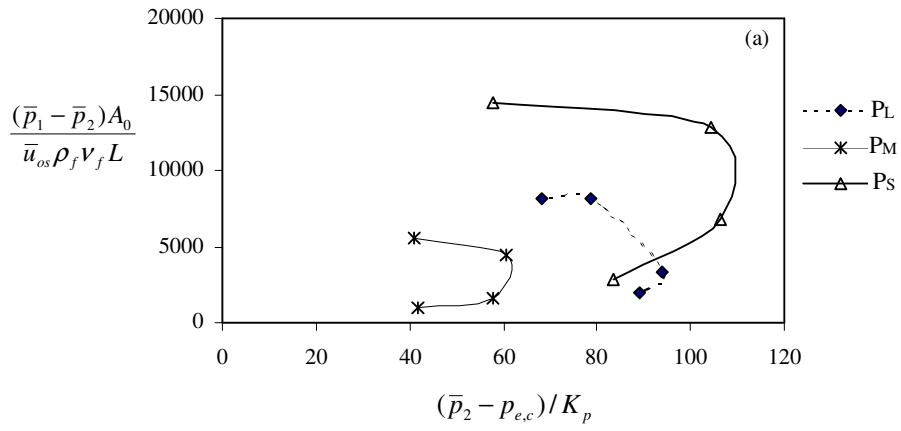


Figure 5.14. Mean flow resistance versus downstream transmural pressure in dimensionless form at the onset of oscillations

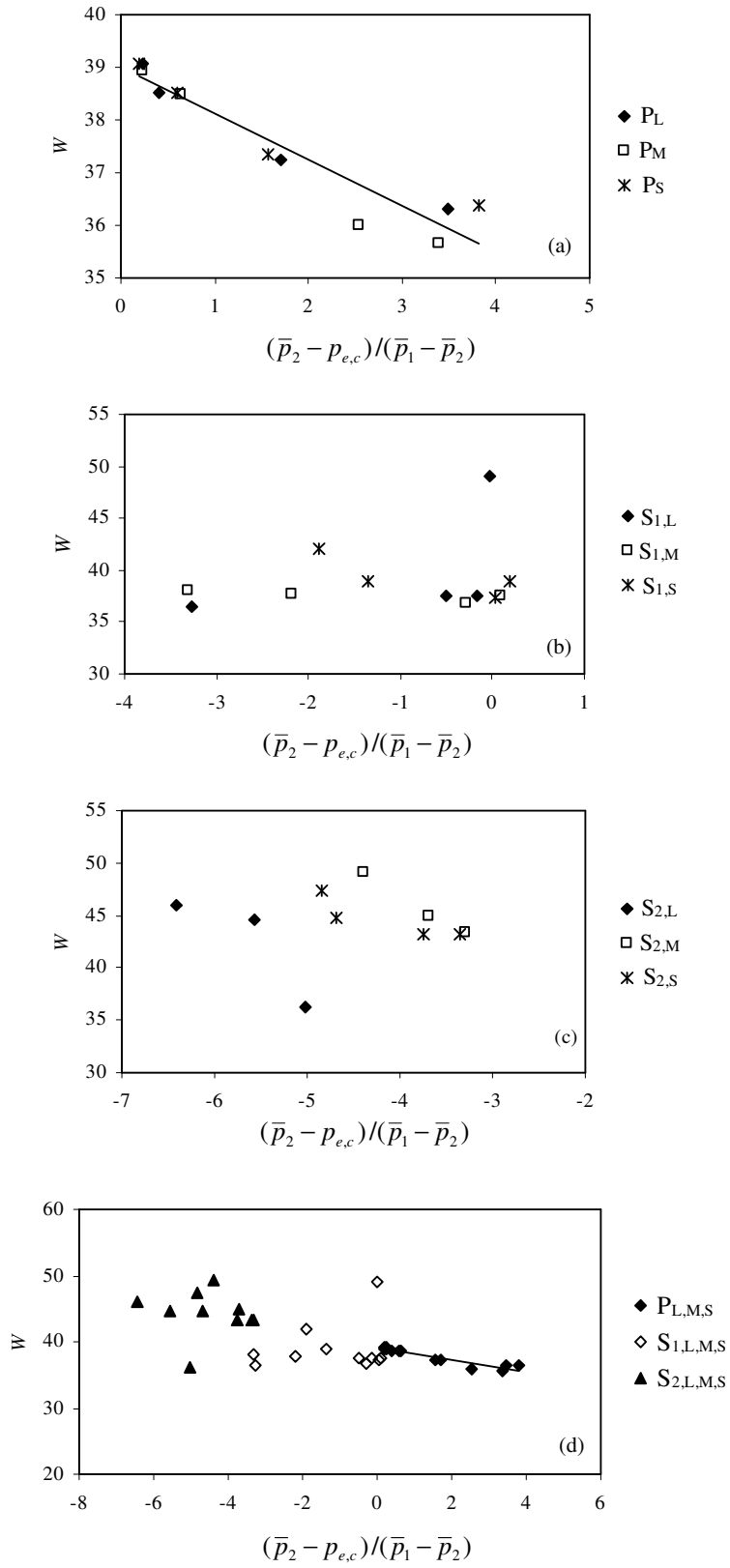


Figure 5.15. Variation of Womersley number with dimensionless downstream transmural pressure at the onset of oscillations

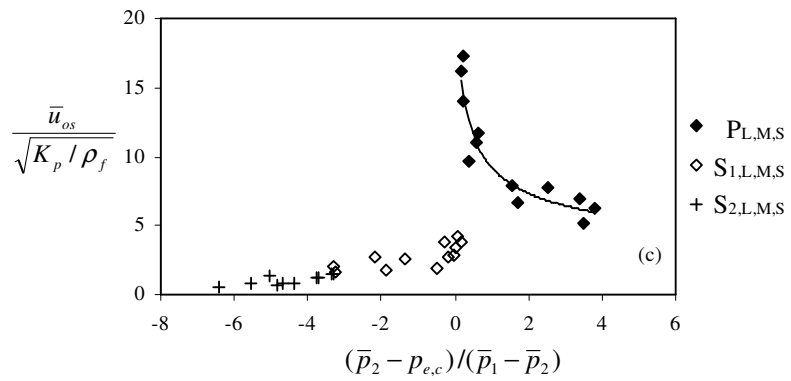
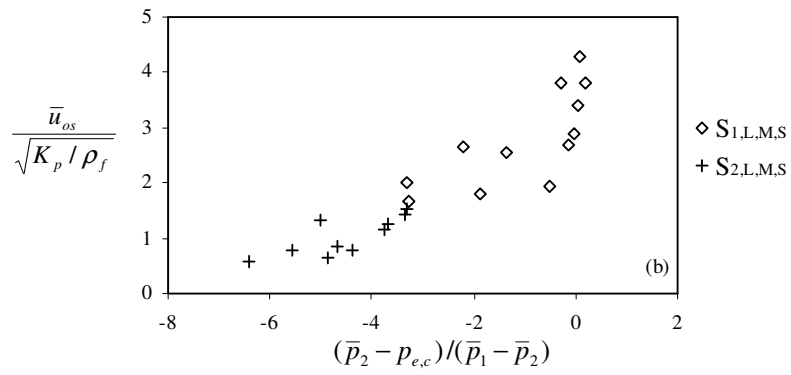
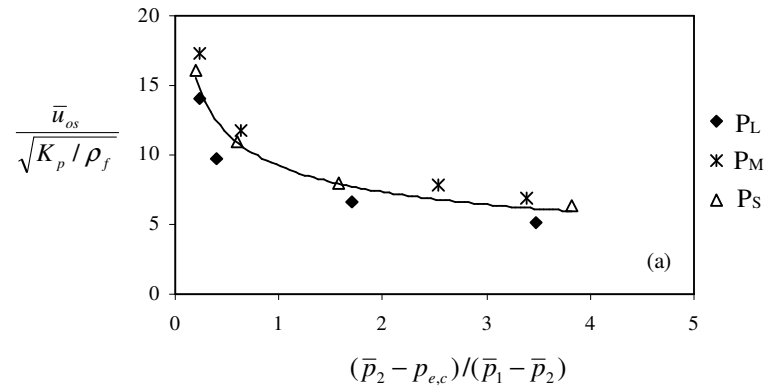


Figure 5.16. Mean oscillating flow velocity versus downstream transmural pressure in dimensionless form at the onset of oscillations

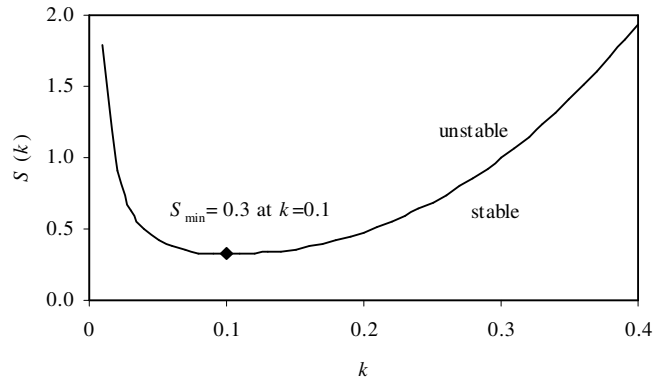


Figure 6.1. Relationship between dimensionless fluid speed (S) and wave number (k) given in reference [13] for $b/D_0 = 0.108$

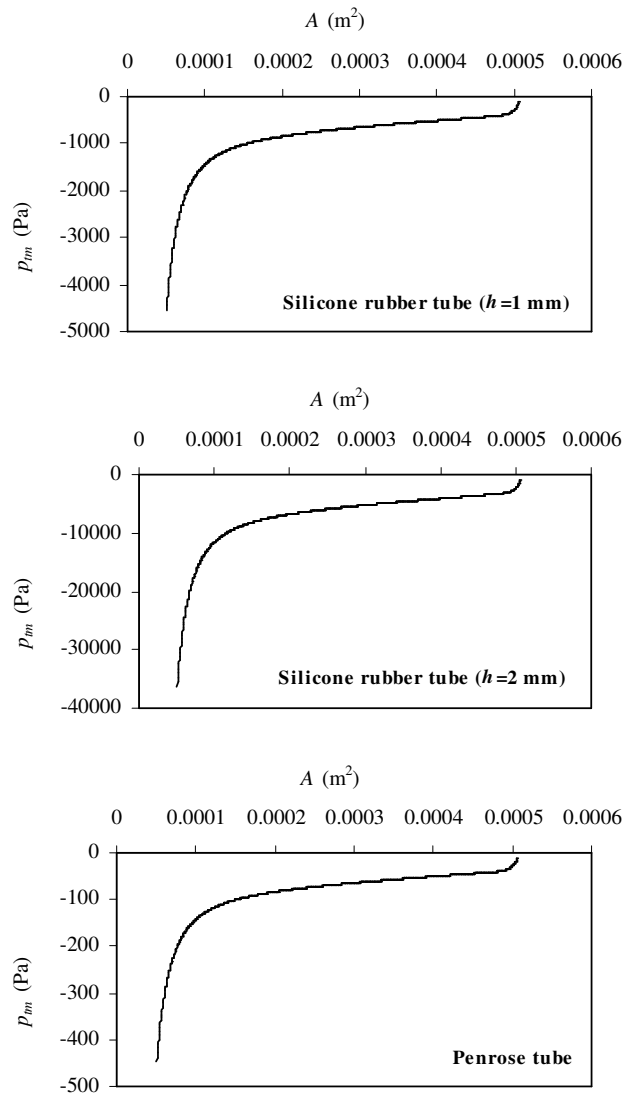


Figure 6.2. Tube law for the test tubes obtained by using equations (6.14 and 6.15)

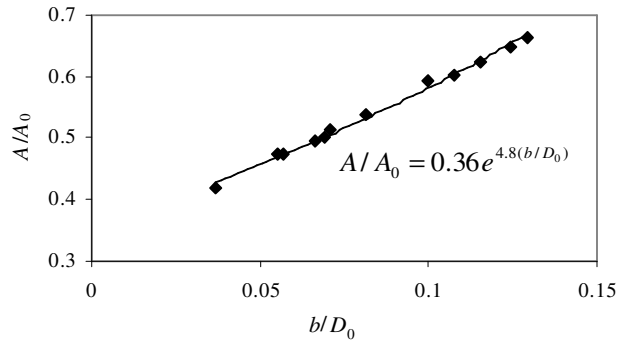


Figure 6.3. The relationship between A/A_0 and b/D_0 obtained by utilizing the experimental data presented in reference [8]

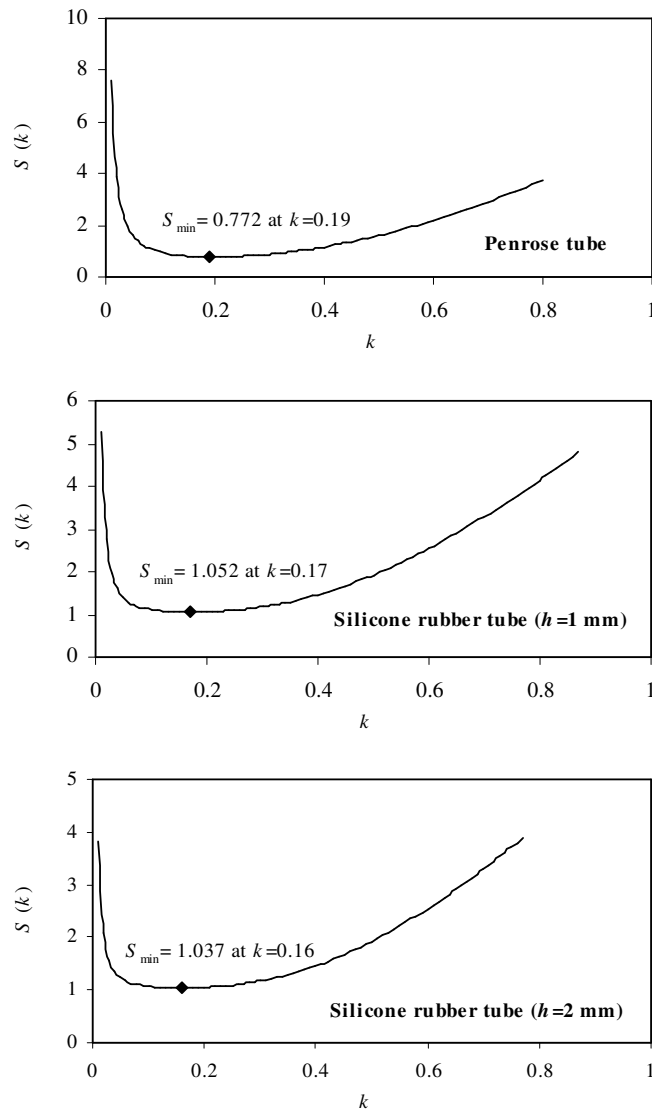


Figure 6.4. The relationship between S and k determined by using linear stability theory presented in reference [13] for $b/D_0 = 0.108$

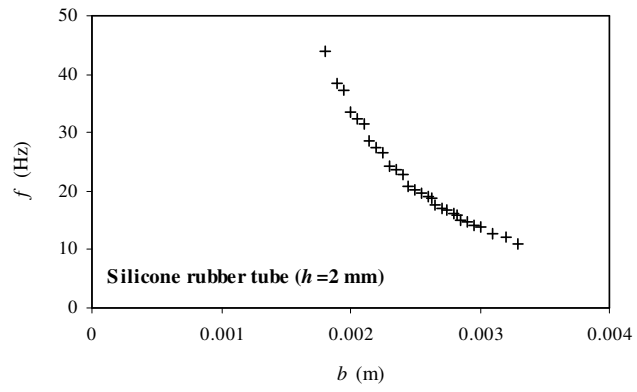
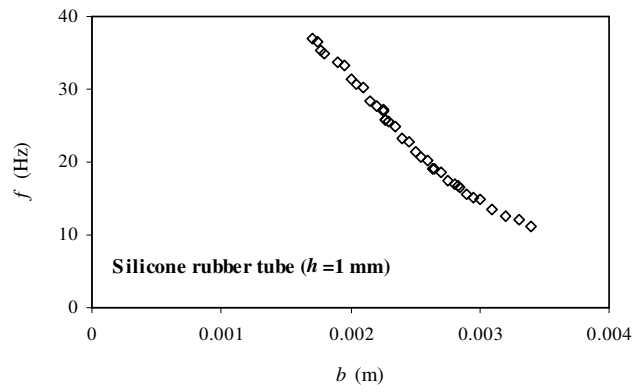
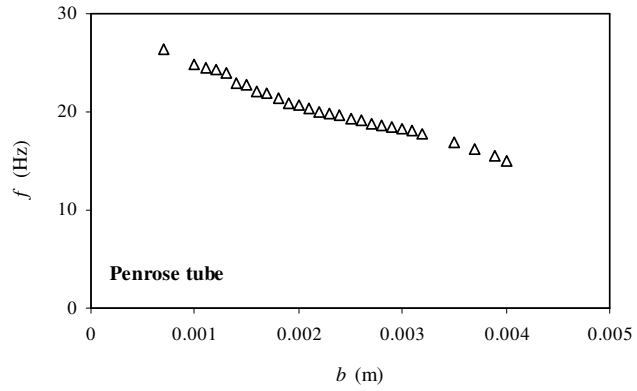


Figure 6.5. Variation of f with b determined by using linear stability theory for the flow through test tubes at the onset of oscillations

APPENDICES

APPENDIX 1

SPECIFICATIONS OF THE COMPRESSOR

Model	: LUPAMAT, LKV 30/8 (PLC)
Type	: Screw
Motor power	: 30 kW
Maximum pressure	: 8 bar
Maximum flow rate	: 0.08 m ³ /s
Length	: 1100 mm
Width	: 1200 mm
Height	: 1250 mm
Weight	: 750 kg

The components of the compressor:

<u>Component:</u>	<u>Type or property</u>
Screw	VMXa 037R
Suction control valve	LEKV 65
Suction control valve piston	45 x 166.5
Minimum pressure valve	LMBV32
Maximum pressure selection relay	LP _{max}
Proportional control valve	LOKV
Solenoid valve	3/2 way; R1/8"
Thermostatic valve	X1-306-71000
Safety valve	R3/4"
Oil filter element (2 units)	6750558246
Separator	49 000 50 111
Oil (28 liter)	Mobil Heavy Medium
Electric motor	30 KW/40HP-3000-B3
Electric Motor	1.1KW/1.5HP-3000-B3
Belt (4 units)	XPA; LP=1500
Fan	355/8-8/40/3HL
Air filter component	3-6 m ³ /min.
Oil level indicator glass	48 x 12
Air hose	1 1/4" x 520 (D+D) R1
Oil Hose	3/4" x 330 (D+90) R1
Pneumatic hose	6 x 8, translucent
Gasket	Presbant VMXa 037R, 120 x 120 x 1
Contactora (1 unit)	3TF40-10
Contactora (1 unit)	3TF42-11
Contactora (2 units)	3TF44-22
Thermic relay	2.5-4A
Thermic relay	25-36A
Time relay	7PU, 0-20SN
N Automatic (1 unit)	Three-phase (4A) C Type
N Automatic (2 units)	Mono-phase (2A; 5SQ2 170 2YA02)
N Automatic (2 units)	Mono-phase (6A; 5SQ2 270 2YA06)
Stop button	XB2-BS542, cork-locked
Transformer	220/220 AC 250 Watt

APPENDIX 2

SPECIFICATIONS of PRESSURE TRANSMITTER for p_e MEASUREMENT

Manufacturer	: BOURDON HAENNI
Model	: E913
Measurement range	: 0.....250 mbar
Output signal	: 4-20 mA
Supply voltage	: 11....40 Vdc
Insulation	: > 100 M Ω at 250 Vdc
Maximum input current	: 6 mA
Load impedance (+M / -M)	: $R_{\Omega} \leq (U_{supply} - 11)/0.02$
CE Conformity	: Directive 89/336 CE (EN50082-1 and -2, EN50081-1 and -2) with screened cable, screen connected at both ends Directive 97/23/CE: 3.3 for $p < 200$ bar
Global error (linearity, hysteresis, and repeatability) by reference to BFSL	Typically: $\pm 0.2\%$ of F.S. / Max.: $\pm 0.3\%$ of F.S.
Operating temperature	
Ambient (T_a)	: -25.....+85 °C
Fluid	: -25.....+100 °C ($T_a \leq 50$ °C)
Storage temperature	: -40.....+85 °C)
Compensated temperature range (zero and sensitivity)	: -10.....+55 °C
Zero thermal drift	: $\pm 0.025\%$ F.S./ °C max. (except $p \leq 1$ bar $\pm 0.06\%$ F.S./°C)
Span thermal drift	: Typically $\pm 0.01\%$ / °C Max. $\pm 0.015\%$ / °C
Wetted parts	: Ceramic + stainless steel 1.4404 (316L) + Viton seal (standard) for ranges ≤ 250 mbar
Standard connection	
Electrical	: DIN 43650 connector
Pressure	: G ½
Protection rating (EN60529)	Standard: IP65 (DIN connector)
Typical response time	: ≤ 3 ms
Vibration resistance (IEC 68-2-6)	: 1.5 mm (10-55 Hz), 20 g (55 Hz to 2 kHz)
Shock resistance (IEC 68-2-32)	: 25 falls from 1 m on concrete ground

APPENDIX 3

TECHNICAL DATA OF ASCON (M1-3000) DIGITAL PROCESS CONTROLLER

Features at env. 25°C	Description			
Total configurability	From keypad or serial communications, the user selects: type of input – associated functions and corresponding outputs - type of control algorithm - type of output and safe conditions - alarm types and functionality - control parameter values			
PV input	Common characteristics	A/D converter with 50.000 points Update measurement time : 0.2 sec Sampling time : 0.5 sec Input shift : + 60 digits Input filter : 1...30 sec (OFF= 0)		
	Accuracy	0.25% ± 1 digit (T/C and RTD) 0.1% ± 1 digit (mA and mV)	Between 100 and 240V~ error is minimal	
	Resistance thermometer for ΔT: R1+R2 must be <320Ω	Pt100Ω at 0°C IEC 751) C /°F selectable	2 or 3 wire connection	Line:20Ω max(3 wire) Thermal drift 0.1°C/10°C env. T. <0.1°C/10Ω line resist.
	Thermocouple	L,J,T,K,S IEC 584) °C /°F selectable	Internal cold junction compensation	Line: 150Ω max Thermal drift <2μV/°C env. T. <0.5μV/10Ω line resist
	DC input (current)	0/4...20mA with 2.5W ext. Shunt Rj > 10MW	Engineering units, floating decimal point, Low Range -999...9999 High Range -999...9999 100 digits minimum	Input drift: <0.1% / 20°C env. T.
	DC input (voltage)	0/10...50mV, Rj >10MW		
	PV Input type	0/4...20 mA 0/10...50 mV	Configurable engineering units mA, mV, V, bar, psi, Rh, ph	
Operating modes	1 single action PID loop or ON/OFF with 1 alarm			
Control mode	Algorithm	P.I.D. with overshoot control or ON/OFF		
	Proport. band (P)	0.5...999.9%		
	Integral time (I)	0.1...100.0 min	OFF = 0	P.I.D. algorithm
	Derivative time (D)	0.01...10.00 min		
	Cool cycle time	1...200 sec.		
	Overshoot control	0.01...1.00		
	High limit	100.0...10.0% (heat) -100.0...-10.0% (cool)		
	Hysteresis	0.1...10.0%		ON/OFF algorithm
OP1 output	SPST relay N.O., 2A/250V~ for resistive load Triac, 1A/250V~ for resistive load			
OP2 output	SSR drive not isolated: 5V-, ± 10%, 30mA max SPST relay N.O., 2A/250V~ for resistive load			
AL1 alarm (indicator with 2 alarms)	Hysteresis 0.1 ... 10.0% of range			
	Active high	Absolute threshold, whole range		
	Active low			

Features at env. 25°C	Description	
Setpoint	Up and down ramps	0.1...999.9 digit/min (OFF = 0)
	Low limit	from low range to high limit
	High limit	from low limit to high range
OP4 (option) PV or SP retransm. output	Galvanically isolated: 500V~/1min Resolution: 12bit (0.025%) Accuracy: 0.1%	In current 0/4...20mA 750Ω/15V max
One-shot Fuzzy-Tuning	Depending on the process condition, the controller applies the best method	Step response
		Natural frequency
Operational safety	Measure input	Detection of out of range, short circuit or sensor break with automatic activation of the safety strategies and alerts on display
	Control output	Safety value (user enabled/disabled): 0%, 100%
	Parameters	A non volatile memory stores for unlimited time all the parameter and configuration values
	Password	A password protects the access to the instrument configuration and parameters
General characteristics	Power supply	100-240V~ (-15% +10%) 50/60Hz or 24V~(-25% +12%), 50/60Hz and 24V- (-15% +25%). Power consumption 1.6W max
	Safety	Compliance EN61010-1 (IEC 1010-1), installation class 2 (2500V), pollution class 2, class II instrument
	Electromagnetic compatibility	Compliance to the CE standards for industrial system and equipment
	Protection EN60529 (IEC 529)	IP65 front panel
	Overall dimensions	1/16 DIN - 48 x 48, depth 120 mm, weight 130g appr.
Panel cut-out: 45 ^{+0.6} x 45 ^{+0.6} mm		

APPENDIX 4

TECHNICAL SPECIFICATIONS OF PRESSURE TRANSDUCERS for p_1 and p_2 MEASUREMENT

Manufacturer	: OMEGA ENGINEERING
Model	: PX951-010G5V
<u>Electrical</u>	
Excitation	: 24 to 40 Vdc @ 25 mA
Output	: 0-5 Vdc (4-wire)
Insulation Resistance	: 5 M Ω @ 75 Vdc
<u>Performance</u>	
Measurement range	: 0 to 10 psi (0 to 68.947 kPa)
Accuracy	: $\pm 0.15\%$ (Combined effect of linearity, hysteresis and repeatability)
Hysteresis	: $\pm 0.10\%$ typical
Repeatability	: $+0.05\%$ typical
Zero Balance	: $\pm 1\%$
Zero and Span Adjustments	: $\pm 20\%$
Shunt Value	: 80% Full Scale
Frequency Response	: 3 kHz
Operable Temperature Range	: 0 to 185°F (-18 to 85°C)
Compensated Temperature Range	: 60 to 160°F (16 to 71°C)
Thermal Zero Effect	: $\pm 0.005\%$ full scale/°F
Thermal Sensitivity Effect	: $\pm 0.005\%$ Reading/°F
Proof Pressure	: 150% Range
Burst Pressure	: 300% Range
<u>Construction</u>	
Body Material	: 17-4 PH Stainless Steel
Diaphragm Material	: 17-4 PH Stainless Steel
Pressure Port	: 1/4 - 18 NPT Male Thread 10 to 1,000 psi; Female thread 3,000 to 7,500 psi
Weight	: 13.5 oz (383 g)

APPENDIX 5

TECHNICAL SPECIFICATIONS OF THE HOT-WIRE ANEMOMETER and ITS PROBE

The hot-wire anemometer used for the axial velocity measurement was consisted of the 56C01 CTA main unit, the 56C17 CTA bridge, and the 56N21 linearizer. The hot-wire anemometer and the 55P14 type miniature wire probe have the following technical specifications:

Hot-Wire Anemometer

56C01 Main Unit

Manufacturer	: DANTEC Electronic Ltd.
Input White Noise	: $2.2 \text{ nV} / (\text{Hz})^{1/2}$
Input Temperature Drift	: $3 \text{ } \mu\text{V} / ^\circ\text{C}$
Upper Frequency Limit	: 330 kHz at AC gain 1100
AC Gain in FLOW Position (over 100 kHz)	: $146 (1+10/R \text{ [k}\Omega])$ for wire
DC Gain in FLOW Position	: $146 (1+383/R \text{ [k}\Omega])$
Gain in TEMP. Position	: Controlled by CTA Bridge
Max. Input Common Mode Range	: 0 to approx. 5 V
Maximum Output Voltage (with 50 Ω load)	: 6 V
Output Current Limiting	: 0.095 A
Frequency of Square-Wave Test Signal	: approx. 1 kHz
Output Impedance	: 10 Ω

56C17 CTA Bridge

Probe Resistance Range	: 3-30 Ω
Bridge Ratio	: 1:20
Upper Frequency Limit	: 150 kHz
Maximum Probe Current	: 315 mA
Typical Output Noise Level	: 0.02 % Turbulence
Output Impedance	: 10 Ω
Output Voltage Range	: 0-12 V
Maximum Gain AC	: 1111
Maximum Gain DC	: 38783
Maximum Length of Transducer Cable	: 100 m
Uncertainty in Resistance Measurement	: <5 %
Ambient Temperature Range	: 5-40 $^\circ\text{C}$
Ambient Humidity Range	: 20-80 %

56N21 Linearizer

Type of Linearization Principle	: Exponential
Accuracy of linearity	: 0.5% reading, +0.15 % full scale
Upper Frequency Limit	: 300 kHz
Input Impedance	: $10^4 \text{ M}\Omega$
Output Impedance	: 100 Ω
Input Voltage Range	: 0-12 V
Output Voltage Range	: 0-10 V
Stability	: 0.05 % / $^\circ\text{C}$

55P14 Miniature Wire Probe

Probe Support	: 4 mm-dia. Probe supports
Mounting	: 4 mm-dia. Mounting tubes
Sensor Type	: Miniature Wire sensors
Sensor Material	: Platinum-plated tungsten
Sensor Dimensions	: 5 μ m dia. 1.25 mm long
Sensor Resistance R_{20}	: 3.5 Ω
Temp. Coefficient of Resistance α_{20}	: 0.36 % / $^{\circ}$ C
Maximum Sensor Temperature	: 300 $^{\circ}$ C
Maximum Ambient Temperature	: 150 $^{\circ}$ C
Maximum Ambient pressure	: Depends on type of mounting
Minimum Velocity	: 0.2 m/s for air
Maximum Velocity	: 500 m/s for air
Frequency Limit f_{cpo}	: 90 Hz for air
Frequency Limit f_{cmax}	: 400 kHz for air
Recommended Medium	: Air and distilled water

APPENDIX 6

FEATURES OF THE DAS-1602 HARDWARE

The DAS-1600 Series of boards is a family of high-performance analog and digital I/O boards for IBM PC AT, and equivalent computers. The DAS-1602 board provide the following features:

1. Board is switch-configurable for 1+ single-ended or 8 differential analog input channels.
2. Analog inputs are is switch-configurable for either unipolar (0 to 10 V) or bipolar (± 10 V) signals.
3. Analog input channels are individually programmable for gains of 1, 2, 4 and 8.
4. Analog input sampling is maximum of 100 ksamples/sec with 12-bit resolution.
5. The base I/O address and Direct Memory Address (DMA) channel are is switch-configurable, interrupt levels are is switch-configurable.
6. Burst mode sampling capability emulates simultaneous sample-and-hold (SSH) operation.
7. Analog to Digital (A/D) conversions run by any of the following methods:
 - software command
 - onboard pacer clock
 - external pacer clock
8. External SSH hardware is supported
9. Data transfer can run by any of the following methods
 - program control
 - interrupt service routines
 - DMA transfer
10. A 3-channel programmable counter/timer (82C54) provides timing for analog input operations or generation of output pulses at any rate from 1 pulse/hour to 100 kHz.
11. The board have four unidirectional digital inputs and four unidirectional digital outputs.
12. The board have two 12-bit digital to analog converter (DAC) channels. The output of these channels have switch configurable output ranges 0 to 5 V, 0 to 10 V, ± 5 V and ± 10 V full scale.

APPENDIX 7

TESTING AND CALIBRATION OF THE DAS-1602 HARDWARE

Testing of the Hardware Board Operation

The functions of the installed board were tested by the control panel program, CTL1600.exe, furnished in the standard software package. The below steps were followed during the test:

- i. Directory was changed to the directory containing the CTL1600.exe program.
- ii. After the control panel started, the name of the configuration file compatible with the switch settings of the board was selected.
- iii. The control panel displayed buttons and a list box that allowed acquiring the data.
- iv. The appropriate buttons were selected to set up and perform the analog and digital I/O operations.
- v. The information on the set-up and performance of the hardware operations was obtained as satisfactorily from the control panel program.
- vi. Exit from the program to calibrate the internals of the hardware.

Calibration of the Hardware Board Internals

The board had been initially calibrated at the factory. CAL1600.exe calibration utility program included in the standard software was used to calibrate the board. The following equipment were also used during calibration of the board internals:

- A digital voltmeter accurate to a minimum of 5 ½ digits
- A DC voltage source with a range of ± 10 V
- A STA-16 screw terminal accessory box with C-1800 cable for connections of input voltages and measuring output voltages.
- A small screwdriver for adjusting pots.

These equipments were used in connection with the potentiometers and test points of the board. The preliminary set-up of the board required for the calibration was that the DAS-1602 board installed to the computer and connected to the STA-16 accessory box with C-1800 cable. After the set-up of the board for calibration was

completed, the calibration utility was started by changing to its directory. In the program the following option values were settled as consistent with the board configuration parameters:

Options	Default Settings
A/D input mode	Bipolar
A/D Cal Chan#1	0
A/D Cal Chan#2	1
DAC0 reference	-5.0
DAC0 mode	Bipolar
DAC1 reference	-5.0
DAC1 mode	Bipolar

Then the following calibrations were done due to the guides of the program

1. Input Amplifier Zero Calibration:

- i. The positive gate of the Digital Volt Meter, DVM(+) was connected to the test point 1, TP1 of the board and DVM(-) was connected to the TP2. Then the DVM was settled to measure millivolts.
- ii. On the STA-16 accessory box, the positive (HI) and the negative (LO) gates of the analog input channel 0 were connected to the low level ground (LLGND).
- iii. The preamplifier offset was nulled by trimming an input offset at the high gain and the output offset low gain. Adjustment of the amplifier required that the pots be alternately adjusted until readings on the DVM were balanced close to 0 volts ± 1.0 millivolts.

2. A/D Bipolar Input Offset Calibration:

- i. On the STA-16 accessory box, the calibration voltage -9.9609 V from the DC power source was connected to the HI of the analog input channel 1. The return of the calibration voltage was connected to the both the LO of the channel 1 and the LLGND.
- ii. The previously connected test leads from TP1 and TP2 were removed.
- iii. The related pot was then trimmed by the screwdriver for reading of -2040.0 count value in the calibration utility.

3. A/D Bipolar Input Full Scale Calibration:

- i. On the STA-16 accessory box, the calibration voltage +9.9609 V from the DC power source was connected to the HI of the analog input channel 1. The return of the calibration voltage was connected to the both the LO of the channel 1 and the LLGND.
- ii. The related pot was then trimmed by the screwdriver for reading of +2040.0 count value in the calibration utility.

4. D/A 0 Bipolar Input Offset and Full Scale Calibration:

- i. On the STA-16 accessory box, DVM(+) was connected to the DAC0 output of the board and DVM(-) was connected to the LLGND.
- ii. The spacebar of the computer keyboard was used to alternate between offset and full-scale calibrations.
- iii. The related pot was then trimmed by the screwdriver for reading of 5.0 V value on the DVM display.

5. D/A 1 Bipolar Input Offset and Full Scale Calibration:

- i. On the STA-16 accessory box, DVM(+) was connected to the DAC1 output of the board and DVM(-) was connected to the LLGND.
- ii. The spacebar of the computer keyboard was used to alternate between offset and full-scale calibrations.
- iii. The related pot was then trimmed by the screwdriver for reading of 5.0 V value on the DVM display.

Thus the calibration of the board internals had been finished for using in the data acquisition system of the experimental set-up.

APPENDIX 8

TIME DEPENDENT DATA ACCUMULATION CONTROL PROGRAM

```
VERSION 5.00
Object = "{4DE9E2A3-150F-11CF-8FBF-444553540000}#4.0#0"; "DLXOCX32.OCX"
Object = "{F9043C88-F6F2-101A-A3C9-08002B2F49FB}#1.2#0"; "COMDLG32.OCX"
Begin VB.Form frmMain
    Caption      = "DAS 1602 Data "
    ClientHeight = 5355
    ClientLeft   = 60
    ClientTop    = 630
    ClientWidth  = 10830
    LinkTopic    = "Form1"
    ScaleHeight  = 5355
    ScaleWidth   = 10830
    StartUpPosition = 1 'CenterOwner
Begin VB.TextBox txtChan
    Height      = 405
    Left        = 7950
    TabIndex    = 24
    Text        = "0"
    Top         = 3840
    Width       = 1395
End
Begin VB.TextBox txtDelay
    Height      = 405
    Left        = 2940
    TabIndex    = 23
    Text        = "10000"
    Top         = 180
    Width       = 1785
End
Begin VB.CommandButton cmdDelayed
    Caption     = "Start As Delayed"
    Height      = 555
    Left        = 2940
    TabIndex    = 22
    Top         = 630
    Width       = 1845
End
Begin VB.CommandButton Command2
    Caption     = "Save Data As ASCII..."
    Height      = 525
    Left        = 1650
    TabIndex    = 20
    Top         = 2610
    Width       = 2115
End
Begin VB.Timer tmrDoEvents
    Enabled     = 0 'False
    Left        = 1110
    Top         = 3840
End
Begin VB.CommandButton cmdLoad
    Caption     = "Load Channel 0 Data As Binary..."
    Height      = 555
    Left        = 7890
```

```

    TabIndex    = 19
    Top         = 870
    Width      = 1815
End
Begin VB.CommandButton cmdSave
    Caption     = "Save Data As Binary..."
    Height     = 525
    Left       = 1650
    TabIndex   = 17
    Top        = 2070
    Width      = 2115
End
Begin MSComDlg.CommonDialog CD
    Left       = 990
    Top        = 3360
    _ExtentX   = 847
    _ExtentY   = 847
    _Version   = 393216
End
Begin VB.CommandButton Command1
    Caption     = "Graph Channel #"
    Height     = 735
    Left       = 7920
    TabIndex   = 16
    Top        = 90
    Width      = 1755
End
Begin VB.CommandButton cmdFill
    Caption     = "FillData"
    Height     = 465
    Left       = 7950
    TabIndex   = 15
    Top        = 4230
    Width      = 1485
End
Begin VB.ListBox List
    Height     = 4740
    Index      = 0
    Left       = 6150
    TabIndex   = 14
    Top        = 0
    Width      = 1695
End
Begin VB.Timer tmrTime
    Left       = 1020
    Top        = 4320
End
Begin VB.Timer tmrData
    Left       = 540
    Top        = 4380
End
Begin VB.CommandButton cmdStop
    Caption     = "Stop"
    Height     = 525
    Left       = 1680
    TabIndex   = 12
    Top        = 1260
    Width      = 1245
End
Begin VB.Timer tmrStatus

```

```

Left      = 30
Top       = 4350
End
Begin VB.Frame Frame1
Caption   = "Select Channels"
ForeColor = &H00FF0000&
Height    = 3195
Left      = 60
TabIndex = 2
Top       = 120
Width     = 1455
End
Begin VB.CheckBox Check1
Caption   = "Channel 3"
Height    = 345
Index     = 3
Left      = 120
TabIndex = 6
Top       = 1365
Value     = 1 'Checked
Width     = 1155
End
Begin VB.CheckBox Check1
Caption   = "Channel 2"
Height    = 345
Index     = 2
Left      = 120
TabIndex = 5
Top       = 1020
Value     = 1 'Checked
Width     = 1155
End
Begin VB.CheckBox Check1
Caption   = "Channel 1"
Height    = 345
Index     = 1
Left      = 120
TabIndex = 4
Top       = 675
Value     = 1 'Checked
Width     = 1155
End
Begin VB.CheckBox Check1
Caption   = "Channel 0"
Height    = 345
Index     = 0
Left      = 120
TabIndex = 3
Top       = 330
Value     = 1 'Checked
Width     = 1155
End
Begin VB.CommandButton cmdStart
Caption   = "Start"
Height    = 525
Left      = 1680
TabIndex = 1
Top       = 630
Width     = 1245
End

```

```

Begin DlsrLib.DriverLINXLDD LDDD
  Index      = 9
  Left       = 540
  Top        = 3840
  _Version   = 262144
  _ExtentX   = 741
  _ExtentY   = 741
  _StockProps = 64
  _Version   = 262144
  _ExtentX   = 741
  _ExtentY   = 741
  _StockProps = 64
End
Begin DlsrLib.DriverLINXLDD LDD
  Left       = 540
  Top        = 3360
  _Version   = 262144
  _ExtentX   = 741
  _ExtentY   = 741
  _StockProps = 64
  _Version   = 262144
  _ExtentX   = 741
  _ExtentY   = 741
  _StockProps = 64
End
Begin DlsrLib.DriverLINXSR SR
  Left       = 90
  Top        = 3360
  _Version   = 262144
  _ExtentX   = 741
  _ExtentY   = 741
  _StockProps = 64
End
Begin VB.Label Label1
  Caption    = "Enter Here Channel Number"
  Height     = 435
  Left       = 7920
  TabIndex   = 25
  Top        = 3420
  Width      = 1545
End
Begin VB.Label lblMeanData
  Caption    = "Label1"
  Height     = 435
  Left       = 90
  TabIndex   = 18
  Top        = 4320
  Width      = 5055
End
Begin VB.Label lblTime
  Alignment  = 2 'Center
  ForeColor  = &H00FF0000&
  Height     = 315
  Left       = 4050
  TabIndex   = 13
  Top        = 4860
  Width      = 1725
End
Begin VB.Label lblStatus
  BackStyle  = 0 'Transparent

```

```

BorderStyle = 1 'Fixed Single
BeginProperty Font
  Name      = "MS Sans Serif"
  Size      = 8.25
  Charset   = 162
  Weight    = 700
  Underline = 0 'False
  Italic    = 0 'False
  Strikethrough = 0 'False
EndProperty
ForeColor   = &H000000FF&
Height     = 405
Left       = 60
TabIndex   = 11
Top        = 4800
Width      = 3855
End
Begin VB.Menu MnFile
  Caption   = "File"
  Begin VB.Menu MnLoadFile
    Caption  = "Load Data File..."
  End
  Begin VB.Menu MnSave
    Caption  = "Save Data To File..."
  End
End
Begin VB.Menu MnExit
  Caption   = "Exit"
End
End
Attribute VB_Name = "frmMain"
Attribute VB_GlobalNameSpace = False
Attribute VB_Creatable = False
Attribute VB_PredeclaredId = True
Attribute VB_Exposed = False
Option Explicit

Dim dummy As Single
ReDim ChanData(UBound(chanList()) - 1, 0 To NumOfData - 1) As Single
lblStatus.Caption = "Started Acquiring..."

For i = 0 To delaytime
  DoEvents
  'doNothing
Next

CurrentDataIndex = CurrentDataIndex + 1
Loop
'lblStatus.Caption = "Total Data=" & Format(CurrentDataIndex, "####,###,###")
tmrStatus.Enabled = True
cmdStart.Enabled = True
Exit Sub
errhandler:
MsgBox "error when getting data"
MsgBox Err.Description
Exit Sub
End Sub
Private Sub cmdStop_Click()
Dim ii As Long

```

```

cmdStart.Enabled = True
cmdDelayed.Enabled = True
DoAcquiring = False
tmrData.Enabled = False
tmrTime.Enabled = False
EndTime = GetTickCount
GraphEndTime = EndTime
StartTime = 0
EndTime = 0
Exit Sub
End If
lblTime = CStr(EndTime - StartTime) & " ms"
TotalEllapsedTime = Val(lblTime.Caption)

lblStatus.Caption = "Total Data per Channel=" & CurrentDataIndex + 1
lblMeanData.Caption = (CurrentDataIndex / ((EndTime - StartTime) / 1000)) & " data per channel
/sec"
StartTime = 0

For ii = 0 To 7
Check1(ii).Enabled = True
Next
cmdStart.Enabled = True
End Sub

Private Sub cmdLoad_Click()
Dim datano As Long, temp As Single
On Local Error GoTo errline
Dim i As Long, ChanNo As Integer

List(0).Clear

CD.DialogTitle = "Open Data To File"
CD.InitDir = "c:\belgelerim"
CD.Filter = "All Files | *.*"
CD.DefaultExt = ".txt"
CD.CancelError = True
CD.ShowOpen
filenametobeLoaded = CD.FileName
filenumber = FreeFile
Open filenametobeLoaded For Binary Access Read As #filenumber

If LOF(filenumber) > 32500 Then
CurrentDataIndex = 32500 \ 4
Else
CurrentDataIndex = LOF(filenumber) \ 4
End If
'CurrentDataIndex = 100
MsgBox CurrentDataIndex & " data found in the file"

For i = 0 To (CurrentDataIndex - 1) Step 4
Get #filenumber, i + 1, temp
List(0).AddItem CStr(Format(temp, "###0.#0")) & " Volts"
Next

Close filenumber
Exit Sub
errline:
MsgBox StrConv("err when file ops", vbProperCase)
End Sub

```

```

Private Sub cmdSave_Click()
Call MnSave_Click
End Sub

Private Sub Command1_Click()
frmGraph.Show
End Sub

Private Sub Check1_Click(Index As Integer)
'MsgBox Check1(Index).Value
End Sub

Private Sub cmdFill_Click()
On Local Error GoTo errhandler
Dim i As Long
ChanNo = Val(txtChan.Text)
List(0).Clear
For i = 0 To CurrentDataIndex - 1
List(0).AddItem Format(ChanData(ChanNo, i), "#0.##")
Next
Exit Sub
errhandler:
MsgBox "You are trying to reach to an Unused Channel"
End Sub

Private Sub cmdSingle_Click()
With SR
.Req_DLL_name = "c:\drvlinx4\kmbdas16.dll"
.Req_device = 0
.Req_subsystem = DL_DEVICE
.Req_mode = DL_OTHER
.Req_op = DL_INITIALIZE
.Refresh
End With

With SR
.Req_subsystem = DL_AI
.Req_mode = DL_POLLED
.Req_op = DL_START

.Evt_Tim_type = DL_NULLEVENT
.Evt_Str_type = DL_COMMAND
.Evt_Stp_type = DL_TCEVENT

.Sel_chan_format = DL_tNATIVE
.Sel_chan_N = 1
.Sel_chan_start = 0
.Sel_chan_startGainCode = .DLGain2Code(-1)

.Sel_chan_stop = 1 ' stop at chan 3 for 4 channels total...0 through 3
.Sel_chan_stopGainCode = .DLGain2Code(-1) ' use this gain for all channels except start chan

.Sel_buf_N = 0
.Sel_buf_samples =

.Res_Sta_typeStatus = DL_IOVALUE
End With

SR.Refresh

```



```

MsgBox Format(SR.DLCode2Volts(SR.Res_Sta_ioValue), "#0.###0")

End Sub

Private Sub cmdStart_Click()
Dim ebrdata() As Single

Dim ii As Long
On Local Error GoTo errhandler
Call FillChannelList ' determine which channels will be used
cmdStart.Enabled = False
cmdDelayed.Enabled = False
NumOfData = 1000000

lblMeanData.Caption = ""
tmrData.Interval = 1000
tmrData.Enabled = True
tmrTime.Interval = 1000
tmrTime.Enabled = True

For ii = 0 To 7
Check1(ii).Enabled = False
Next
cmdStart.Enabled = False

Dim dummy As Single
ReDim ChanData(UBound(chanList()) - 1, 0 To NumOfData - 1) As Single
MsgBox "inited"
lblStatus.Caption = "Started Acquiring..."
DoAcquiring = True
CurrentDataIndex = 0
StartTime = GetTickCount
GraphStartTime = StartTime
Do Until DoAcquiring = False
    For ChanNo = 0 To UBound(chanList()) - 1
        With SRR(ChanNo)
            .Refresh
            ChanData(ChanNo, CurrentDataIndex) = .DLCode2Volts(.Res_Sta_ioValue)
        End With
    Next
    If CurrentDataIndex > NumOfData Then
        MsgBox CurrentDataIndex
        MsgBox "Total Time=" & (GetTickCount - StartTime) / 1000
        cmdStart.Enabled = True
        DoAcquiring = False
        tmrData.Enabled = False
        tmrTime.Enabled = False
        EndTime = GetTickCount
        Exit Do
    End If
DoEvents
CurrentDataIndex = CurrentDataIndex + 1
Loop
lblStatus.Caption = "Total Data=" & Format(CurrentDataIndex, "####,###,###")
tmrStatus.Enabled = True
cmdStart.Enabled = True
Exit Sub
End Sub

```

CURRICULUM VITAE

PERSONAL INFORMATION

Surname, Name: Oruç, VEDAT
Nationality: Turkish (TC)
Date and Place of Birth: 20 September 1975, Diyarbakır
Marital Status: Single
Phone: +90 412 248 84 03
Fax: +90 412 248 84 05
email: voruc@dicle.edu.tr

EDUCATION

Degree	Institution	Year of Graduation
MS	Gaziantep University, Graduate School of Natural and Applied Sciences	2001
BS	Gaziantep University Department of Mechanical Engineering	1998
High School	Fatih Lisesi (DİYARBAKIR)	1992

WORK EXPERIENCE

Year	Place	Enrollment
1998- Present	Dicle University Department of Mechanical Engineering Diyarbakır	Research Assistant

FOREIGN LANGUAGES

English

PUBLICATIONS

1. Çarpınlioğlu, M.Ö., Özbelge, T.A., **Oruç, V.** (2002). Flow frictional resistance in pneumatic conveying of solid particles through inclined lines. *Powder Technology*, **125**, 292-297.
2. Çarpınlioğlu, M.Ö., **Oruç, V.** (2004). A correlation study for the positional dependence of friction factor in dilute phase flows. *Particulate Science and Technology*, **22**, 93-103.
3. **Oruç, V.**, Çarpınlioğlu, M.Ö. A test rig for the investigation of airflow through collapsible tubes. *Proceedings of the Institution of Mechanical Engineers, Part C: Journal of Mechanical Engineering Science* (In press)

4. Çarpınlioğlu, M.Ö., Özbelge, T.A., **Oruç, V.** (2001). Flow frictional resistance in pneumatic conveying of solid particles through inclined lines. *Proceedings of the 4th International Conference on Multiphase Flow, ICMF 2001*, June New Orleans, LA. U.S.A, Particle Dynamics Session, 27th May-1st June, CD-ROM, paper no: 853, 11 pages.
5. Çarpınlioğlu, M.Ö., **Oruç, V.** (2006). Presentation of a Sample Test Case on the Self- Excited Oscillations in Collapsible Tube Flows. *Proceedings of ILSA'06, 31st International Lung Sounds Association Conference*, Halkidiki, Greece, September 8-9, Session I: Airflow, Asthma, Wheeze, pp. 5-6.
6. **Oruç, V.**, Çarpınlioğlu, M.Ö. (2006). Elastik tüplerdeki akışların araştırılmasına yönelik bir deney düzeneğinin tanıtımı. *GAP V. Mühendislik Kongresi Bildiriler Kitabı*, 26-28 Nisan, Şanlıurfa, pp. 305-310.
7. **Oruç, V.**, Çarpınlioğlu, M.Ö. (2006). *Elastik tüplerdeki akışlarda kendiliğinden oluşan salınımların analizine yönelik deneysel bir araştırma. III. Ulusal Biomekanik Kongresi*, İTÜ, 1-2 Aralık.

HOBBIES

Travelling, swimming, fishing, internet searching, music.